Single-Molecule Protein Dynamics at the Solid-Liquid Interface

by

James Sullivan Weltz

B.S., Chemical Engineering and Biomedical Engineering, Carnegie Mellon University, 2013

A thesis submitted to the Faculty of the Graduate School of the University of Colorado in partial fulfillment of the requirement for the degree of Doctor of Philosophy

Department of Chemical and Biological Engineering

2019

This thesis entitled:

"Single-Molecule Protein Dynamics at the Solid-Liquid Interface"
written by James Sullivan Weltz

has been approved for the Department of Chemical and Biological Engineering

Joel L. Kaar	Date
Daniel K. Schwartz	Date

The final copy of this thesis has been examined by the signatories, and we find that both the content and the form meet acceptable presentation standards of scholarly work in the above-mentioned discipline.

ABSTRACT

James Sullivan Weltz (Department of Chemical and Biological Engineering)
"Single-Molecule Protein Dynamics at the Solid-Liquid Interface"
Thesis directed by Professors Joel L. Kaar and Daniel K. Schwartz

The objective of this work was to increase understanding of protein dynamics at solid-liquid interfaces using single-molecule methods to improve immobilized enzyme technologies. First, we identified a unique, dynamic mechanism of protein unfolding at solid-liquid interfaces where folded protein efficiently explored the surface before encountering sparsely distributed, nanoscale surface features, upon which the enzyme rapidly unfolded. Notably, passivation of the intensity and frequency of these surface features by site blocking did not significantly hinder protein unfolding due to the efficiency of this interfacial search process. With this molecular understanding of protein unfolding, we sought the design of an enzyme immobilization strategy which both reduced surface heterogeneity and inhibited searching of the surface, which involved covalent attachment of enzymes to polymer brushes. Notably, significant activity retention was observed for an industrially important lipase upon immobilization, suggesting little to no surface induced unfolding occurred. Interestingly, we observed a significant difference in stability of this lipase at elevated temperatures immobilized on two commonly employed polymers in biologically interfacing materials. Single-molecule observations of folding dynamics explained the difference in elevated-temperature stability as a change in both the temperature dependence of folding and unfolding rate constants. Notably, this difference in stability between polymer supports was not observed with other similar lipases, indicating this behavior was enzyme specific. Lastly, we exerted control over the dynamics of immobilized lipase by increased the number of sites of

attachment per enzyme. This reduced both folding dynamics and thermally driven fluctuations of the enzyme, which resulted in a tradeoff between immobilized enzyme stability and activity.

ACKNOWLEDGMENTS

I am grateful for my advisors, professors Joel L. Kaar and Daniel K. Schwartz, for mentorship throughout my graduate school career. Joel selflessly offered his limited time and extensive experience to solve technical challenges. Dan provided impressive intellect and diverse knowledge to answer many questions. Both provided a well-funded environment to pursue impactful, interesting research, including my own intellectual pursuits, and took a personal interest in my development as a scientist and professional. I would also like to express gratitude to my committee, Professors Ted Randolph, Joe Falke, and Hendrik Heinz, for critical feedback which significantly improved my dissertation.

I have also enjoyed working with many other great scientists and engineers. I would like to thank Daniel Kienle and Gregory Morrin for lending expertise toward fruitful collaborations. I would also like to thank Joshua Mabry, Mark Kastantin, Erik Nordwald, and Joseph Plaks for their support when I started this work. I appreciated countless discussions with and thoughtful feedback from Blake Langdon, Michael Skaug, Nathaniel Nelson, Garrett Chado, David Faulón Marruecos, Andres Chaparro Sosa and the rest of the Kaar and Schwartz labs. Lastly, Samantha Summers's friendship, perseverance, and optimism in the face of adversity remain a constant source of inspiration.

My scientific endeavors were only possible with financial support, which included grants from the U.S. Defense Threat Reduction Agency (award HDTRA1-16-1-0045), the graduate research fellowship from the NIH/CU Molecular Biophysics Training Program, and the Army Research Office (award W911NF-12-01115).

I was fortunate to mentor several talented students, including Clare Wise, Patrick Heenan, Kevin Sun, and Sam Blackman. Through teaching comes mastery, and their attentive questions and hard work provided a valuable aspect to my graduate education.

I would like to recognize my parents, Dana and Jim, and brother, Adam, for encouraging lifelong learning and leading by example. A big thank you to the wonderful Boulder friends I met along the way, including Tobin, Boris, Zoban, Spencer, Ian, Parker, and Julia. Together we have enjoyed much of what Colorado has to offer. Last, but certainly not least, I would like to thank Rachel for the love and joy she brings to my life.

TABLE OF CONTENTS

TABLE OF FIGURES

Chapter 1 Introduction

1.1 Interfacial Dynamics of Proteins

Proteins and enzymes are biological polymers composed of amino acids that often fold into precise three-dimensional structures[1]. These macromolecules mediate many of the diverse chemical and physical processes involved in biology and, therefore, are attractive for numerous technological applications[2–5]. For example, the ability of enzymes to catalyze reactions under mild conditions with exquisite selectivity make them exceptional catalysts[6–10]. This selectivity, coupled with high affinity, enables detection and quantification of small analyte concentrations in complex sample matrices[11–14]. The specificity of protein-protein interactions enables nanoscale self-assembly[15–17]. In these technologies, interaction of proteins with solid-liquid interfaces is often desired, as with the immobilization of enzymes to facilitate catalyst recycling[18–20], to make protein recognition compatible with a sensing modality[21–23], and to direct self-assembly in two dimensions[24–26]. Additionally, proteins interact with solid-liquid interfaces during purification and storage[27–29]. Therefore, the ubiquity of protein-surface interactions has motived decades of study[30–32].

Protein-surface interactions are typically studied with measurements of interfacial dynamics, including adsorption and desorption[33–35], diffusion[36–38], and changes in conformation[39–41]. Understanding adsorption and desorption is critical for creating stable immobilized enzyme catalysts with high loading and minimal leaching[42–44]. Diffusion is critical for effective chromatographic purification and efficient protein-directed self-assemblies[45–47]. Most importantly, preserving the native conformations of proteins at interfaces is required to preserve function[48–50]. Macroscopic measurements of interfacial dynamics have provided valuable, comparative information about the effects of, for example, surface chemistry[51–53], solution conditions[54–56], and

protein type[57–59] on adsorption and unfolding. However, the particular dynamic mechanisms of protein adsorption, diffusion, and unfolding cannot be directly determined from these ensemble-averaged measurements[60]. In the Schwartz and Kaar labs, we are interested in the development and application of single-molecule techniques to directly observe interfacial diffusion[61], aggregation[62], and unfolding[63] in order to provide engineering guidance for the technological applications of proteins at interfaces.

1.1.1 Adsorption and Desorption

Typically, ensemble measurements of protein adsorption monitor the quantity of adsorbed protein over time after contact with a protein containing solution[64–66]. Desorption kinetics are similarly measured by monitoring the loss of protein over time after exchange to a protein-free solution[67–69]. The amount of adsorbed protein is typically measured with techniques such as quartz crystal microbalance[70], sum frequency generation[71], surface plasmon resonance[72], and total internal reflection fluorescence[73], with high sensitivity enabling measurement of quantities significantly less than that of a monolayer. Notably, comparative studies of surfaces functionalized with self-assembled monolayers and polymers identified interfaces which significantly reduce the quantity of adsorbed protein[74–76] and are used as biomaterial surface coatings[77–79]. Additionally, low adsorption coatings functionalized with selective capture moieties are employed as sensors of specific proteins in whole blood[80,81].

Changes in the surface coverage of proteins are typically observed over minutes to hours with ensemble techniques[65,82]. However, increasingly complex observations led to considerable speculation regarding the molecular behaviors of adsorption and desorption that lead to these changes. For example, the well-documented Vroman effect, where an adsorbed protein layer is exchanged with a different soluble protein with higher surface affinity, suggest a contact-time

dependence on desorption rate[83–85]. Additionally, desorption of protein is often, to some degree, irreversible, with some amount of protein remaining on the surface over timescales longer than the experiment, typically hours to days[65,86,87]. Studies employing techniques sensitive to the conformation of surface bound protein suggested this long-lived species contained unfolded protein[50,67]. Alternatively, investigations of chromatographic stationary phases implicated lateral surface heterogeneity on long lived adsorbed species, which can be reduced through chemical passivation[29,88,89].

Dynamic single-molecule (SM) fluorescence methods enable simultaneous quantification of protein adsorption and desorption at interfaces without ensemble averaging[90–93]. Notably, these measurements observe a majority of proteins reside on the surface for hundreds of milliseconds[94], indicating exchange between the bulk and interface is highly dynamic. Additionally, the distributions of residence times suggest heterogeneous barriers to desorption[38,94], and SM methods have implicated surface heterogeneity[95,96], aggregation state[96,97], and protein conformation[63] on long-residing protein. Together, SM experiments have been invaluable for the unambiguous determination of adsorption and desorption dynamics of proteins at interfaces.

1.1.2 Diffusion

Interfacial diffusion of proteins, as well as small molecules, polymers, and surfactants, is essential for understanding fundamental technologies such as tribology[98], self-assembly[99], and chromatography[100]. As with adsorption and desorption, diffusion has traditionally been studied using ensemble-averaged, macroscopic techniques, including fluorescence recovery after photobleaching[36,101,102]. More recent work by the Schwartz group and others employing widefield SM particle tracking demonstrated proteins, polymers, and fluorophores undergo bulk-mediated diffusion at bare and functionalized silica-water interfaces[38,61,103]. This involves desorption,

subsequent three-dimensional random walk in the adjacent solution, followed by readsorption, as the primary mode of transport at solid-liquid interfaces[104]. Notably, bulk-mediated diffusion enables efficient searching of the surface compared to two-dimensional random walk confined to the interface[105], which is important for the efficiency of interfacial self-assembly, heterogeneous catalysis, and sensing.

Bulk-mediated diffusion at the solid-liquid interface can be described as a continuous time random walk were adsorbates exhibit variable waiting times and step sizes[106]. Notably, single-molecule tracking enables direct measurements of the distributions of both waiting times and step sizes, the latter being a distribution of "flights" in the adjacent bulk solution[107]. Flight-length distributions represent the number of collisions between the protein and the surface and the probability of readsorption with each collision (*i.e.* sticking coefficient)[38]. Since readsorption represents a competition between adsorbate and solvent, flight-length distributions of small molecules can be controlled by tuning the composition of the solvent, as with reverse phase chromatography[45], although this method of control is not compatible with many protein systems. Alternatively, flight-length distributions may be controlled with nanoscale topography of the surface, creating physical barriers to long flights[108]. Waiting-times represent a measurement of the energy barriers of desorption, and power-law distributed waiting times have been observed in a variety of contexts, indicating significant heterogeneity in the energy barriers to desorption[38,61,103].

1.1.3 Conformation

The first reports of the loss of enzyme function at interfaces were made nearly one-hundred years ago[109] and were soon after attributed to changes in enzyme conformation[110]. Since these early reports, surface-induced protein denaturation has been implicated in many technological challenges, including the loss of immobilized enzyme activity[111], sensor sensitivity[112], and the

safety of protein-based therapeutics[27]. Therefore, understanding the mechanisms of protein denaturation at interfaces, as well as the particular physical and chemical properties of surfaces that lead to protein denaturation are of significant interest.

The precise, three dimensional conformation of proteins have been determined in atomistic detail using x-ray crystallography[113], cryo-electron microscopy[114], and nuclear magnetic resonance[115], although these methods are generally incompatible with proteins at solid-liquid interfaces. Other biophysical methods, such as fluorescence[116] and circular dichroism[117], can be used to monitor protein structure loss in micro- and nanoparticle suspensions, although interpretation is complicated by the protein remaining in solution and significant light scattering. Therefore, methods sensitive to protein only at an interface, such as Fourier transform infrared attenuated total reflection spectroscopy[118], total internal reflection fluorescence[119], and surface plasmon resonance[120] have been invaluable in measuring the kinetics of protein structure loss at interfaces and identifying surfaces that limit protein unfolding.

Studies of the kinetics of protein structure loss at interfaces generally observe transitions from mostly folded to mostly unfolded protein over minutes to hours, which has been attributed to relaxation of adsorbed protein layers over these timescales[39,82,121]. While this is reasonable and represents the simplest explanation of the observation, alternative interpretations are possible. For example, rapid exchange of protein between the surface and solution and a higher affinity between unfolded protein and the surface could result in the surface acting as a collector of unfolded protein from solution[94]. While this interpretation is more complex and speculative, it is consistent with a more dynamic picture of proteins at interfaces as suggested by observations of the Vroman effect[84]. Lastly, these measurements are insensitive to surface heterogeneity, which has been indirectly implicated protein unfolding at chromatographic interfaces[88,89,122].

Recent developments in single-molecule methods enable the direct observation of protein structure at interfaces without ensemble averaging. Notably, single-molecule studies of organophosphorous hydrolase on fused silica observed a majority of unfolding events occurring within one second of adsorption. Additionally, a majority of unfolded protein readily desorbed, suggesting surfaces may be a source of unfolded protein in solution[63]. Single-molecule measurements of peptide conformation on functionalized fused silica surfaces demonstrated a dependence of conformation on underlying surface chemistry and further implicated surface heterogeneity in surface-induced protein unfolding[95].

1.2 Approaches of Enzyme Immobilization

Enzyme immobilization facilitates recycling of the otherwise soluble catalyst[59], makes enzyme catalysis compatible with various sensing modalities[12], and, in some cases, imparts additional enzyme stability[123]. Given the diverse applications of immobilized enzymes, equally diverse approaches for enzyme immobilization have been developed. For example, in amperometric sensing of glucose, glucose oxidase is immobilized on the surface of an electrode, enabling facile quantification of glucose in whole blood[14,124]. In the preparation of lipases, an important industrial catalyst, immobilization and crude purification are combined to simplify production and reduce costs[125]. In biomaterials, protein signals are desired at low concentration to direct wound healing and, importantly, misfolded protein at low concentrations may cause a deleterious host responses[126].

While these examples highlight the different engineering and design requirements for applications of immobilized enzymes, in all cases high stability is desired[6]. High operational stability of industrial biocatalysts enables long operational lifetimes[2] and enables operation at elevated temperatures, resulting in higher catalytic rates, increased substrate solubility[127], reduced

probability of microbial contamination[128], and reduced feed viscosity[5]. In biosensing, the response of the sensor must be consistent and robust against chemical denaturation due to the wide variety of sample matrices in which detection is desired[13]. In cell culture and tissue engineering, cellular responses may occur over days, and protein signals must remain active over these timescales[129].

1.2.1 Adsorption

Perhaps the most common approach for immobilization of lipases, an industrially important class of enzymes which catalyze the hydrolysis of fatty acid esters, is adsorption[130]. Several industrially employed examples of immobilized lipase employ microporous, hydrophobic plastic supports to which lipases spontaneously adsorb[125]. The high affinity of lipases to the hydrophobic supports enable direct immobilization from industrial fermentations, combining somewhat crude purification with immobilization, as done with *Candida antarctica* lipase B[131]. Fortuitously, increases in thermostability, as measured indirectly as an increase in activity retention over time at elevated temperatures or in non-aqueous solvents, have been observed for *Bacillus thermocatenulatus*, porcine pancreas, and *Pseudomonas fluorescens* lipases adsorbed to hydrophobic supports[125,130,132]. Additionally, the activity per enzyme has increased upon immobilization to hydrophobic supports for several lipases, including *Rhizomucor miehei* and *Candida rugosa* lipases, upon adsorption[132–134]. This so called "interfacial activation" is typically ascribed to the stabilization of an "open" conformation, where an aliphatic domain near the active site no longer hinders substrate binding[135–137].

Despite the advantages of immobilization by adsorption, the reversibility of immobilization results in leaching of enzyme from the support and subsequent loss of activity[43,138]. In drug delivery, desorption is desired and, therefore, proteins are often immobilized by adsorption to porous carriers, including mesoporous silica, for controlled release[139,140]. Notably, significant

increases in thermostability has been reported for proteins within mesoporous silicas and other supports with a confining dimension on the order of the size of an individual protein[141,142]. This thermodynamic stabilization can be well modeled as a reduction in unfolded-state entropy, the primary thermodynamic penalty of protein folding[143–145]. In applications were desorption is undesired, as with lipase biocatalysts, co-deposition of enzymes with polysiloxanes[146] and polyethylenimine[147] reduced enzyme leaching, thereby improving catalyst longevity.

1.2.2 Entrapment

Entrapment typically involves polymerization of a gel around an enzyme. Notably, as with confinement of protein within mesoporous solids, entrapment can result in significant enzyme stabilization with minimal leaching. Stabilization by entrapment within silica sol-gels has been achieved with numerous enzymes, including model systems with catalase, peroxidase, and trypsin, as well as systems of applied biocatalysis and biosensing using lipases and glucose oxidase[148–150]. In addition to gelation, DNA nanoassemblies[151], polyurethane foams[152], and agarose[153] have been employed for entrapment and stabilization of several enzymes. Presumably, stabilization is due to confinement, as with adsorption within mesoporous silicas. However, significant differences in enzyme stability with modification of sol-gel chemistry have been observed, indicating other interactions between the protein and support also significantly influence stability[154–156]. Although significant stabilization of immobilized enzymes has been observed, a major disadvantage of entrapment is hindered substrate and product transport[43,157]. Additionally, even in examples where enzyme stabilization occurs, typically less than 10% of the enzyme remains active after immobilization, indicating significant protein unfolding during the immobilization process[152,158]. Therefore, entrapment is typically employed where high stability, rather than overall activity, is desired.

1.2.3 Carrier-Free Approaches

Carrier-free approaches to enzyme immobilization most often consist of crosslinked enzyme crystals and aggregates (CLECs and CLEAs, respectively)[146,159,160]. These involve crystallization or aggregation of an enzyme while preserving activity, followed by crosslinking, although several protocols have combined both steps[59,161]. Notably, exceptional stability against chemical denaturants, solvents, surfactants, and elevated temperatures have been reported with carrier-free immobilization of lipases[7,162]. Additionally, carrier-free approaches sometimes combine immobilization and purification through a crude, selective precipitation of the target enzyme from cell culture media, which often simplifies preparation[146]. While CLECs and CLEAs have been employed successfully in industry for several enzymes, including *Rhizomucor miehei* lipase, identification of conditions to aggregate or crystalize protein while retaining activity requires empirical screening and have not identified for many enzymes[59]. Additionally, as with entrapment, reduced activities due to diffusional limitations and poor activity retention is observed and, therefore, carrier-free immobilization approaches are also employed when high stability, rather than activity, is desired[163].

1.2.4 Covalent Conjugation

Covalent immobilization of enzymes prevents leaching and can reduce mass transport limitations associated with immobilization by adsorption, entrapment, and carrier-free approaches. Typically, reactive groups are introduced on the support surface, such as epoxides or aldehydes, which randomly react with enzyme surface groups, resulting in a monolayer of immobilized enzyme[21,123,164]. While there are numerous reports of immobilization using this approach, immobilization with significant activity retention and stability requires an empirical, trial-and-error to identify support surfaces, chemistries of attachment, and solution conditions for successful

immobilization[59,165,166]. Therefore, numerous support chemistries, including hydrophilic agarose gels[167,168], hydrophobic cross-linked polymers[123,169], and polyelectrolytes[170,171], have been investigated.

Additionally, the means of covalent attachment can affect the stability of an immobilized enzyme.[123,168,172] In cases where attachment to native sites on the surface on the enzyme causes inactivation, control of the location of the attachment has been achieved through genetic methods, including incorporation of a unique thiol-containing cysteine[22,52,173], target peptide sequence for enzyme-mediated post-translational modification[174–176], or biorthogonal non-natural amino acids[177–179]. Additionally, attachment to a reactive group on the enzyme near the active site can prevent substrate access and, therefore, bulky substrates and substrate analogs have been added to immobilization reactions to sterically inhibit covalent attachment at locations close to the active site[180]. Changes in solution pH and temperature can also be used to favor attachment to particular reactive groups. This has been employed to preferentially immobilize enzymes *via* the N-terminus, which often exhibits a different pK_a than primary amines found on lysine residues[181,182].

1.3 Single-Molecule Fluorescence at Solid-Liquid Interfaces

Fluorescence methods rely on the adsorption of light by fluorophores, typically conjugated aromatic molecules, which emit red shifted light with a high efficiency[183]. The difference in wavelength between excitation and emitted light (*i.e.*, Stokes shift), combined with the high brightness (the product of adsorption coefficient and the quantum yield) enable detection of these molecules at low concentration[184]. This low detection limit, combined with many strategies for the conjugation of fluorophores to biomolecules, has made fluorescence methods widespread in the life sciences.

1.2.1 Total Internal Reflection Fluorescence Microscopy

In fluorescence microscopy, fluorophores are excited with a high intensity and images are generated by wavelength dependent filtering of red shifted emission collected by the objective of a microscope. There are numerous illumination geometries available depending on the application[185]. The goal of many illumination strategies is to limit excitation to a small volume within the focal plane of the objective, reducing emission of fluorophores that do not contribute to the focused image, therefore, reducing the background[186].

On approach to limit background and only excite fluorophores near a solid-liquid interface is total internal reflection fluorescence microscopy (TIRFM). In this geometry, excitation light, in the form of a focused laser, is incident on the interface at an angle greater than the critical angle, as shown in Figure 1-1 for prism-based TIRFM. Excitation light does not propagate into the adjacent liquid, but forms an exponentially decaying evanescent wave with intensity at a given distance normal to the interface, z, given by:

$$I(z) = I_0 e^{-z/d}$$

The characteristic distance, d, depends on the index of refraction of the solid and liquid, n_s and n_l, respectively, the wavelength of incident light, λ, and the angle of incident light relative to the surface normal, θ, and is approximately 83 nm for 491 nm light incident at the fused silica-water interface at 75º from the surface normal[187].

$$d = \frac{\lambda}{4\pi\sqrt{n_s^2 \sin^2(\theta) - n_l^2}}$$

Notably, this significantly reduces the background from fluorophores in solution, enabling localization and tracking of single-molecules at the interface.

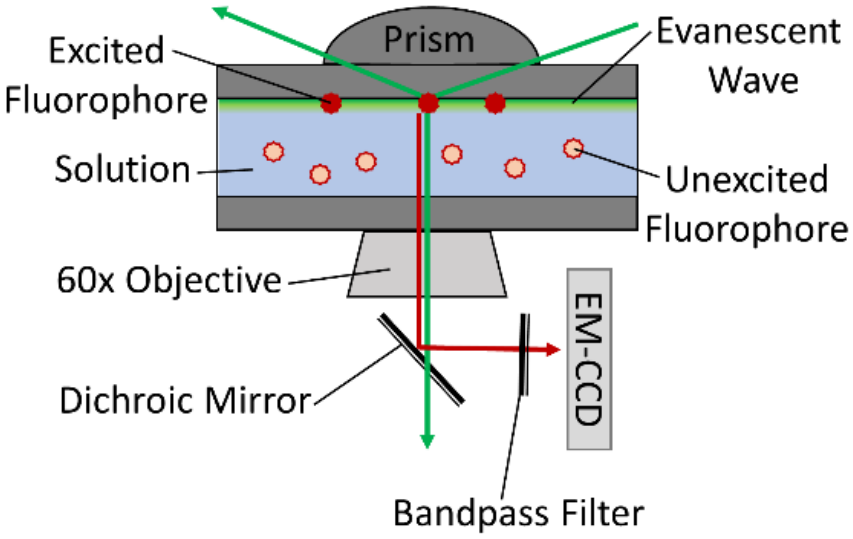

Figure 1-1: Prism-Based TIRFM. Laser excitation is incident on the sample at an angle greater than the critical angle and, therefore, does not propagate into the solution. Excitation occurs by an evanescent wave within approximately 100 nm of the surface.

1.2.2 Förster Resonance Energy Transfer

Förster resonance energy transfer (FRET) is the non-radiative energy transfer from a donor fluorophore to an acceptor fluorophore, where the emission spectrum of the donor and adsorption spectrum of acceptor overlap[188]. The energy transfer occurs over distances between 1 and 10 nm and the efficiency of energy transfer from donor to acceptor, E, given a donor-acceptor separation, r, is:

$$E = \frac{I_A}{I_D + I_A} = \frac{1}{\left(1 + \left(\frac{r}{R_0}\right)^6\right)}$$

Where I_A and I_D are the intensity of acceptor and donor emission, respectively, and the constant, R_0, depends on the emission spectrum of donor, excitation spectra of acceptor, the index of

refraction of the medium between fluorophores, and the orientation between fluorophores[189]. The rotation of donor and acceptor fluorophores are often assumed to be rapid enough such that random, isotropic averaging is achieved over the fluorescence lifetime of the donor[190].

The utility of FRET in many biophysical applications comes from the strong distance dependence of energy transfer. Accurate distance measurements of, for example, conformational changes in peptides, proteins, and DNA have been achieved with FRET[191]. While the parameter E is often reported in biophysical methods, there are several parameterization of FRET data in the published literature. A useful approach is the relative distance parameter, d, which is defined as:

$$d = \left(\frac{I_D}{I_A}\right)^{\frac{1}{6}}$$

The parameter d is proportional to the absolute distance between fluorophores by R_0 and is therefore useful when comparing relative changes in fluorophore-fluorophore distance.

One design strategy for conformationally sensitive, FRET-active proteins is to covalently attach donor and acceptor fluorophores at proximal sites on the solvent-accessible surface of the folded state and far apart in the primary sequence[192]. Therefore, the folded state is observed with high energy transfer (low d) while unfolded states have a greater average fluorophore-fluorophore distance and, therefore, significantly decreased energy transfer (high d). Importantly, determination of protein conformation with FRET requires the site-specific labeling of donor and acceptor fluorophores at known locations on the surface of the protein, enabling interpretation in changes in fluorophore-fluorophore distance as changes in protein structure[193]. Fortunately, there have been significant development of bioconjugation strategies for fluorophore labeling of proteins.

1.2.3 Site-Specific Bioconjugation of Fluorophores for FRET

Site-specific conjugation of donor and acceptor fluorophores has been achieved through numerous methods, including genetic fusion with fluorescent proteins[189], enzyme-directed post-translational modification[176], and non-natural amino acids (NNAAs)[194]. Fusion with fluorescent proteins has been invaluable when FRET-labeling intracellular proteins in living cells, however, challenges arise from the large size of fluorescent proteins and the relatively low photostability compared to modern chemical fluorophores[189]. Enzyme-directed post-translational modifications, including sortase and lipoic acid ligase mediated approaches, require incorporation of enzyme recognition sequences, typically 5-12 amino acids, within the protein without significantly altering stability, structure, or function[174,176].

NNAAs are increasingly employed due the large number of biorthogonal chemistries available and the requirement of only one amino acid insertion compared with fluorescent protein or enzyme-mediated approaches[194]. NNAA incorporation into recombinantly expressed protein in bacteria is achieved by additional expression of an engineered tRNA and tRNA synthetase pair[195]. The mutant tRNA synthetase specifically charges mutant tRNA with a NNAA supplemented into the cell culture medium. Typically, the mutant, aminoacyl-tRNA is complementary to the amber stop codon and outcompetes binding of the native release factor during protein synthesis in the ribosome[196]. This stop codon suppression effectively recodes the amber stop codon from peptide termination into the codon for a new, non-natural amino acid. Notably, mutant tRNA synthetases have been engineered to incorporate over three-hundred unique, non-natural amino acids, including biorthogonal “click-chemistries” and entire small-molecule fluorophores. However, non-natural amino acids have limited efficiency of incorporation due to premature peptide termination from native release factors. Therefore, significant improvements, including genome

engineering of expression organisms to remove the native release factor, were required to incorporate multiple non-natural amino acids into one protein[197].

1.4 Objectives

The objective of this work was to investigate protein dynamics at solid-liquid interfaces using single-molecule methods to better understand the technological challenges involving enzymes at interfaces and improve methods for enzyme immobilization. To that end, three specific aims were addressed in this work.

1. Identify a dynamic molecular mechanism of protein unfolding at silica-water interfaces
2. Engineer strategies for enzyme immobilization that preserve the folded, active conformation
3. Control the conformational dynamics of immobilized enzymes to improve stability

1.4.1 Identify a dynamic molecular mechanism of protein unfolding at silica-water interfaces

In the first specific aim, single-molecule particle tracking combined with FRET was used to identify a dynamic mechanism of protein unfolding at a solid-liquid interface. These single-molecule methods enabled the observation that folded enzymes rapidly explored the surface *via* bulk-mediated surface diffusion before encountering sparsely distributed, nanoscale surface features, upon which the enzyme rapidly unfolded. Notably, passivation of the intensity and frequency of these surface features by site blocking did not significantly hinder protein unfolding due to the efficiency of this interfacial search process.

1.4.2 Engineer strategies for enzyme immobilization that preserve the folded, active conformation

With this molecular understanding of protein unfolding, we sought the design of an enzyme immobilization strategy which both reduced surface heterogeneity and inhibited searching of the surface. To that end, we employed dense polymer brush surfaces as the immobilization support to inhibit interaction between enzymes and the underlying solid. To both facilitate immobilization and prevent searching, reactive moieties were incorporated into the brush matrix to rapidly and irreversibly tether the enzyme. Notably, significant activity retention was observed for lipase A from *Bacillus subtilis* (lipA), an important enzyme for industrial catalysis, suggesting that little to no surface induced unfolding occurred. Interestingly, we observed a significant increase in the elevated temperature stability of immobilized lipA on polymer brushes composed of zwitterionic poly(sulfobetaine methacrylate) relative to the same enzyme on poly(poly(ethylene glycol) methacrylate), two common polymers employed on biologically interfacing materials. Single-molecule observations of lipA dynamics demonstrated that this difference in stability was due to reduction in the temperature dependence of folding and unfolding rate constants of on the stabilizing support. Interestingly, this difference in stability between supports, where the zwitterionic polymer appeared stabilizing, was also observed for the lipase from *Rhizomucor miehei*, but not for *Candida antarctica* lipase B or *Candida rugosa* lipase, and therefore, stabilization by zwitterionic supports was not universal. Future work will attempt to relate structural properties of an enzyme and chemical properties of these polymer brush supports to gain predictive capability to enzyme stabilization by immobilization.

1.4.3 Control the conformational dynamics of immobilized enzymes to improve stability

Due to the stabilizing interactions between the zwitterionic polymer brush support and immobilized lipA, we hypothesized that multipoint covalent immobilization (MPCI), attachment of the enzyme to the support at multiple locations on the enzyme surface, would further stabilize

the enzyme. Increased numbers of attachments per enzyme increased both the activity retention of immobilized lipA at elevated temperatures and the temperature optimum of activity, both suggestive of enzyme stabilization. Single-molecule measurements of immobilized lipA showed a dramatic decrease of the rate of unfolding, demonstrating that increasing the number of attachments per enzyme increased the free energy barrier(s) to unfolding. Additionally, increasing number of attachments per enzyme reduced the thermally driven fluctuations of unfolded enzyme, and therefore, the conformational entropy of the unfolded state, a major thermodynamic penalty for protein folding, was identified as a potential source of thermodynamic stabilization by MPCI. Lastly, increasing number of covalent attachments significantly decreased thermally driven fluctuations in the folded state, which corresponded to decreases in the specific activity of immobilized enzyme. Therefore, stabilization of enzymes by MPCI represented a tradeoff between high temperature stability and activity by restricting structural dynamics required for catalysis.

1.5 References

1. Fersht, A. *Structure and Mechanism in Protein Science*. **13409**, (W. H. Freeman and Company, 1997).
2. Bommarius, A. S. Biocatalysis: A Status Report. *Annu. Rev. Chem. Biomol. Eng.* **6**, 319–345 (2015).
3. Schmid, A. *et al.* Industrial Biocatalysis Today and Tomorrow. *Nature* **409**, 258–268 (2001).
4. DiCosimo, R., McAuliffe, J., Poulose, A. J. & Bohlmann, G. Industrial use of immobilized enzymes. *Chem. Soc. Rev.* **42**, 6437–74 (2013).
5. Dordick, J. S. An Introduction to Industrial Biocatalysis. in *Biocatalysts for Industry* (ed. Dordick, J. S.) (Springer, 1991). doi:https://doi.org/10.1007/978-1-4757-4597-9
6. Adams, M. W. W., Perler, F. B. & Kelly, R. M. Extremozymes: Expanding the limits of biocatalysis. *Nature Biotechnology* **13**, 662–668 (1995).
7. Sheldon, R. A., Schoevaart, R. & Van Langen, L. M. Cross-linked enzyme aggregates (CLEAs): A novel and versatile method for enzyme immobilization (a review). *Biocatal. Biotransformation* **23**, 141–147 (2005).

8. Bornscheuer, U. T. *et al.* Engineering the third wave of biocatalysis. *Nature* **485**, 185–194 (2012).

9. Gumulya, Y. *et al.* Engineering highly functional thermostable proteins using ancestral sequence reconstruction. *Nat. Catal.* **1**, 878–888 (2018).

10. Schmid, R. D. & Verger, R. Lipases: Interfacial Enzymes with Attractive Applications. *Angew. Chemie Int. Ed.* **37**, 1608–1633 (1998).

11. Iqbal, S. S. *et al.* A review of molecular recognition technologies for detection of biological threat agents. *Proc. SPE Int. Improv. Oil Recover. Conf. Asia Pacific* **15**, 549–578 (2003).

12. Smith, R. G., D'Souza, N. & Nicklin, S. A review of biosensors and biologically-inspired systems for explosives detection. *Analyst* **133**, 571–584 (2008).

13. Berberich, J. A., Yang, L. W., Bahar, I. & Russell, A. J. A stable three enzyme creatinine biosensor. 2. Analysis of the impact of silver ions on creatine amidinohydrolase. *Acta Biomater.* **1**, 183–191 (2005).

14. Bruen, D., Delaney, C., Florea, L. & Diamond, D. Glucose sensing for diabetes monitoring: Recent developments. *Sensors (Switzerland)* **17**, 1–21 (2017).

15. Shenton, W., Pum, D., Sleytr, U. B. & Mann, S. Synthesis of cadmium sulphide superlattices using self-assembled bacterial S-layers. *Nature* **389**, 585–587 (1997).

16. Zhong, C. *et al.* Strong underwater adhesives made by self-assembling multi-protein nanofibres. *Nat. Nanotechnol.* **9**, 858–866 (2014).

17. Huang, X. *et al.* Interfacial assembly of protein-polymer nano-conjugates into stimulus-responsive biomimetic protocells. *Nat. Commun.* **4**, 1–9 (2013).

18. Klibanov, A. M. Immobilized enzymes and cells as practical catalysts. *Science (80-.).* **219**, 722–727 (1983).

19. Prasad, S. & Roy, I. Converting Enzymes into Tools of Industrial Importance. *Recent Pat. Biotechnol.* **12**, 33–56 (2017).

20. Feng, D. *et al.* Stable metal-organic frameworks containing single-molecule traps for enzyme encapsulation. *Nat. Commun.* **6**, 1–8 (2015).

21. Scouten, W. H., Luong, J. H. T. & Stephen Brown, R. Enzyme or protein immobilization techniques for applications in biosensor design. *Trends Biotechnol.* **13**, 178–185 (1995).

22. Berberich, J. A., Yang, L. W., Madura, J., Bahar, I. & Russell, A. J. A stable three-enzyme creatinine biosensor. 1. Impact of structure, function and environment on PEGylated and immobilized sarcosine oxidase. *Acta Biomater.* **1**, 173–181 (2005).

23. Berberich, J. A., Chan, A., Boden, M. & Russell, A. J. A stable three-enzyme creatinine biosensor. 3. Immobilization of creatinine amidohydrolase and sensor development. *Acta Biomater.* **1**, 193–199 (2005).

24. Yan, H., Park, S. H., Finkelstein, G., Reif, J. H. & LaBean, T. H. DNA-templated self-assembly of protein arrays and highly conductive nanowires. *Science (80-.).* **301**, 1882–1884 (2003).

25. Zhang, S. Fabrication of novel biomaterials through molecular self-assembly. *Nat. Biotechnol.* **21**, 1171–1178 (2003).

26. Knowles, T. P. J., Oppenheim, T. W., Buell, A. K., Chirgadze, D. Y. & Welland, M. E. Nanostructured films from hierarchical self-assembly of amyloidogenic proteins. *Nat. Nanotechnol.* **5**, 204–207 (2010).

27. BEE, J. S., RANDOLPH, T., CARPENTER, J. F., BISHOP, S. M. & DIMITROVA, M. N. Effects of Surfaces and Leachables on the Stability of Biopharmaceuticals. *J. Pharm. Sci.* **100**, 4158–4170 (2011).

28. Burke, C. J. *et al.* The adsorption of proteins to pharmaceutical container surfaces. *Int. J. Pharm.* **86**, 89–93 (1992).

29. Jungbauer, A., Machold, C. & Hahn, R. Hydrophobic interaction chromatography of proteins: III. Unfolding of proteins upon adsorption. *J. Chromatogr. A* **1079**, 221–228 (2005).

30. Norde, W. & Lyklema, J. Thermodynamics of Protein Adsorption. *J. Colloid Interface Sci.* **71**, 350–366 (1979).

31. Ramsden, J. J. Puzzles and paradoxes in protein adsorption. *Chem. Soc. Rev.* **24**, 73 (1995).

32. Gray, J. J. The interaction of proteins with solid surfaces. *Curr. Opin. Struct. Biol.* **14**, 110–5 (2004).

33. Whitesides, G. M. & Prime, K. L. Self-assembled organic monolayers: model systems for studying adsorption of proteins at surfaces. *Science (80-.).* **252**, 1164–1167 (1991).

34. Calonder, C., Tie, Y. & Tassel, P. R. Van. Protein adsorption: Kinetics and history dependence of protein adsorption kinetics. *Proc. Natl. Acad. Sci.* **98**, 10664–10669 (2001).

35. Lee, R. G. & Kim, S. W. Adsorption of proteins onto hydrophobic polymer surfaces: Adsorption isotherms and kinetics. *J. Biomed. Mater. Res.* **8**, 251–259 (1974).

36. Yuan, Y., Velev, O. D. & Lenhoff, A. M. Mobility of adsorbed proteins studied by fluorescence recovery after photobleaching. *Langmuir* **19**, 3705–3711 (2003).

37. Ries, J., Petrov, E. P. & Schwille, P. Total internal reflection fluorescence correlation spectroscopy: Effects of lateral diffusion and surface-generated fluorescence. *Biophys. J.* **95**, 390–399 (2008).

38. Skaug, M. J., Mabry, J. & Schwartz, D. K. Intermittent Molecular Hopping at the Solid-Liquid Interface. *Phys. Rev. Lett.* **110**, 256101 (2013).

39. Graham, D. E. & Phillips, M. C. Proteins at Liquid Interfaces: Kinetics of Adsorption and

Surface Denaturation. *J. Colloid Interface Sci.* **70**, 403–414 (1978).

40. Shang, W., Nuffer, J. H., Dordick, J. S. & Siegel, R. W. Unfolding of ribonuclease a on silica nanoparticle surfaces. *Nano Lett.* **7**, 1991–1995 (2007).

41. Nakanishi, K., Sakiyama, T. & Imamura, K. On the adsorption of proteins on solid surfaces, a common but very complicated phenomenon. *J. Biosci. Bioeng.* **91**, 233–44 (2001).

42. Essa, H., Magner, E., Cooney, J. & Hodnett, B. K. Influence of pH and ionic strength on the adsorption, leaching and activity of myoglobin immobilized onto ordered mesoporous silicates. *J. Mol. Catal. B Enzym.* **49**, 61–68 (2007).

43. Ansorge-Schumacher, M. B. & Thum, O. Immobilised lipases in the cosmetics industry. *Chem. Soc. Rev.* **42**, 6475–6490 (2013).

44. Bo Chen, Jun Hu, Elizabeth M. Miller, Wenchun Xie, Minmin Cai, R. A. G. *et al.* Candida antarctica Lipase B Chemically Immobilized on Epoxy-Activated Micro- and Nanobeads: Catalysts for Polyester Synthesis. *Biomacromolecules* 463–471 (2008). doi:10.1021/bm700949x

45. Mabry, J. N., Skaug, M. J. & Schwartz, D. K. Single-Molecule Insights into Retention at a Reversed-Phase Chromatographic Interface. (2014).

46. Wirth, M. J., Swinton, D. J. & Ludes, M. D. Adsorption and Diffusion of Single Molecules at Chromatographic Interfaces. *J. Phys. Chem. B* **107**, 6258–6268 (2003).

47. Kisley, L. *et al.* Unified superresolution experiments and stochastic theory provide mechanistic insight into protein ion-exchange adsorptive separations. *Proc. Natl. Acad. Sci. U. S. A.* **111**, 2075–80 (2014).

48. Hlady, V. & Buijs, J. Protein adsorption on solid surfaces. *Curr. Opin. Biotechnol.* **7**, 72–7 (1996).

49. Rabe, M., Verdes, D. & Seeger, S. Understanding protein adsorption phenomena at solid surfaces. *Adv. Colloid Interface Sci.* **162**, 87–106 (2011).

50. Singla, B., Krisdhasima, V. & McGuire, J. Adsorption kinetics of wild type and two synthetic stability mutants of T4 phage lysozyme at silanized silica surfaces. *J. Colloid Interface Sci.* **182**, 292–296 (1996).

51. Prime, K. L. & Whitesides, G. M. Adsorption of Proteins onto Surfaces Containing End-Attached Oligo(ethylene oxide): A Model System Using Self-Assembled Monolayers. *J. Am. Chem. Soc.* **115**, 10714–10721 (1993).

52. Mrksich, M. & Whitesides, G. M. Using Self-Assembled Monolayers to Understand the Interactions of Man-Made Surfaces With Proteins and Cells. *Annu. Rev. Biophys. Biomol. Struct.* **25**, 55–78 (1996).

53. Ostuni, E., Chapman, R. G., Holmlin, R. E., Takayama, S. & Whitesides, G. M. A survey

of structure-property relationships of surfaces that resist the adsorption of protein. *Langmuir* **17**, 5605–5620 (2001).

54. Dismer, F., Petzold, M. & Hubbuch, J. Effects of ionic strength and mobile phase pH on the binding orientation of lysozyme on different ion-exchange adsorbents. *J. Chromatogr. A* **1194**, 11–21 (2008).

55. Wu, X. & Narsimhan, G. Effect of surface concentration on secondary and tertiary conformational changes of lysozyme adsorbed on silica nanoparticles. *Biochim. Biophys. Acta - Proteins Proteomics* **1784**, 1694–1701 (2008).

56. Barbosa, O., Torres, R., Ortiz, C. & Fernandez-Lafuente, R. Versatility of glutaraldehyde to immobilize lipases: Effect of the immobilization protocol on the properties of lipase B from Candida antarctica. *Process Biochem.* **47**, 1220–1227 (2012).

57. Jeon, S. I. & Andrade, J. D. Protein-Surface Interactions in the Presence of Polyethylene Oxide: II. Effect of Protein Size. *J. Colloid Interface Sci.* **142**, 159–166 (1991).

58. Silberberg, A. Adsorption of Collagen , Serum Albumin , and Fibronectin to Glass and to Each Other. **126**, (1988).

59. Cao, L. Immobilised enzymes: Science or art? *Curr. Opin. Chem. Biol.* **9**, 217–226 (2005).

60. Kastantin, M., Langdon, B. B. & Schwartz, D. K. A bottom-up approach to understanding protein layer formation at solid-liquid interfaces. *Adv. Colloid Interface Sci.* **207**, 240–252 (2014).

61. Skaug, M. J., Mabry, J. N. & Schwartz, D. K. Single-Molecule Tracking of Polymer Surface Di ff usion. *J. Am. Chem. Soc.* (2013).

62. Langdon, B. B., Kastantin, M. & Schwartz, D. K. Surface Chemistry Influences Interfacial Fibrinogen Self-Association. *Biomacromolecules* 150910134203000 (2015). doi:10.1021/acs.biomac.5b00869

63. McLoughlin, S. Y., Kastantin, M., Schwartz, D. K. & Kaar, J. L. Single-molecule resolution of protein structure and interfacial dynamics on biomaterial surfaces. *Proc. Natl. Acad. Sci.* **110**, 19396–19401 (2013).

64. Kastl, K. *et al.* Partially reversible adsorption of annexin A1 on POPC/POPS bilayers investigated by QCM measurements, SFM, and DMC simulations. *ChemBioChem* **7**, 106–115 (2006).

65. Krisdhasima, V., Vinaraphong, P. & McGuire, J. Adsorption Kinetics and Elutability of α-Lactalbumin, β-Casein, β-Lactoglobulin, and Bovine Serum Albumin at Hydrophobic and Hydrophilic Interfaces. *Journal of Colloid and Interface Science* **161**, 325–334 (1993).

66. Castillo, E. J., Koenig, J. L., Anderson, J. M. & Lo, J. Protein adsorption on hydrogels. II. Reversible and irreversible interactions between lysozyme and soft contact lens surfaces. *Biomaterials* **6**, 338–345 (1985).

67. Karlsson, M., Ekeroth, J., Elwing, H. & Carlsson, U. Reduction of irreversible protein adsorption on solid surfaces by protein engineering for increased stability. *J. Biol. Chem.* **280**, 25558–64 (2005).

68. Giacomelli, C. E. & Norde, W. The Adsorption–Desorption Cycle. Reversibility of the BSA–Silica System. *J. Colloid Interface Sci.* **233**, 234–240 (2001).

69. Daly, S. M., Przybycien, T. M. & Tilton, R. D. Adsorption of poly(ethylene glycol)-modified lysozyme to silica. *Langmuir* **21**, 1328–1337 (2005).

70. Richert, L., Variola, F., Rosei, F., Wuest, J. D. & Nanci, A. Adsorption of proteins on nanoporous Ti surfaces. *Surf. Sci.* **604**, 1445–1451 (2010).

71. Wang, J., Buck, S. M. & Chen, Z. Sum frequency generation vibrational spectroscopy studies on protein adsorption. *J. Phys. Chem. B* **106**, 11666–11672 (2002).

72. Lau, K. H. A., Bang, J., Hawker, C. J., Dong, H. K. & Knoll, W. Modulation of protein-surface interactions on nanopatterned polymer films. *Biomacromolecules* **10**, 1061–1066 (2009).

73. Daly, S. M., Przybycien, T. M. & Tilton, R. D. Coverage-dependent orientation of lysozyme adsorbed on silica. *Langmuir* **19**, 3848–3857 (2003).

74. Chen, S., Li, L., Zhao, C. & Zheng, J. Surface hydration: Principles and applications toward low-fouling/nonfouling biomaterials. *Polymer (Guildf).* **51**, 5283–5293 (2010).

75. Kane, R. S., Deschatelets, P. & Whitesides, G. M. Kosmotropes form the basis of protein-resistant surfaces. *Langmuir* **19**, 2388–2391 (2003).

76. Zamfir, M. *et al.* Controlled growth of protein resistant PHEMA brushes via S-RAFT polymerization. *J. Mater. Chem. B* **1**, 6027–6034 (2013).

77. Tidwell, C. D. *et al.* Glow discharge plasma deposition of tetraethylene glycol dimethyl ether for fouling-resistant biomaterial surfaces. *J. Biomed. Mater. Res.* **26**, 415–439 (2005).

78. Latour, R. Biomaterials: protein-surface interactions. *... Biomater. Biomed. Eng.* 1–15 (2005). doi:10.1081/E-EBBE-120041856

79. Wang, Y. X., Robertson, J. L., Spillman, W. B. & Claus, R. O. Effects of the chemical structure and the surface properties of polymeric biomaterials on their biocompatibility. *Pharm. Res.* **21**, 1362–1373 (2004).

80. Gautrot, J. E., Huck, W. T. S., Welch, M. & Ramstedt, M. Protein-resistant NTA-functionalized polymer brushes for selective and stable immobilization of histidine-tagged proteins. *ACS Appl. Mater. Interfaces* **2**, 193–202 (2010).

81. Nieba, L. *et al.* BIACORE Analysis of Histidine-Tagged Proteins Using a Chelating NTA Sensor Chip. *Anal. Biochem.* **252**, 217–228 (1997).

82. Wertz, C. F. & Santore, M. M. Fibrinogen adsorption on hydrophilic and hydrophobic

surfaces: Geometrical and energetic aspects of interfacial relaxations. *Langmuir* **18**, 706–715 (2002).

83. Vroman, L. Effect of Adsorbed Proteins on the Wettability of Hydrophilic and Hydrophobic Solids. *Nature* **196**, 1097–1098 (1962).

84. Wojciechowski, P., Ten Hove, P. & Brash, J. . Phenomenology and mechanism of the transient adsorption of fibrinogen from plasma (Vroman effect). *J. Colloid Interface Sci.* **111**, 455–465 (1986).

85. Casals, E., Pfaller, T., Duschl, A., Oostingh, G. J. & Puntes, V. Time evolution of nanoparticle protein corona. **4**, 3623–3632 (2010).

86. Deyme, M., Baszkin, A., Proust, J. E., Perez, E. & Boissonnade, M. M. Collagen at interfaces I. In situ collagen adsorption at solution/air and solution/polymer interfaces. *J. Biomed. Mater. Res.* **20**, 951–962 (1986).

87. Karlsson, M., Ekeroth, J., Elwing, H. & Carlsson, U. Reduction of irreversible protein adsorption on solid surfaces by protein engineering for increased stability. *J. Biol. Chem.* **280**, 25558–25564 (2005).

88. Benedek, K., Dong, S. & Karger, B. L. Kinetics of unfolding of proteins on hydrophobic surfaces in reversed-phase liquid chromatography. *J. Chromatogr. A* **317**, 227–243 (1984).

89. Kulik, E. A., Kalinin, I. D. & Sevastianov, V. I. The heterogeneity of protein/surface interactions and structural alterations of adsorbed albumin and immunoglobulin G. *Artif. Organs* **15**, 386–391 (1991).

90. McUmber, A. C., Randolph, T. W. & Schwartz, D. K. Electrostatic Interactions Influence Protein Adsorption (but Not Desorption) at the Silica-Aqueous Interface. *J. Phys. Chem. Lett.* **6**, 2583–2587 (2015).

91. Walder, R. & Schwartz, D. K. Single molecule observations of multiple protein populations at the oil-water interface. *Langmuir* **26**, 13364–13367 (2010).

92. Kastantin, M., Langdon, B. B., Chang, E. L. & Schwartz, D. K. Single-molecule resolution of interfacial fibrinogen behavior: effects of oligomer populations and surface chemistry. *J. Am. Chem. Soc.* **133**, 4975–83 (2011).

93. Kisley, L. *et al.* High ionic strength narrows the population of sites participating in protein ion-exchange adsorption: A single-molecule study. *J. Chromatogr. A* **1343**, 135–142 (2014).

94. Langdon, B. B., Kastantin, M. & Schwartz, D. K. Apparent activation energies associated with protein dynamics on hydrophobic and hydrophilic surfaces. *Biophys. J.* **102**, 2625–2633 (2012).

95. Mabry, J. N., Kastantin, M. & Schwartz, D. K. Capturing Conformation-Dependent Molecule-Surface Interactions When Surface Chemistry Is Heterogeneous. *ACS Nano* **9**,

7237–7247 (2015).

96. Langdon, B. B. *et al.* Single-Molecule Resolution of Protein Dynamics on Polymeric Membrane Surfaces: The Roles of Spatial and Population Heterogeneity. *ACS Appl. Mater. Interfaces* 150203144035006 (2015). doi:10.1021/am507730k

97. Langdon, B. B., Kastantin, M., Walder, R. & Schwartz, D. K. Interfacial protein-protein associations. *Biomacromolecules* **15**, 66–74 (2014).

98. Bhushan, B., Kwak, K. J., Gupta, S. & Lee, S. C. Nanoscale adhesion, friction and wear studies of biomolecules on silicon based surfaces. *J. R. Soc. Interface* **6**, 719–733 (2008).

99. Bromley, K. M. *et al.* Interfacial self-assembly of a bacterial hydrophobin. *Proc. Natl. Acad. Sci.* **112**, 5419–5424 (2015).

100. Kisley, L. & Landes, C. F. Molecular Approaches to Chromatography Using Single Molecule Spectroscopy. (2015).

101. Yang, Z., Galloway, J. A. & Yu, H. Protein interactions with poly(ethylene glycol) self-assembled monolayers on glass substrates: Diffusion and adsorption. *Langmuir* **15**, 8405–8411 (1999).

102. Tilton, R. D., Robertson, C. R. & Gast, A. P. Lateral diffusion of bovine serum albumin adsorbed at the solid-liquid interface. *J. Colloid Interface Sci.* **137**, 192–203 (1990).

103. Yu, C., Guan, J., Chen, K., Bae, S. C. & Granick, S. Single-molecule observation of long jumps in polymer adsorption. *ACS Nano* **7**, 9735–9742 (2013).

104. Bychuk, O. V. & O'Shaughnessy, B. Anomalous Diffusion at Liquid Surfaces. *Phys. Rev. Lett.* **74**, 1795–1798 (1995).

105. Monserud, J. H. & Schwartz, D. K. Interfacial Molecular Searching Using Forager Dynamics. *Phys. Rev. Lett.* **116**, 098303 (2016).

106. Skaug, M. J. *et al.* Single-molecule diffusion in a periodic potential at a solid-liquid interface. *Soft Matter* **10**, 753–9 (2014).

107. Wang, D., Chin, H.-Y., He, C., Stoykovich, M. P. & Schwartz, D. K. Polymer Surface Transport Is a Combination of in-Plane Diffusion and Desorption-Mediated Flights. *ACS Macro Lett.* **5**, 509–514 (2016).

108. Wang, D., He, C., Stoykovich, M. P. & Schwartz, D. K. Nanoscale Topography Influences Polymer Surface Diffusion. *ACS Nano* (2015).

109. Langmuir, I. & Schaefer, V. J. Activities of Urease and Pepsin Monolayers. *J. Am. Chem. Soc.* **60**, 1351–1360 (1938).

110. Lumry, R. & Eyring, H. Conformation changes of proteins. *J. Phys. Chem* **58**, 110–120 (1954).

111. Norde, W. & Zoungrana, T. Surface-induced changes in the structure and activity of

enzymes physically immobilized at solid/liquid interfaces. *Biotechnol. Appl. Biochem.* **28**, 133–143 (1998).

112. Das, P., Das, M., Chinnadayyala, S. R., Singha, I. M. & Goswami, P. Recent advances on developing 3rd generation enzyme electrode for biosensor applications. *Biosens. Bioelectron.* **79**, 386–397 (2016).

113. Garman, E. F. Developments in X-ray crystallographic structure determination of biological macromolecules. *Science (80-.).* **343**, 1102–1108 (2014).

114. Fischer, N. *et al.* Structure of the E. coli ribosome-EF-Tu complex at <3 Å resolution by Cs-corrected cryo-EM. *Nature* **520**, 567–570 (2015).

115. Cavalli, A., Salvatella, X., Dobson, C. M. & Vendruscolo, M. Protein structure determination from NMR chemical shifts. *Proc. Natl. Acad. Sci.* **104**, 9615–9620 (2007).

116. Huang, R., Carney, R. P., Ikuma, K., Stellacci, F. & Lau, B. L. T. Effects of surface compositional and structural heterogeneity on nanoparticle-protein interactions: Different protein configurations. *ACS Nano* **8**, 5402–5412 (2014).

117. Vertegel, A. a, Siegel, R. W. & Dordick, J. S. Silica nanoparticle size influences the structure and enzymatic activity of adsorbed lysozyme. *Langmuir* **20**, 6800–6807 (2004).

118. Buijs, J., Norde, W. & Lichtenbelt, J. W. T. Changes in the Secondary Structure of Adsorbed IgG and F (ab ′) 2 Studied by FTIR Spectroscopy. *Langmuir* **12**, 1605–1613 (1996).

119. Lensun, L., Smith, T. A. & Gee, M. L. Partial denaturation of silica-adsorbed bovine serum albumin determined by time-resolved evanescent wave-induced fluorescence spectroscopy. *Langmuir* **18**, 9924–9931 (2002).

120. Sota, H., Hasegawa, Y. & Iwakura, M. Detection of Conformational Changes in an Immobilized Protein Using Surface Plasmon Resonance. *Anal. Chem.* **70**, 2019–2024 (1998).

121. Wertz, C. F. & Santore, M. M. Effect of surface hydrophobicity on adsorption and relaxation kinetics of albumin and fibrinogen: Single-species and competitive behavior. *Langmuir* **17**, 3006–3016 (2001).

122. Sadana, A. Protein adsorption and inactivation on surfaces. Influence of heterogeneities. *Chem. Rev.* **92**, 1799–1818 (1992).

123. Mateo, C. *et al.* Immobilization of enzymes on heterofunctional epoxy supports. *Nat. Protoc.* **2**, 1022–1033 (2007).

124. Campbell, A. S. *et al.* Polymer-based protein engineering grown ferrocene-containing redox polymers improve current generation in an enzymatic biofuel cell. *Biosens. Bioelectron.* **86**, 446–453 (2016).

125. Ortiz, C. *et al.* Novozym 435: The 'perfect' lipase immobilized biocatalyst? *Catal. Sci.*

Technol. **9**, 2380–2420 (2019).

126. El Bialy, I., Jiskoot, W. & Reza Nejadnik, M. Formulation, Delivery and Stability of Bone Morphogenetic Proteins for Effective Bone Regeneration. *Pharm. Res.* **34**, 1152–1170 (2017).

127. Klibanov, A. M. Stabilization of Enzymes against Thermal Inactivation. *Adv. Appl. Microbiol.* **29**, 1–28 (1983).

128. Zamost, B. L., Nielsen, H. K. & Starnes, R. L. Thermostable enzymes for industrial applications. *Journal of Industrial Microbiology* **8**, 71–81 (1991).

129. Visser, R., Arrabal, P. M., Becerra, J., Rinas, U. & Cifuentes, M. The effect of an rhBMP-2 absorbable collagen sponge-targeted system on bone formation in vivo. *Biomaterials* **30**, 2032–2037 (2009).

130. Jesionowski, T., Zdarta, J. & Krajewska, B. Enzyme immobilization by adsorption: A review. *Adsorption* **20**, 801–821 (2014).

131. Barbosa, O. *et al.* Strategies for the one-step immobilization-purification of enzymes as industrial biocatalysts. *Biotechnol. Adv.* **33**, 435–456 (2015).

132. Palomo, J. M. *et al.* Purification, immobilization, and stabilization of a lipase from Bacillus thermocatenulatus by interfacial adsorption on hydrophobic supports. *Biotechnol. Prog.* **20**, 630–635 (2004).

133. Verger, R. Interfacial activation of lipases facts and artifacts. *Trends Biotechnol.* **15**, 32–38 (1997).

134. Rodrigues, R. C. & Fernandez-Lafuente, R. Lipase from Rhizomucor miehei as a biocatalyst in fats and oils modification. *J. Mol. Catal. B Enzym.* **66**, 15–32 (2010).

135. Brzozowski, A. M. *et al.* A model for interfacial activation in lipases from the structure of a fungal lipase-inhibitor complex. *Lett. to Nat.* **351**, 491–494 (1991).

136. Grochulski, P. *et al.* Insights into interfacial activation from an open structure of Candida rugosa lipase. *J. Biol. Chem.* **268**, 12843–12847 (1993).

137. Grochulski, P., Li, Y., Schrag, J. D. & Cygler, M. Two conformational states of Candida rugosa lipase. *Protein Sci.* **3**, 82–91 (1994).

138. Zhao, X., Qi, F., Yuan, C., Du, W. & Liu, D. Lipase-catalyzed process for biodiesel production: Enzyme immobilization, process simulation and optimization. *Renew. Sustain. Energy Rev.* **44**, 182–197 (2015).

139. Arruebo, M. Drug delivery from structured porous inorganic materials. *Wiley Interdiscip. Rev. Nanomedicine Nanobiotechnology* **4**, 16–30 (2012).

140. Slowing, I. I., Trewyn, B. G. & Lin, V. S. Y. Mesoporous silica nanoparticles for intracellular delivery of membrane-impermeable proteins. *J. Am. Chem. Soc.* **129**, 8845–8849 (2007).

141. Ravindra, R., Zhao, S., Gies, H. & Winter, R. Protein encapsulation in mesoporous silicate: The effects of confinement on protein stability, hydration, and volumetric properties. *J. Am. Chem. Soc.* **126**, 12224–12225 (2004).

142. Itoh, T. *et al.* Enhancement in thermal stability and resistance to denaturants of lipase encapsulated in mesoporous silica with alkyltrimethylammonium (CTAB). *Colloids Surfaces B Biointerfaces* **75**, 478–482 (2010).

143. Zhou, H. X. & Dill, K. A. Stabilization of proteins in confined spaces. *Biochemistry* **40**, 11289–11293 (2001).

144. Zhou, H.-X., Rivas, G. & Minton, A. P. Macromolecular crowding and confinemment: biochemical, biophysical, and potential physiological consequences. *Annu Rev Biophys* **37**, 375–397 (2010).

145. Eggers, D. K. & Valentine, J. S. Molecular confinement influences protein structure and enhances thermal protein stability. *Protein Sci.* **10**, 250–261 (2001).

146. Sheldon, R. A. Enzyme Immobilization: The Quest for Optimum Performance. *Adv. Synth. Catal.* **349**, 1289–1307 (2007).

147. Mateo, C., Abian, O., Fernandez-Lafuente, R. & Guisan, J. M. Reversible enzyme immobilization via a very strong and nondistorting ionic adsorption on support-polyethylenimine composites. *Biotechnol. Bioeng.* **68**, 98–105 (2000).

148. Avnir, D., Braun, S., Lev, O. & Ottolenghi, M. Enzymes and Other Proteins Entrapped in Sol-Gel Materials. *Chem. Mater.* **6**, 1605–1614 (1994).

149. Dave, B. C., Dunn, B., Valentine, J. S. & Zink, J. I. Sol-Gel Encapsulation Methods for Biosensors. *Anal. Chem.* **66**, 1120A-1127A (1994).

150. Reetz, M. T., Zonta, A. & Simpelkamp, J. Efficient immobilization of lipases by entrapment in hydrophobic sol-gel materials. *Biotechnol. Bioeng.* **49**, 527–534 (1996).

151. Zhao, Z. *et al.* Nanocaged enzymes with enhanced catalytic activity and increased stability against protease digestion. *Nat. Commun.* **7**, 10619 (2016).

152. Drevon, G. F. *et al.* High-activity enzyme-polyurethane coatings. *Biotechnol. Bioeng.* **79**, 785–794 (2002).

153. Liu, H. H. *et al.* Direct electrochemistry and electrocatalysis of heme-proteins entrapped in agarose hydrogel films. *Biosens. Bioelectron.* **20**, 294–304 (2004).

154. Hudson, S., Cooney, J. & Magner, E. Proteins in Mesoporous Silicates. *Angew. Chemie Int. Ed.* **47**, 8582–8594 (2008).

155. Hartono, S. B. *et al.* Functionalized mesoporous silica with very large pores for cellulase immobilization. *J. Phys. Chem. C* **114**, 8353–8362 (2010).

156. Jin, W. & Brennan, J. D. Properties and applications of proteins encapsulated within sol-gel derived materials. *Anal. Chim. Acta* **461**, 1–36 (2002).

157. Huang, J. *et al.* Immobilization of penicillin G acylase on poly [(glycidyl methacrylate)-co-(glycerol monomethacrylate)]-grafted magnetic microspheres. *Macromol. Biosci.* **8**, 508–515 (2008).

158. Koepsel, R. R. & Russell, A. J. Directed capture of enzymes and bacteria on bioplastic films. *Biomacromolecules* **4**, 850–855 (2003).

159. Rodrigues, R. C. & Fernandez-Lafuente, R. Lipase from Rhizomucor miehei as an industrial biocatalyst in chemical process. *Journal of Molecular Catalysis B: Enzymatic* **64**, 1–22 (2010).

160. Bornscheuer, U. T. Immobilizing enzymes: How to create more suitable biocatalysts. *Angew. Chemie - Int. Ed.* **42**, 3336–3337 (2003).

161. Garcia-Galan, C., Berenguer-Murcia, Á., Fernandez-Lafuente, R. & Rodrigues, R. C. Potential of different enzyme immobilization strategies to improve enzyme performance. *Adv. Synth. Catal.* **353**, 2885–2904 (2011).

162. Sheldon, R. A. Cross-linked enzyme aggregates (CLEA®s): stable and recyclable biocatalysts. *Biochem. Soc. Trans.* **35**, 1583–1587 (2007).

163. Mafra, A. C. O. *et al.* Diffusion effects of bovine serum albumin on cross-linked aggregates of catalase. *J. Mol. Catal. B Enzym.* **133**, 107–116 (2016).

164. Tardioli, P. W., Pedroche, J., Giordano, R. L. C., Fernández-Lafuente, R. & Guisán, J. M. Hydrolysis of proteins by immobilized-stabilized Alcalase-glyoxyl agarose. *Biotechnol. Prog.* **19**, 352–360 (2003).

165. Yilmaz, E., Can, K., Sezgin, M. & Yilmaz, M. Immobilization of Candida rugosa lipase on glass beads for enantioselective hydrolysis of racemic Naproxen methyl ester. *Bioresour. Technol.* **102**, 499–506 (2011).

166. Bayramoğlu, G., Kaçar, Y., Denizli, A. & Yakup Arica, M. Covalent immobilization of lipase onto hydrophobic group incorporated poly(2-hydroxyethyl methacrylate) based hydrophilic membrane matrix. *J. Food Eng.* **52**, 367–374 (2002).

167. Guncheva, M. & Zhiryakova, D. Catalytic properties and potential applications of Bacillus lipases. *J. Mol. Catal. B Enzym.* **68**, 1–21 (2011).

168. Palomo, J. M. *et al.* Modulation of the enantioselectivity of lipases via controlled immobilization and medium engineering: Hydrolytic resolution of mandelic acid esters. *Enzyme Microb. Technol.* **31**, 775–783 (2002).

169. Mateo, C. *et al.* Epoxy Sepabeads: A novel epoxy support for stabilization of industrial enzymes via very intense multipoint covalent attachment. *Biotechnol. Prog.* **18**, 629–634 (2002).

170. Zhang, C., Dong, X., Guo, Z. & Sun, Y. Remarkably enhanced activity and substrate affinity of lipase covalently bonded on zwitterionic polymer-grafted silica nanoparticles. *J. Colloid Interface Sci.* **519**, 145–153 (2018).

171. Zaak, H. *et al.* Effect of immobilization rate and enzyme crowding on enzyme stability under different conditions. The case of lipase from Thermomyces lanuginosus immobilized on octyl agarose beads. *Process Biochem.* **56**, 117–123 (2017).

172. Rodrigues, D. S., Mendes, A. A., Adriano, W. S., Gonçalves, L. R. B. & Giordano, R. L. C. Multipoint covalent immobilization of microbial lipase on chitosan and agarose activated by different methods. *J. Mol. Catal. B Enzym.* **51**, 100–109 (2008).

173. Jiang, H. & Xu, F. J. Biomolecule-functionalized polymer brushes. *Chem. Soc. Rev.* **42**, 3394–3426 (2013).

174. Fernández-Suárez, M. *et al.* Redirecting lipoic acid ligase for cell surface protein labeling with small-molecule probes. *Nat. Biotechnol.* **25**, 1483–7 (2007).

175. Puthenveetil, S., Liu, D. S., White, K. a, Thompson, S. & Ting, A. Y. Yeast display evolution of a kinetically efficient 13-amino acid substrate for lipoic acid ligase. *J. Am. Chem. Soc.* **131**, 16430–8 (2009).

176. Warden-Rothman, R., Caturegli, I., Popik, V. & Tsourkas, A. Sortase-tag expressed protein ligation: Combining protein purification and site-specific bioconjugation into a single step. *Anal. Chem.* **85**, 11090–11097 (2013).

177. Hohsaka, T. & Sisido, M. Incorporation of non-natural amino acids into proteins. *Curr. Opin. Biosci. Biotechnol.* **6**, 809–815 (2002).

178. Wang, K. *et al.* Optimized orthogonal translation of unnatural amino acids enables spontaneous protein double-labeling and FRET. *Nat. Chem.* **6**, 393–403 (2014).

179. Lang, K. & Chin, J. W. Cellular incorporation of unnatural amino acids and bioorthogonal labeling of proteins. *Chem. Rev.* **114**, 4764–806 (2014).

180. Mateo, C., Palomo, J. M., Fernandez-Lorente, G., Guisan, J. M. & Fernandez-Lafuente, R. Improvement of enzyme activity, stability and selectivity via immobilization techniques. *Enzyme Microb. Technol.* **40**, 1451–1463 (2007).

181. Janssen, K. P. F. *et al.* Single molecule methods for the study of catalysis: from enzymes to heterogeneous catalysts. *Chem. Soc. Rev.* **43**, 990–1006 (2014).

182. Rao, S. V., Anderson, K. W. & Bachas, L. G. Oriented immobilization of proteins. *Mikrochim. Acta* **128**, 127–143 (1998).

183. Lavis, L. D. & Raines, R. T. Bright Ideas for Chemical Biology. *ACS Chem. Biol.* **3**, (2007).

184. Zheng, Q. *et al.* Ultra-stable organic fluorophores for single-molecule research. *Chemical Society Reviews* **43**, 1044–1056 (2014).

185. Hu, Y. S., Zimmerley, M., Li, Y., Watters, R. & Cang, H. Single-molecule super-resolution light-sheet microscopy. *ChemPhysChem* **15**, 577–586 (2014).

186. Leung, B. O. & Chou, K. C. Review of super - Resolution fluorescence microscopy for

biology. *Appl. Spectrosc.* **65**, 967–980 (2011).

187. Axelrod, D. Total internal reflection fluorescence microscopy in cell biology. *Methods Enzymol.* **361**, 1–33 (2003).

188. Roy, R., Hohng, S. & Ha, T. A practical guide to single-molecule FRET. **5**, 507–516 (2008).

189. Piston, D. W. & Kremers, G.-J. Fluorescent protein FRET: the good, the bad and the ugly. *Trends Biochem. Sci.* **32**, 407–414 (2007).

190. Wallace, B. & Atzberger, P. J. Förster resonance energy transfer: Role of diffusion of fluorophore orientation and separation in observed shifts of FRET efficiency. *PLoS One* **12**, 1–17 (2017).

191. Lerner, E. *et al.* Toward dynamic structural biology: Two decades of single-molecule Förster resonance energy transfer. *Science (80-.).* **359**, eaan1133 (2018).

192. Rhoades, E., Cohen, M., Schuler, B. & Haran, G. Two-state folding observed in individual protein molecules. *J. Am. Chem. Soc.* **126**, 14686–14687 (2004).

193. Kipper, K. *et al.* Structure-guided approach to site-specific fluorophore labeling of the lac repressor LacI. *PLoS One* **13**, 1–17 (2018).

194. Miyake-Stoner, S. J. *et al.* Probing protein folding using site-specifically encoded unnatural amino acids as FRET donors with tryptophan. *Biochemistry* **48**, 5953–5962 (2009).

195. Jackson, J. C., Duffy, S. P., Hess, K. R. & Mehl, R. A. Improving nature's enzyme active site with genetically encoded unnatural amino acids. *J. Am. Chem. Soc.* **128**, 11124–11127 (2006).

196. Mehl, R. A. *et al.* Generation of a bacterium with a 21 amino acid genetic code. *J. Am. Chem. Soc.* **125**, 935–939 (2003).

197. Heinemann, I. U. *et al.* Enhanced phosphoserine insertion during Escherichia coli protein synthesis via partial UAG codon reassignment and release factor 1 deletion. *FEBS Lett.* **586**, 3716–3722 (2012).

Chapter 2 Surface-Mediated Protein Unfolding as a Search Process for Denaturing Sites

Previously published as: Weltz, J. S., Schwartz, D. K., & Kaar, J. L. (2015). Surface-Mediated Protein Unfolding as a Search Process for Denaturing Sites. *ACS Nano*, *10*, 730–738. https://doi.org/10.1021/acsnano.5b05787

2.1 Abstract

Surface-induced protein denaturation has important implications for the development of materials that are resistant and/or innocuous to biomolecules. Here, we studied the mechanism of lysozyme (T4L) unfolding on fused silica (FS) using single-molecule methods that provided direct insight into the cause of denaturation. Unfolding of T4L was monitored by Förster resonance energy transfer while simultaneously tracking the adsorption, diffusion, and desorption of individual molecules at the solid−solution interface. Results of high-throughput single-molecule analysis suggested that the unfolding of T4L on FS was mediated by surface diffusion and occurred on isolated nanoscale sites, which were relatively rare and distinct from the majority of the surface. These observations suggest that surface-mediated protein unfolding is a search process that is based on the exploration for denaturing sites by the protein. Ultimately, these findings have important implications for the design of protein-compatible surfaces.

Keywords: Single-molecule tracking, Förster resonance energy transfer, Total internal reflection fluorescent microscopy, Particle Adsorption, Protein-surface interactions, Interfacial protein diffusion, Surface heterogeneity

2.2 Introduction

Many biotechnology applications require that bio- molecules retain biological function in the presence of a surface or within a high surface area material.[1] However, proteins are often observed to adopt non-native conformations and reduced activity in these environments.[2] While

such observations are ubiquitous, the causal mechanisms, and certainly the specific dynamic mechanisms that lead to changes in conformation and activity, remain elusive and a matter of speculation.[3] This issue is of direct relevance, for example, to the efficacy and safety of protein-based vaccines, sensitivity and specificity of biosensors, catalytic efficiency of immobilized enzymes, and biological response of implantable scaffolds, which may all be significantly impacted by protein or enzyme unfolding upon contact with natural or synthetic materials.[4−6] From a practical perspective, there is a particular interest in identifying and understanding the salient physicochemical features of a surface that induce protein unfolding.

The mechanistic understanding of protein unfolding on surfaces has been limited by the availability of methods to resolve protein structure at the solution−solid interface. Traditional biophysical techniques (e.g., circular dichroism, fluorescence, FTIR, NMR, crystallography) are sometimes challenging to apply to interfacial systems (e.g., due to poor signal/background ratios)[7] and, when used, often lead to data that are difficult to interpret because they provide ensemble-averaged information about highly heterogeneous systems.[8] As a result, conventional approaches to monitor changes in protein structure on surfaces have often entailed the use of indirect measurements from which structure must be inferred using ad hoc parametric theoretical models. For example, structural changes are often inferred from measurements of protein adsorption, including the total amount of adsorbed protein, as well as surface elutability.[9,10] From these measurements, the average conformation of the adsorbed protein is reported to "relax" over minutes to hours, presumably due to the presence of irreversibly bound protein molecules.[11,12] In general, the (sometimes unarticulated) models and assumptions used to interpret these measurements ignore or minimize the potential for various types of spatial, dynamic, and/or population heterogeneity in the system being studied.[3,8] While this is understandable in the absence

of direct knowledge about the types of heterogeneity (and represents a way to minimize the number of undetermined parameters), this "top-down" approach has the unfortunate potential to be vastly over- simplified or even completely incorrect. For example, such approaches generally neglect the potential for dynamic exchange of unfolded as well as folded protein molecules between the surface and bulk solution, leading to a situation where the apparent relaxation may, in fact, be the result of differences in surface residence times of the folded and unfolded species.[13] Moreover, in cases where conventional ensemble-averaging methods for monitoring structure are used (i.e., to measure protein structure on the surface of nanoparticles),[14] the exact mechanism of unfolding cannot be determined from the average measurement of conformation alone. Additionally, traditional ensemble-averaging methods are completely insensitive to spatial heterogeneity, and, therefore, the analysis of these measurements generally assumes that the surface is homogeneous.[15,16]

We previously reported an approach to monitor protein unfolding in near-surface environments using single-molecule intramolecular Förster resonance energy transfer (smFRET), which involves high-throughput smFRET imaging of individual protein molecules using total internal reflection fluorescence microscopy (TIRFM).[17] A key aspect of this approach is site-specific attachment of donor and acceptor fluorophores, which allows one to directly relate fluctuations in smFRET efficiency to changes in protein structure. Notably, using this approach, changes in conformation can be directly correlated with other dynamic phenomena - such as adsorption, diffusion, and desorption - by tracking 10^4–10^6 molecules and performing large-scale multivariate computational analyses. Using related methods to study helical peptides, we showed that, in addition to making connections with adsorption and desorption, molecular conformation can also be correlated with spatial heterogeneity (e.g., of surface chemistry).[18]

Herein, smFRET−TIRFM was used to investigate the molecular mechanism of protein unfolding at the solution-solid interface using lysozyme as a model protein. Specifically, the unfolding of T4 bacteriophage lysozyme (T4L) on fused silica (FS) was studied with the goal of identifying relevant factors, such as spatial heterogeneity, that lead to unfolding on surfaces. Notably, silica is widely used as a material for the storage of therapeutic proteins,[19] chromatography resin for protein purification,[20] protein immobilization,[21] and implantable biomaterials,[22] underscoring the importance of understanding protein adsorption and denaturation on FS. To enable smFRET, T4L, a well-established model protein for studying protein-surface interactions,[23−25] was site-specifically labeled via engineering a unique cysteine and incorporation of the unnatural amino acid p-azidophenylalanine (AzF). Our results suggest a novel paradigm for the mechanism of protein unfolding on surfaces and provide new insights into strategies for preventing surface-induced protein unfolding.

2.3 Results

2.3.1 smFRET Signatures of Folded and Unfolded Adsorbed T4L

For smFRET analysis, the cysteine-free, pseudo-wild-type construct T4L C54T/C97A (T4L WT*) was used, which is similar in structure and stability to native T4L[26] and, like native T4L, lacks disulfide bonds. The T4L WT* construct was labeled with donor (dibenzocyclooctyne−Alexa Fluor 555) and acceptor (maleimide−Alexa Fluor 647) fluorophores via mutation of Tyr at position 139 and Asp at position 61 to AzF and Cys, respectively. To replace Tyr at position 139 with AzF, the amber stop codon (TAG) was introduced at this site in T4L WT*, which was subsequently coexpressed with orthogonal tyrosyl−tRNA/tRNA synthetase from Methanococcus jannaschii.[27] These residues were carefully chosen based on solvent exposure and lack of side

chain interactions with neighboring residues, which may perturb conformation and stability if disrupted. As anticipated, differences in the structure of T4L WT* D61C/Y139AzF (referred to as $T4L_{FRET}$) were minimal as determined by circular dichroism (Figure C-3). Moreover, as confirmation that the FRET signature of the labeled construct was sensitive to changes in conformation, changes in FRET were monitored in solution upon addition of denaturant (Figure C-4).

Labeled $T4L_{FRET}$ was diluted to a concentration suitable for single-molecule detection (1.0×10^{-10} M) and subsequently exposed to a clean FS surface in a flow cell at room temperature. Molecules at the solution-solid interface were illuminated using 532 nm light via total internal reflection and subsequently imaged in spatially aligned, but spectrally distinct, channels to capture donor and acceptor emission intensities. The conformation of labeled $T4L_{FRET}$ was parametrized using the relative fluorophore-to-fluorophore distance $d = \left(\frac{F_D}{F_A}\right)^{1/6}$, where F_D and F_A are the emission intensities of the donor and acceptor, respectively. Changes in d, which is approximately proportional to the absolute distance between labels, provide direct information about changes in the folding state (i.e., tertiary structure). Notably, only molecules that yielded fluorescence emission in both the donor and acceptor channel at some point during the trajectory were included in the FRET analysis. This criterion allowed us to exclude molecules lacking a functional acceptor label. While this filtering could potentially remove properly labeled protein molecules in sufficiently extended conformations, it is unlikely that molecules would adopt this conformation over the entire trajectory. As evidence of this, the denatured state of the protein was modeled using a two- and three-dimensional random walk model,[28] which predicted that the fraction of molecules with unmeasurable acceptor intensity (with greater than ~9 nm end-to-end distance between labeling sites) would be 13% and 2%, respectively. Furthermore, the elimination of properly

labeled molecules that lacked acceptor emission over the entire trajectory would not alter the analysis of unfolding.

To classify individual molecules based on folding state, the distribution of the time-average d value for all molecules upon adsorption was analyzed (Figure C-5). From this analysis, we found that surface-adsorbed molecules existed predominately in two distinct states, which were labeled as folded (low-d) or unfolded (high-d). This was evident by the presence of two primary populations that had midpoint values of d = 0.85 and d = 1.27, which corresponded to values of FRET efficiencies of 0.73 and 0.19, respectively. The low-d and high-d states could be attributed to folded and unfolded states based on solution FRET measurements of the native and denatured states of the protein. In solution, the d value for the native and denatured states closely matched the midpoint values for the low-d and high-d states, respectively, for surface-adsorbed molecules (Figure C-4 and Figure C-5). Based on this, a critical threshold for d ($\leq$1.05), corresponding to the minimum probability between the observed populations, was assigned as a cutoff for distinguishing folded from unfolded molecules as well as, importantly, identifying conformational transitions upon surface adsorption of protein molecules.

2.3.2 Connecting molecular trajectories and conformation

The dynamics of T4LFRET unfolding on FS was directly connected to the diffusive motion of individual protein molecules using molecular tracking. Specifically, surface trajectories for all individual molecules on FS were examined, and each trajectory step was assigned a conformation using the criteria described above to distinguish folded from unfolded states. This analysis indicated that the diffusive motion of $T4L_{FRET}$ on FS was qualitatively consistent with the intermittent diffusion observed previously for other molecules, including proteins, nucleic acids,

surfactants, and small-molecule dyes.[29] Specifically, T4L$_{FRET}$ trajectories exhibited periods of immobilization/confinement interspersed with flights (Figure 2-1A), some of which were quite long. Our previous work showed that these flights were consistent with the theoretically predicted desorption-mediated diffusion process, in which a molecule desorbs into the near-surface environment, executes a rapid three-dimensional random walk ("hop") in the aqueous phase, re-encounters the surface where it may readsorb, potentially repeating this process until readsorbing at the end of a "flight" (which may consist of multiple "hops"). This type of motion incorporates long surface displacements, allowing a molecule to efficiently "search" large surface regions to identify sparse target sites. This type of transport has been described mathematically using a continuous time random walk formalism, which incorporates "waiting- time" and "flight-length" distributions as generalizations of a simple random walk, which involves constant step sizes and constant waiting times.[29] The distribution of waiting times is representative of the energy barrier(s) for desorption, and the step-size distribution is mainly determined by the readsorption probability (i.e., the sticking coefficient).[29]

By segmenting the surface trajectories by folding state, the connection between this intermittent surface diffusion and conformation for T4L$_{FRET}$ on FS was directly observed. Interestingly, we found that, for >95% of unfolding events, the protein unfolded within the first frame after readsorption, coinciding with the start of a waiting time (Figure C-6). Since protein unfolding is rapid, it was expected that the molecules would unfold within the acquisition time of the camera; however, it is remarkable that unfolding almost universally correlated with readsorption after a flight. While the ensemble unfolding of lysozyme in solution has been shown to be much slower than the time scale measured here (i.e., on the order of minutes), these unfolding times are representative of the rate of change of the relative fraction of folded and unfolded

molecules, rather than the transition of an individual molecule from folded-to-unfolded state. The unfolding time scale for the lysozyme in our studies is consistent with that shown for other proteins in single-molecule unfolding experiments.[30]

One hypothetical explanation for this observation is that unfolding occurred randomly upon readsorption, regardless of the nature of the adsorption site. Although this cannot be ruled out a priori, it is difficult to reconcile this hypothesis with the observation that proteins almost never unfolded during waiting periods. An alternative hypothesis is that protein molecules unfolded upon encountering unique surface sites, distinct from the majority of the surface, which favored interactions with the denatured state of the protein. This hypothesis essentially posits the existence of anomalous denaturing sites and mathematically equates surface-mediated unfolding to a search process in which an adsorbed protein explores the surface to "find" a denaturing site (Figure 2-1B). In the case of FS, anomalous sites have been previously observed[8] and may be due to a variety of nanoscale chemical and/or physical factors, including heterogeneous surface density of silanol and siloxane groups,[31] varied orientations of surface moieties,[32] or topographical variations (i.e., roughness).[33] Given the inherent spatial heterogeneity associated with virtually all surfaces, we felt that the latter "denaturing site" hypothesis was intuitively reasonable and, therefore, tested this hypothesis via systematic passivation of the hypothetical denaturing sites.

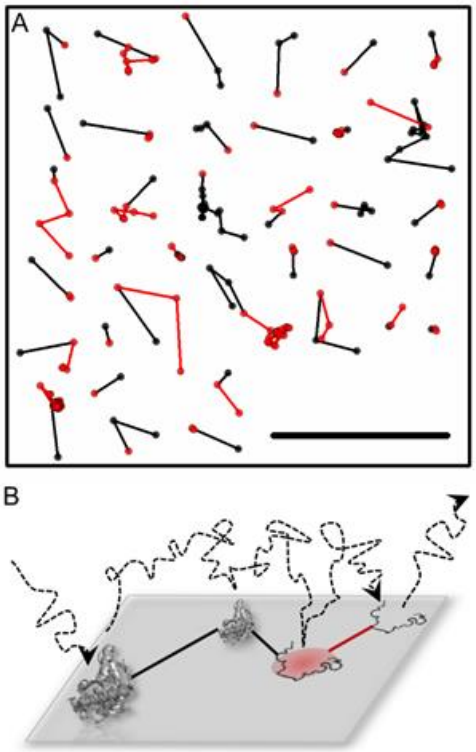

Figure 2-1**.** Molecular surface trajectories for $T4L_{FRET}$ on FS as a function of conformation. (A) Thirty-six randomly selected surface trajectories of labeled $T4L_{FRET}$ that undergo unfolding in the presence of $7.0x10^{-8}$ M unlabeled T4L WT*. Black and red segments of the trajectories represent folded and unfolded portions of each trajectory, respectively. The scale bar represents 5 μm. (B) Proposed model of surface-induced unfolding of $T4L_{FRET}$ on anomalous denaturing sites on FS.

2.3.3 Protein coverage influences surface heterogeneity

To test the hypothesis that spatial heterogeneity was a source of surface-mediated protein unfolding, the heterogeneity of FS was controlled by varying protein surface coverage. Specifically, we hypothesized that increased protein surface coverage would passivate putative denaturing sites, resulting in decreased surface heterogeneity. Systematically increasing concentrations of unlabeled T4L WT* were added to labeled $T4L_{FRET}$, the concentration of which was held fixed to facilitate single-molecule localization and tracking. Surface coverages were estimated from the ratio of labeled-to-unlabeled protein, the approximate footprint of T4L WT*, and the number of surface- adsorbed molecules. For estimating the footprint of T4L WT*, a "side-

on" orientation and rectangular projection with a width (3 nm) and length (4 nm) using the maximum dimensions measured in the crystal structure (PDB 1L63)[34] was used. The lowest concentration (1.0×10^{-10} M labeled $T4L_{FRET}$ with 0 M unlabeled T4L WT*) corresponded to a fractional surface coverage of 2×10^{-6}, while increased concentration conditions (5.0×10^{-10} M labeled $T4L_{FRET}$ with 1.0×10^{-9}, 5.0×10^{-9}, and 7.0×10^{-8} M unlabeled T4L WT*) corresponded to surface coverages of 5×10^{-6}, 2×10^{-5}, and 2×10^{-4}, respectively (Figure C-7). When low surface coverages were employed, sparse heterogeneous sites were passivated without significantly obstructing the bulk surface.

To characterize the degree of surface heterogeneity in the presence of unlabeled T4L WT*, the density of strong adsorption sites was determined by spatial mapping using the motion blur point accumulation for imaging in nanoscale topography (mbPAINT) method[35–37] as a function of protein concentration. As seen in Figure 2-2, the regions on the surface with anomalously high adsorption decreased in frequency with increasing amounts of unlabeled T4L WT* for the same number of randomly selected trajectories (~47,000) at each concentration condition. To quantify this observation, strong adsorption sites were defined as regions upon which more than one protein molecule adsorbed over the course of an experiment. Given the low surface coverage, the probability of observing more than one adsorption event in the same 100 nm region of the surface was extremely low if adsorption was random.[8] Using this definition, we found that the number of adsorption events per strong site decreased with increasing protein surface coverage (Figure C-8). Taken together, these results confirmed that, as protein surface coverage increased, even within the range of very low overall coverage, the apparent homogeneity of the surface also increased, which likely resulted in passivation of the denaturing sites. Notably, all data were collected within

the first 10 min of protein contacting the surface to minimize the effect of surface aging on protein adsorption behavior.

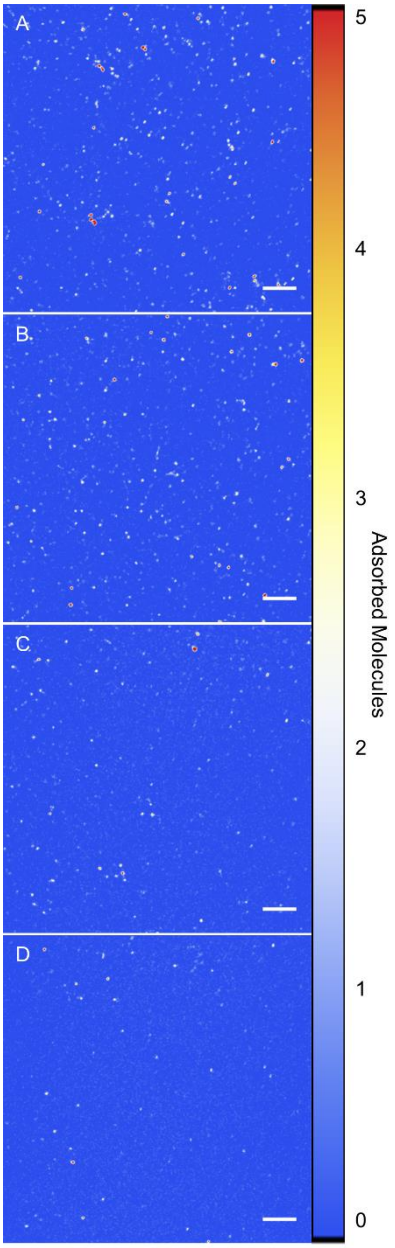

Figure 2-2. Super-resolution mapping of surface adsorption of labeled $T4L_{FRET}$ on FS using mbPAINT for total protein concentrations (fractional surface coverages) of (A) $1.0x10^{-10}$ M ($2x10^{-6}$), (B) $1.5x10^{-9}$ M ($5x10^{-6}$), (C) $5.5x10^{-9}$ M ($2x10^{-5}$), and (D) $7.1x10^{-8}$ M ($2x10^{-4}$). Scale bars represent 10 µm.

2.3.4 Surface heterogeneity influences surface-mediated diffusion and unfolding

The diffusion of $T4L_{FRET}$ on FS in the folded state was significantly altered by the passivation of strong adsorption sites. To quantify this change, we analyzed the distributions of waiting times and of step sizes as a function of increasing protein surface concentration/coverage (Figure 2-3). As protein surface coverage increased, the apparent number of long waiting times between hops decreased, suggesting that molecules underwent more frequent hopping motion. Specifically, the distribution of waiting times decayed more rapidly, as shown in Figure 2-3A. Over the range of measurable time intervals, each waiting-time distribution was well-described by a power-law function, consistent with the presence of a continuum of binding energies.[38] The power-law exponent could therefore be used as a convenient parameter to describe the decay of this distribution. As shown in Figure 2-3A, the waiting-time distribution was broader at low protein coverage, corresponding to a power-law exponent of −2.1, and narrowed systematically with increasing surface coverage to an exponent of −2.9. Similarly, the probability of long flights increased significantly with protein surface coverage, as indicted by the systematic broadening of the step-size distribution (see Figure 2-3B). This indicated a lower probability of readsorption, consistent with the blocking of strong adsorption sites (and decreased surface heterogeneity),[8] resulting in flights comprising more hops. While consistent with the blocking of strong adsorption sites, the apparent decrease in waiting times and increase in step size led to enhanced surface-mediated diffusion.

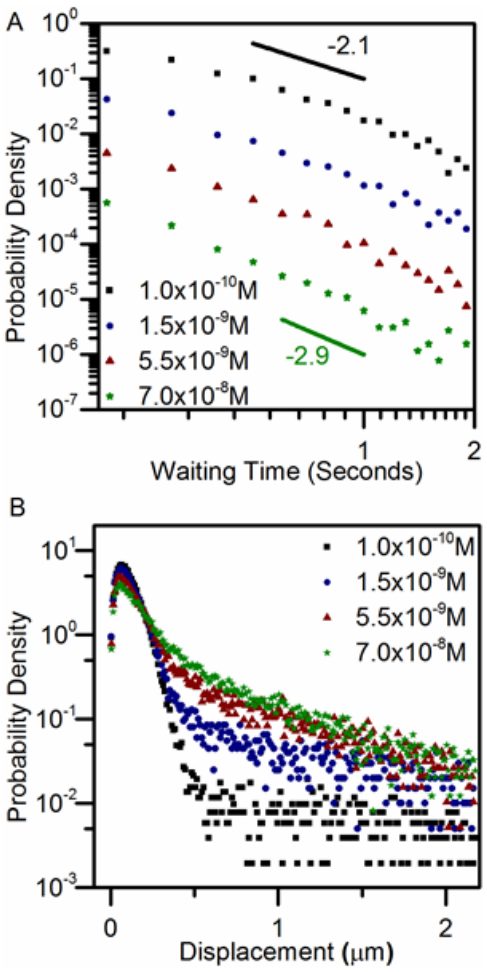

Figure 2-3. Distributions of (A) waiting times between hops and (B) step sizes between waiting times for folded T4L$_{FRET}$ on FS for total protein concentrations (fractional surface coverages) of $1.0x10^{-10}$ M ($2x10^{-6}$), $1.5x10^{-9}$ M ($5x10^{-6}$), $5.5x10^{-9}$ M ($2x10^{-5}$), and $7.1x10^{-8}$ M ($2x10^{-4}$). Waiting times are offset by a factor of 1/10, 1/100, and 1/1000 for the $1.5x10^{-9}$ M, $5.5x10^{-9}$ M, and $7.1x10^{-8}$ M concentrations, respectively. Slopes from power-law fits are shown in (a) for the highest and lowest concentrations.

Given the enhancement in surface-mediated diffusion with the blocking of strong surface sites, one would expect increasing protein surface coverage to facilitate increased exploration of the surface prior to protein unfolding. This was investigated by comparing surface trajectories of folded molecules before unfolding as a function of protein surface coverage. Figure 2-4 shows randomly selected trajectories for molecules that adsorbed in the folded state and were folded for 10 frames (1.0 s) before unfolding for the lowest and highest concentrations of added unlabeled

T4L WT*. As expected, the size of the surface trajectories increased qualitatively with increasing protein surface coverage, suggesting that denaturing sites were indeed passivated at the highest surface coverage.

Given the enhancement in surface-mediated diffusion with the blocking of strong surface sites, one would expect increasing protein surface coverage to facilitate increased exploration of the surface prior to protein unfolding. This was investigated by comparing surface trajectories of folded proteins before unfolding as a function of protein surface coverage. Figure 2-4 shows randomly selected trajectories for molecules that adsorbed in the folded state and were folded for 10 frames (1.0 s) before unfolding, for the lowest and highest concentrations of unlabeled T4L WT* that was added. As expected, the size of the surface trajectories increased qualitatively with increasing protein surface coverage, suggesting that denaturing sites were indeed passivated at the highest surface coverage.

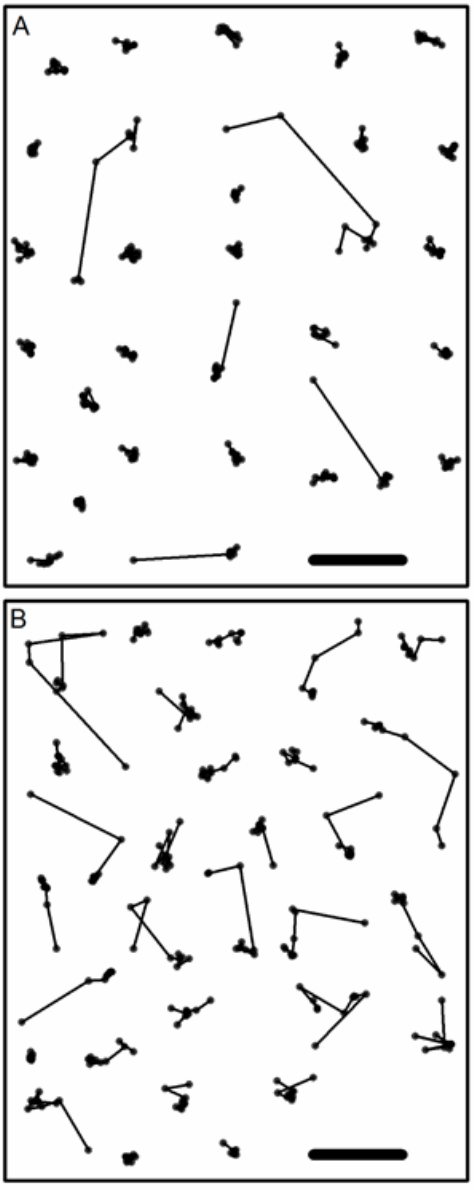

Figure 2-4. Molecular surface trajectories for $T4L_{FRET}$ on FS prior to unfolding for (A) $1.0x10^{-10}$ M and (B) $7.1x10^{-8}$ M total protein. Scale bars represent 500 nm.

The increase in trajectory size was further quantified by constructing distributions of the Euclidean distance between the initial adsorption location and the eventual unfolding site (Figure 2-5). Consistent with the qualitative trend indicated in Figure 2-4, these distributions broadened systematically and significantly with increasing protein surface coverage. Specifically, at the

lowest surface coverage, the distribution was characterized by a distinct peak centered at about 200 nm, suggesting that the vast majority of proteins unfolded within ~400 nm of their adsorption location. With increasing protein surface concentration, as denaturing sites were systematically blocked, the magnitude of this short-distance peak decreased dramatically, and the distributions developed broad tails extending out to at least 2 μm. These observations suggested a correlation between the blocking of strong adsorption sites and of denaturing sites, perhaps due to the fact that these sites actually coincided (Figure C-5). In any case, it is likely that the anomalous adsorption sites favor interaction with the unfolded protein. These findings ultimately support the hypothesis that protein unfolding is the result of a search process, which is mediated by intermittent diffusion and density of denaturing sites.

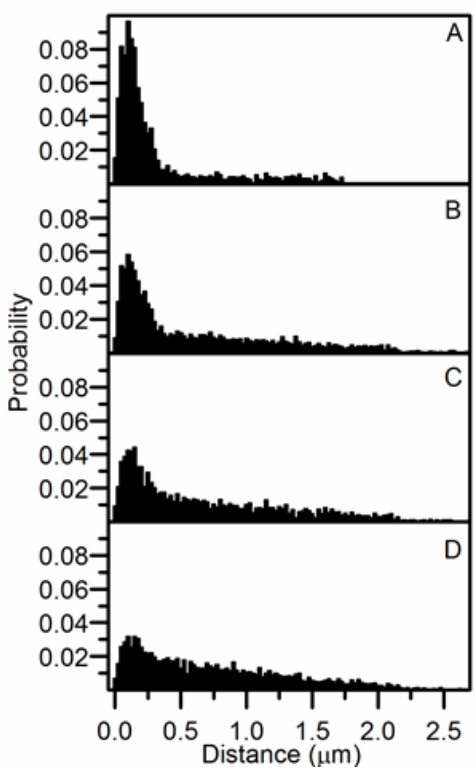

Figure 2-5. Distribution of the length of surface trajectories prior to unfolding for $T4L_{FRET}$ on FS for total protein concentrations (fractional surface coverages) of (A) $1.0x10^{-10}$ M ($2x10^{-6}$), (B) $1.5x10^{-9}$ M ($5x10^{-6}$), (C) $5.5x10^{-9}$ M ($2x10^{-5}$), and (D) $7.1x10^{-8}$ M ($2x10^{-4}$).

2.4 Discussion

Our results show that surface-induced protein denaturation and the dynamic interfacial behavior of proteins upon surface adsorption are tightly connected. This connection was elucidated using single-molecule methods, which uniquely permitted the direct observation of protein unfolding and interfacial dynamics at the solution-solid interface. Specifically, we found that protein unfolding on surfaces is analogous to a search process, which involves exploration of a surface that contains localized denaturing sites. Through exploring the surface via intermittent diffusion, the protein molecules probe local changes in chemical and physical properties of the surface that result from spatial heterogeneity, some of which stabilize the unfolded state of the protein. It should be noted that, in many areas, nanoscale heterogeneities are often intentionally introduced into materials, including, for example, the inclusion of nanoparticles and nanotubes within biomaterials for drug delivery, making the development of methods to characterize the interaction of proteins with such heterogeneities of critical importance.[39–41]

In the case of FS, it is difficult to determine the exact nature or size of the heterogeneities that favor interactions with the unfolded state of $T4L_{FRET}$ upon readsorption. However, it is widely acknowledged that even carefully prepared FS substrates, such as those used herein, exhibit inherent chemical and topographical heterogeneities.[8,31,32] Such surfaces, in particular, may consist of spatial differences in the density of hydrophobic siloxane and hydrophilic silanol moieties, resulting in regions with varying hydrophobicity. Based on this, we speculate that regions of increased siloxane density, and, therefore, increased local hydrophobicity, may represent sites that promote protein unfolding. These regions would presumably preferentially retain unfolded protein due to favorable hydrophobic interactions between the hydrophobic core of the protein and surface,

resulting in long residence times of the unfolded protein. Moreover, these sites would exhibit anomalously high adsorption due to weakly bound vicinal water, which reduces the barrier to adsorption.[42] Alternatively, some denaturing sites may result from nanoscale surface defects, including topographical features (e.g., edge sites arising from surface roughness) to which protein binding is entropically stabilized.[43] It is also plausible that the denaturing sites may have a different charge density then the rest of the surface. Additional negative charge at these sites could lead to enhanced adsorption of T4L, which is positively charged at the buffer conditions (pH 6.8) used in our experiments (the pI of T4L and FS is 9.8 and 3, respectively). Notably, it has previously been shown that FS surfaces may exhibit electrostatic heterogeneity, which supports this hypothesis.[44]

Although the precise nature of the denaturing sites cannot be determined using the methods applied here, our findings have important implications for reducing protein denaturation on surfaces. While most strategies for preventing surface protein unfolding have focused on altering the overall hydrophobicity of a surface via a uniform coating process,[45,46] the results presented here highlight the importance of reducing spatial heterogeneity. One approach to eliminate surface heterogeneity, and thus the frequency of denaturing sites on the surface, is to use blocking agents (e.g., protein or surfactant) as was used via the addition of unlabeled T4L WT*. This approach is akin to the use of bovine serum albumin in enzyme-linked immunosorbent assays to prevent nonspecific binding of proteins or biomolecules to unoccupied surface sites. While increasing homogeneity with increasing surface coverage (i.e., blocking) has been demonstrated in numerous applications, it is possible that, in actuality, increasing surface coverage decreases surface homogeneity. However, our results explicitly show the opposite is true for our experimental system, and that the surface becomes more homogeneous as a function of protein surface coverage.

Since the addition of soluble factors is not always appropriate, it may be desirable to chemically passivate strong sites with covalently bound blocking agents that display protein-resistant moieties such as polyethylene glycol or other hydrophilic polymers (e.g., zwitterionic polymers such as polysulfobetaine).[47] Additionally, the effects of residual surface heterogeneity on protein unfolding can be minimized by reducing/confining protein surface mobility. Interfacial protein mobility may be confined or reduced by the presence of nanoscale features that block protein hopping, which, in turn, limit the exploration of the surface by the protein. As a demonstration of this approach, Wang and co-workers recently showed that surface patterning with nanoscale pillars resulted in reduced polymer diffusion on surfaces.[43] Notably, the extent by which molecular diffusion was reduced was dependent on pillar height, which directly impacted the waiting-time and step-size distribution of the polymer.

In conclusion, we present a new model for protein denaturation at the solid-liquid interface where folded protein molecules undergo a search process, resulting in unfolding on distinct surface sites. These findings were enabled by the use of novel single-molecule methods that combined FRET and high-throughput particle tracking, permitting the simultaneous observation of diffusive behavior and changes in protein conformation. Importantly, these heterogeneities would be invisible by the use of conventional ensemble-averaging methods for investigating the structure of proteins at interfaces. Furthermore, because interfacial dynamics and conformation cannot be directly observed using ensemble methods, the role of diffusion on unfolding would be inaccessible using such methods. Ultimately, our results address a fundamental question about the mechanism of protein unfolding on surfaces and also suggest a somewhat different approach to rationally tailor surfaces for improved biocompatibility. Finally, although our findings underscore the role of surface heterogeneity in protein denaturation, these results do not rule out the

contribution of other mechanisms of protein unfolding on surfaces. Additional studies that investigate the role of other sources of heterogeneity such as interfacial protein aggregation are critical to fully elucidate the sources of surface-induced protein unfolding.

2.5 Materials and Methods

2.5.1 Cloning, Expression, and Purification of T4L

Plasmid DNA encoding the gene for T4L WT* was obtained from Addgene (plasmid number 18111). Residues 139 and 61 were mutated to the TAG stop codon and cysteine, respectively, using the Quikchange mutagenesis kit (Agilent). The primers used for the D61C and Y138AzF mutations, which were confirmed by sequence, were 5′-GGCGTAAT-ACTAATGGTGTAATTACAAAATGTGAAGCTGAAAAACT- CTTTAATCAAG-3′ and 5′-CTTAGCTAAAAGTAGATG- GTAGAATCAAACAACTAATCGCGC-3′, respectively.

T4L WT* and $T4L_{FRET}$ were cotransformed in BL21 (DE3) Escherichia coli with the pDule2 pCNF RS plasmid (courtesy of Ryan Mehl, Oregon State). Transformed cells were plated on agar containing spectinomycin (50 μg/mL) and ampicillin (50 μg/mL) and subsequently expressed and purified as described previously.[48] For purification, an additional size-exclusion step was included using a Bio- Rad SEC 70 10 × 300 mm column (Figure C-1). Exposure of the protein to ultraviolet light was minimized during purification to prevent photodegradation of the azide group in the $T4L_{FRET}$ double mutant.

2.5.2 Site-specific Dual Labeling of $T4L_{FRET}$

Following purification, $T4L_{FRET}$ was dialyzed against 50 mM sodium phosphate buffer (pH 6.80) at 4 °C and concentrated by centrifugation to 2 mg/mL for labeling. To the concentrated

protein was added dibenzocyclooctyne-activated Alexa Fluor 555 (Life Technologies) at a 5:1 molar ratio of fluorophore-to-protein for 18 h in the dark. Next, tris(2-carboxyethyl)- phosphine hydrochloride (TCEP, Fischer Scientific) was added to reduce the lone cysteine prior to labeling at a 5:1 molar ratio of TCEP-to-protein for 30 min at 4 °C. Finally, maleimide-activated Alexa Fluor 647 (Life Technologies) was added in a 5:1 molar ratio of fluorophore-to-protein for an additional 18 h conjugation in the dark at 4 °C.

After both reactions, separation of the dual-labeled protein from residual free dye in solution was performed using size-exclusion chromatography using a Bio-Rad SEC 70 10 × 300 mm column (Figure C-2). Labeling efficiency was determined using the molar extinction coefficient for each dye (155 000 M^{-1} cm^{-1} for Alexa Fluor 555 at 565 nm and 270 000 M^{-1} cm^{-1} for Alexa Fluor 647 at 668 nm)[49] and the estimated adsorption coefficient of T4L WT* at 280 nm (25 440 M^{-1} cm^{-1}).[50] Correcting for absorbance of the dyes at 280 nm, we found the labeling efficiency to be between 65% and 80% for each dye.

2.5.3 Surface Preparation

Fused silica wafers were cleaned with a 2% micro-90 solution (International Product Corp.) and thoroughly rinsed with ultrapure 18 MΩ·cm water. The wafers were then submersed in warm piranha solution (70% hydrochloric acid, 30% hydrogen peroxide solution) for 1 h. Following piranha treatment, the wafers were subsequently rinsed with ultrapure water, dried under ultrapure nitrogen, and treated with UV-ozone also for 1 h. Before use, the wafers were again rinsed in ultrapure water and dried under nitrogen and characterized by contact angle goniometry to ensure complete wetting (contact angle ∼0°).

2.5.4 Single-molecule TIRF Imaging

Details of the experimental setup have been described previously.[51] Briefly, samples were imaged on a custom prism TIRF microscope using a Nikon Eclipse TE-2000 platform, a 60× water immersion objective, and 1.5× post-objective magnification. Total internal reflection excitation was achieved using a 532 nm 50 mW diode-pumped solid-state laser (Samba, Cobolt) with a custom prism illumination system. Fluorescence emission from donor and acceptor fluorophores was separated using an Optosplit III beam splitter (Cairn Research) containing a dichroic mirror with a separation wavelength of 610 nm (model T610LPXR, Chroma). Donor and acceptor channels were filtered with FF01-585/40-25 band-pass filter (Semrock) centered at 585 nm with a 90% transmission width of 40 nm and a LP02-647RU-25 band-pass filter (Semrock), respectively. The channels were projected onto different regions of a Cascade-II: 512 EMCCD camera (Photometrics) maintained at −80 °C. Images were collected with an acquisition time of 100 ms (i.e., a frame rate of 10 s^{-1}).

2.5.5 Image Processing and Molecule Tracking

The methodology for object identification, tracking, and FRET quantification has been described in detail elsewhere.[52] Briefly, diffraction-limited objects in the donor channel were identified by convolution with a disk matrix and thresholding. Diffraction-limited spots were localized according to their centroid and their intensity quantified after subtracting the local background intensity. The same object identification procedure was used for the acceptor channel, and objects that coincided spatially in both channels for a given frame were used to quantify FRET. To measure diffusive behavior, diffraction-limited objects were connected as a molecular trajectory if they were localized in consecutive frames within a threshold distance of 2.2 μm. To

minimize erroneous tracking of different molecules into the same molecular trajectory (false connections), the surface coverage of labeled molecules was limited to fewer than 100 objects per frame by choosing an appropriate bulk concentration of labeled protein. Objects that were already adsorbed in the first frame or remained adsorbed after the final frame were excluded from analysis to ensure the accurate calculation of waiting times. Additionally, objects that did not have measurable intensity in either the donor or acceptor channel, which likely represented mislabeled protein molecules or contaminants, were excluded from analysis.

The Alexa Fluor 555 and 647 dyes were spectrally well separated, and given the properties of the optics used, we would not expect any measurable fluorescence from donor in the acceptor channel and vice versa. Indeed, previous work utilizing the same optical path, filters, dichroic, fluorophores, and similar excitation intensity demonstrated no crosstalk between channels.[17] Photobleaching, the irreversible destruction of a fluorophore, can cause significant changes in the apparent FRET. However, in this work, observations were ignored if they did not exhibit measurable intensity in either channel during the molecular trajectory. Therefore, photobleaching of either donor or acceptor fluorophore was not appreciably responsible for the apparent protein unfolding behavior. Previous smFRET experiments utilizing this donor and acceptor fluorophore also demonstrated that photoblinking did not cause significant changes in apparent FRET.[17]

2.5.6 Surface Adsorption Mapping (mbPAINT)

To characterize surface heterogeneity, adsorption events were spatially mapped on the surface. These maps identified anomalous sites with adsorption rates that would not be expected given random adsorption to a homogeneous surface, which can be described by Poisson statistics.[8] Briefly, these surface adsorption maps were generated by binning adsorption events onto a

pseudoimage with 15 nm pixels. A Gaussian blur was applied to this pseudoimage with a radius of 100 nm to account for positional uncertainty. Anomalous sites were identified as simply connected regions after thresholding the image with a threshold of one adsorption event per pixel. A distribution of the number of adsorption events per identified site was fit to a three-component Poisson mixture model (Figure C-8).

2.5.7 Step Size and Waiting Time Distributions

The step-size distribution for folded proteins was constructed by calculating the two-dimensional Euclidean distance between the same object in sequential frames for steps where the molecule appeared in the folded state. Steps were ignored if the molecule appeared in the unfolded state in either frame of a step. Waiting-time distributions were calculated by determining the time intervals during which a folded molecule appeared within a distance threshold of 0.2 μm in consecutive frames. If a molecule moved more than this distance between frames, the motion was considered significant, ending the waiting period. The trends observed in the waiting-time distribution as a function of T4L concentration was insensitive to changes in this threshold distance.

2.6 References

(1) Hlady, V.; Buijs, J. Protein Adsorption on Solid Surfaces. Curr. Opin. Biotechnol. 1996, 7,72−77.

(2) Gray, J. J. The Interaction of Proteins with Solid Surfaces. Curr. Opin. Struct. Biol. 2004, 14, 110−115.

(3) Kastantin, M.; Langdon, B. B.; Schwartz, D. K. A Bottom-Up Approach to Understanding Protein Layer Formation at Solid-Liquid Interfaces. Adv. Colloid Interface Sci. 2014, 207, 240−252.

(4) Rabe, M.; Verdes, D.; Seeger, S. Understanding Protein Adsorption Phenomena at Solid Surfaces. Adv. Colloid Interface Sci. 2011, 162,87−106.

(5) Haynes, C. A.; Norde, W. Globular Proteins at Solid/Liquid Interfaces. Colloids Surf., B 1994, 2, 517−566. (6) Ramsden, J. Puzzles and Paradoxes in Protein Adsorption. Chem. Soc. Rev. 1995, 24,73−78.

(7) Nakanishi, K.; Sakiyama, T.; Imamura, K. On the Adsorption of Proteins on Solid Surfaces, a Common but Very Complicated Phenomenon. J. Biosci. Bioeng. 2001, 91, 233−244.

(8) Langdon, B. B.; Mirhossaini, R. B.; Mabry, J. N.; Sriram, I.; Lajmi, A.; Zhang, Y.; Rojas, O. J.; Schwartz, D. K. Single-Molecule Resolution of Protein Dynamics on Polymeric Membrane Surfaces: The Roles of Spatial and Population Heterogeneity. ACS Appl. Mater. Interfaces 2015, 7, 3607−3617.

(9) Karlsson, M.; Ekeroth, J.; Elwing, H.; Carlsson, U. Reduction of Irreversible Protein Adsorption on Solid Surfaces by Protein Engineering for Increased Stability. J. Biol. Chem. 2005, 280, 25558− 25564.

(10) Singla, B.; Krisdhasima, V.; McGuire, J. Adsorption Kinetics of Wild Type and Two Synthetic Stability Mutants of T4 Phage Lysozyme at Silanized Silica Surfaces. J. Colloid Interface Sci. 1996, 182, 292−296.

(11) Wertz, C. F.; Santore, M. M. Fibrinogen Adsorption on Hydrophilic and Hydrophobic Surfaces: Geometrical and Energetic Aspects of Interfacial Relaxations. Langmuir 2002, 18, 706−715.

(12) Wertz, C. F.; Santore, M. M. Effect of Surface Hydrophobicity on Adsorption and Relaxation Kinetics of Albumin and Fibrinogen: Single-Species and Competitive Behavior. Langmuir 2001, 17, 3006− 3016.

(13) Kastantin, M.; Langdon, B. B.; Chang, E. L.; Schwartz, D. K. Single-Molecule Resolution of Interfacial Fibrinogen Behavior: Effects of Oligomer Populations and Surface Chemistry. J. Am. Chem. Soc. 2011, 133, 4975−4983.

(14) Vertegel, A. A.; Siegel, R. W.; Dordick, J. S. Silica Nanoparticle Size Influences the Structure and Enzymatic Activity of Adsorbed Lysozyme. Langmuir 2004, 20, 6800−6807.

(15) Sethuraman, A.; Belfort, G. Protein Structural Perturbation and Aggregation on Homogeneous Surfaces. Biophys. J. 2005, 88, 1322− 1333.

(16) Felsovalyi, F.; Patel, T.; Mangiagalli, P.; Kumar, S. K.; Banta, S. Effect of Thermal Stability on Protein Adsorption to Silica Using Homologous Aldo-Keto Reductases. Protein Sci. 2012, 21, 1113−1125.

(17) McLoughlin, S. Y.; Kastantin, M.; Schwartz, D. K.; Kaar, J. L. Single-Molecule Resolution of Protein Structure and Interfacial Dynamics on Biomaterial Surfaces. Proc. Natl. Acad. Sci. U. S. A. 2013, 110, 19396−19401.

(18) Mabry, J. N.; Kastantin, M.; Schwartz, D. K. Capturing Conformation-Dependent Molecule−Surface Interactions When Surface Chemistry Is Heterogeneous. ACS Nano 2015, 9, 7237−7247.

(19) Buijs, J.; Norde, W.; Lichtenbelt, J. W. T. Changes in the Secondary Structure of Adsorbed IgG and F (ab') 2 Studied by FTIR Spectroscopy. Langmuir 1996, 12, 1605−1613.

(20) Towns, J. K.; Regnier, F. E. Capillary Electrophoretic Separations of Proteins Using Nonionic Surfactant Coatings. Anal. Chem. 1991, 63, 1126−1132.

(21) Luckarift, H. R.; Spain, J. C.; Naik, R. R.; Stone, M. O. Enzyme Immobilization in a Biomimetic Silica Support. Nat. Biotechnol. 2004, 22, 211−213.

(22) Arcos, D.; Vallet-Regí, M. Sol−Gel Silica-Based Biomaterials and Bone Tissue Regeneration. Acta Biomater. 2010, 6, 2874−2888.

(23) Lee, W.-K.; McGuire, J.; Bothwell, M. K. Competitive Adsorption of Bacteriophage T4 Lysozyme Stability Variants at Hydrophilic Glass Surfaces. J. Colloid Interface Sci. 2004, 269, 251− 254.

(24) Jacobsen, K.; Hubbell, W. L.; Ernst, O. P.; Risse, T. Details of the Partial Unfolding of T4 Lysozyme on Quartz Using Site-Directed Spin Labeling. Angew. Chem., Int. Ed. 2006, 45, 3874−3877.

(25) Billsten, P.; Wahlgren, M.; Arnebrant, T.; McGuire, J.; Elwing, H. Structural Changes of T4 Lysozyme Upon Adsorption to Silica Nanoparticles Measured by Circular Dichroism. J. Colloid Interface Sci. 1995, 175,77−82.

(26) Matsumura, M.; Becktel, W. J.; Levitt, M.; Matthews, B. W. Stabilization of Phage T4 Lysozyme by Engineered Disulfide Bonds. Proc. Natl. Acad. Sci. U. S. A. 1989, 86, 6562−6566.

(27) Chin, J. W.; Santoro, S. W.; Martin, A. B.; King, D. S.; Wang, L.; Schultz, P. G. Addition of p-Azido-L-Phenylalanine to the Genetic Code of Escherichia coli. J. Am. Chem. Soc. 2002, 124, 9026−9027.

(28) Des Cloizeaux, J. Lagrangian theory for a self-avoiding random chain. Phys. Rev. A: At., Mol., Opt. Phys. 1974, 10, 1665−1669.

(29) Skaug, M. J.; Mabry, J.; Schwartz, D. K. Intermittent Molecular Hopping at the Solid-Liquid Interface. Phys. Rev. Lett. 2013, 110, 256101.

(30) Chung, H. S.; Louis, J. M.; Eaton, W. A. Experimental determination of upper bound for transition path times in protein folding from single-molecule photon-by-photon trajectories. Proc. Natl. Acad. Sci. U. S. A. 2009, 106, 11837−11844.

(31) Vigil, G.; Xu, Z.; Steinberg, S.; Israelachvili, J. Interactions of Silica Surfaces. J. Colloid Interface Sci. 1994, 165, 367−385.

(32) Bolis, V.; Cavenago, A.; Fubini, B. Surface Heterogeneity on Hydrophilic and Hydrophobic Silicas: Water and Alcohols as Probes for H-Bonding and Dispersion Forces. Langmuir 1997, 13, 895−902.

(33) Rädlein, E.; Frischat, G. H. Atomic Force Microscopy as a Tool to Correlate Nanostructure to Properties of Glasses. J. Non-Cryst. Solids 1997, 222,69−82.

(34) Nicholson, H.; Anderson, D.; Dao Pin, S.; Matthews, B. Analysis of the Interaction Between Charged Side Chains and the Alpha-Helix Dipole Using Designed Thermostable Mutants of Phage T4 Lysozyme. Biochemistry 1991, 30, 9816−9828.

(35) Chen, J.; Bremauntz, A.; Kisley, L.; Shuang, B.; Landes, C. F. Super-Resolution mbPAINT for Optical Localization of Single- Stranded DNA. ACS Appl. Mater. Interfaces 2013, 5, 9338−9343.

(36) Kisley, L.; Chen, J.; Mansur, A. P.; Dominguez-Medina, S.; Kulla, E.; Kang, M. K.; Shuang, B.; Kourentzi, K.; Poongavanam, M.- V.; Dhamane, S. High Ionic Strength Narrows the Population of Sites Participating in Protein Ion-Exchange Adsorption: A Single-Molecule Study. J. Chromatogr. A 2014, 1343, 135−142.

(37) Mabry, J. N.; Skaug, M. J.; Schwartz, D. K. Single-Molecule Insights into Retention at a Reversed-Phase Chromatographic Interface. Anal. Chem. 2014, 86, 9451−9458.

(38) Skaug, M. J.; Lacasta, A. M.; Ramirez-Piscina, L.; Sancho, J. M.; Lindenberg, K.; Schwartz, D. K. Single-Molecule Diffusion in a Periodic Potential at a Solid−Liquid Interface. Soft Matter 2014, 10, 753−759.

(39) Ahadian, S.; Ramón-Azcón, J.; Estili, M.; Liang, X.; Ostrovidov, S.; Shiku, H.; Ramalingam, M.; Nakajima, K.; Sakka, Y.; Bae, H. Hybrid hydrogels containing vertically aligned carbon nanotubes with anisotropic electrical conductivity for muscle myofiber fabrication. Sci. Rep. 2014, 4, 4271.

(40) Gaharwar, A. K.; Patel, A.; Dolatshahi-Pirouz, A.; Zhang, H.; Rangarajan, K.; Iviglia,G.; Shin,S.-R.;Hussain,M.A.; Khademhosseini, A. Elastomeric nanocomposite scaffolds made from poly (glycerol sebacate) chemically crosslinked with carbon nanotubes. Biomater. Sci. 2015, 3,46−58.

(41) Hosseinkhani, H.; Hosseinkhani, M.; Gabrielson, N. P.; Pack, D. W.; Khademhosseini, A.; Kobayashi, H. DNA nanoparticles encapsu- lated in 3D tissue-engineered scaffolds enhance osteogenic differ- entiation of mesenchymal stem cells. J. Biomed. Mater. Res., Part A 2008, 85,47−60.

(42) Honciuc, A.; Baptiste, D. J.; Campbell, I. P.; Schwartz, D. K. Solvent Dependence of the Activation Energy of Attachment Determined by Single Molecule Observations of Surfactant Adsorption. Langmuir 2009, 25, 7389−7392.

(43) Wang, D.; He, C.; Stoykovich, M. P.; Schwartz, D. K. Nanoscale Topography Influences Polymer Surface Diffusion. ACS Nano 2015, 9, 1656−1664.

(44) Taboada-Serrano, P.; Vithayaveroj, V.; Yiacoumi, S.; Tsouris, C. Surface Charge Heterogeneities Measured by Atomic Force Microscopy. Environ. Sci. Technol. 2005, 39, 6352−6360.

(45) Ostuni, E.; Grzybowski, B. A.; Mrksich, M.; Roberts, C. S.; Whitesides, G. M. Adsorption of Proteins to Hydrophobic Sites on Mixed Self-Assembled Monolayers. Langmuir 2003, 19, 1861−1872.

(46) Chen, X.; Ferrigno, R.; Yang, J.; Whitesides, G. M. Redox Properties of Cytochrome C Adsorbed on Self-Assembled Mono- layers: A Probe for Protein Conformation and Orientation. Langmuir 2002, 18, 7009−7015.

(47) Zhang, Z.; Finlay, J. A.; Wang, L.; Gao, Y.; Callow, J. A.; Callow, M. E.; Jiang, S. Polysulfobetaine-Grafted Surfaces as Environmentally Benign Ultralow Fouling Marine Coatings. Langmuir 2009, 25, 13516−13521.

(48) Tsugita, A.; Inouye, M.; Terzaghi, E.; Streisinger, G. Purification of Bacteriophage T4 Lysozyme. J. Biol. Chem. 1968, 243, 391−397.

(49) Johnson, I. The Molecular Probes Handbook: A Guide to Fluorescent Probes and Labeling Technologies,11th ed.; Life Technologies Corporation, 2010.

(50) Gill, S. C.; Von Hippel, P. H. Calculation of Protein Extinction Coefficients from Amino Acid Sequence Data. Anal. Biochem. 1989, 182, 319−326.

(51) Kastantin, M.; Keller, T. F.; Jandt, K. D.; Schwartz, D. K. Single-Molecule Tracking of Fibrinogen Dynamics on Nanostructured Poly(ethylene) Films. Adv. Funct. Mater. 2012, 22, 2617−2623.

(52) Walder, R.; Kastantin, M.; Schwartz, D. K. High Throughput Single Molecule Tracking for Analysis of Rare Populations and Events. Analyst 2012, 137, 2987−2996.

Chapter 3 Dramatic Increase in Catalytic Performance of Immobilized Lipases by their Stabilization on Polymer Brush Supports

Previously published as: Weltz, J. S., Kienle, D. F., Schwartz, D. K. & Kaar, J. L. Dramatic Increase in Catalytic Performance of Immobilized Lipases by Their Stabilization on Polymer Brush Supports. *ACS Catal.* 4992–5001 (2019). doi:10.1021/acscatal.9b01176

3.1 Abstract

Despite their widespread use in biocatalysis, the marginal stability of lipases can significantly limit their catalytic performance in industrial biotransformations. Here, we demonstrate that this limitation can be overcome by immobilization on poly(sulfobetaine methacrylate) (PSBMA) polymer brushes. Specifically, the immobilization of *Bacillus subtilis* lipase A (lipA) on PSBMA brushes resulted in a 100-fold enhancement in turnover frequency relative to ambient conditions at the temperature optimum of the immobilized enzyme, which was also improved by immobilization. This significant enhancement in catalytic performance was due to the structural stabilization of lipA as well as changes in lipA conformational dynamics as measured using single-molecule Förster Resonance Energy Transfer. Interestingly, the enhancement in catalytic performance of lipases depended strongly on the chemistry of the brush. These findings demonstrate that tuning the brush chemistry can lead to marked improvements in the catalytic efficiency of immobilized lipases, which may have major ramifications in industrial biocatalysis.

Keywords: Biocatalysis, Enzyme immobilization, Enzyme stability, Lipase, Polymer brushes, Single-molecule FRET

3.2 Introduction

Microbial lipases are broadly used as biocatalysts in industrial chemical transformations, with a global market exceeding $500 million and growing[1–5]. Specifically, these enzymes are widely employed to catalyze the hydrolysis of ester molecules as well as alcoholysis reactions (e.g., esterifications, transesterifications, polyesterifications) in anhydrous media[6]. The major uses of microbial lipases for industrial biocatalysis include the production of pharmaceuticals (e.g., ibuprofen)[7–10], renewable fuels (e.g., biodiesels)[11,12], foodstuffs (e.g., flavor enhancers, butter, cheese)[13,14], and personal care products (e.g., soaps)[15,16]. However, microbial lipases, like most enzymes, are only marginally stable and are thus active only over a narrow range of environmental operating conditions, including temperature[17]. Unfortunately, the requirement of low-temperature operation limits the accessible catalytic rates of industrial processes, which are dictated by the laws of chemical kinetics. In principle, small improvements in the stabilization of lipases could lead to dramatic improvements in catalytic performance by enabling their use at elevated temperatures[18–20].

In light of the desirability of elevated-temperature operation, the development of practical methods for the stabilization of lipases has been pursued for decades. A popular approach for stabilizing lipases, which has been adopted industrially and has numerous advantages, including enabling enzyme recycling, improving activity, altering specificity, and facilitating purification, involves immobilization[21–27]. Perhaps the most widely used example of an immobilized lipase is Novozym 435, which consists of *Candida antarctica* lipase, type B (CALB) adsorbed onto a macroporous acrylic support[28]. Studies have shown that Novozym 435 has a longer half-life than soluble CALB in aqueous reaction media; however, the improvement in catalytic performance

with increasing temperature is only modest[29]. For example, the optimal temperature for Novozym 435 and soluble CALB are the same, and the relative increase in activity with temperature is improved only two-fold compared to the soluble enzyme[10,30]. In addition to improving stability, there are many examples where immobilization can increase lipase activity upon immobilization via interfacial activation. Such activation has been shown to be the result of the opening of an amphiphilic lid that covers the active site of many lipases through interactions with the surface[31–34].

Recently, polymer brushes have received considerable attention as enzyme immobilization supports for biocatalysis and sensing applications due to several of their characteristic properties[35]. This interest has been motivated in part by the non-fouling and biocompatible nature of polymer brushes towards proteins and cells in biological settings, including upon implantation *in vivo*[36]. It is widely presumed that polymer brushes prevent protein unfolding and thus provide a stabilizing environment for enzymes compared to other surfaces[37]. A particularly intriguing aspect of polymer brushes is tunability. Notably, by adjusting the polymer chemistry, molecular weight, and grafting density, the physical and chemical properties of the brush may be rationally controlled[38]. This, in turn, provides an opportunity to modify the molecular details of the brush, which may influence enzyme structure and dynamics at the brush-solution interface.

Here, we report a dramatic increase in the stability and activity of the industrially important lipase A from *Bacillus subtilis* lipase A (lipA) at elevated temperatures via its covalent immobilization on zwitterionic poly(sulfobetaine methacrylate) (PSBMA) brushes. PSBMA brushes are commonly employed in biomaterial applications, where the non-fouling and biocompatible nature is typically ascribed to reduced unfolding of proteins at these interfaces[39–41]. When immobilized to PSBMA brushes, lipA exhibited a >100-fold activity enhancement at the

optimum temperature relative to ambient conditions (i.e., 20°C). The magnitude of this enhancement is markedly greater than that observed by immobilization of lipases on other surfaces, or by other methods of stabilization, including protein engineering[21,37,42–46]. Notably, the optimum temperature of the enzyme also increased by 20°C upon immobilization, suggesting an enhancement in conformational stability. To understand the mechanistic basis for this stabilization, the conformational dynamics of lipA immobilized on PSBMA and on poly(poly(ethylene glycol) methacrylate) (PEGMA) brushes was studied using single-molecule (SM) methods. Additionally, the influence of the chemical details of the brush layer on the catalytic performance of other lipases, including *Rhizomucor miehei* lipase (RML), *Candida rugosa* lipase (CRL), and *Candida antarctica* lipase B (CALB), was also investigated. We observed increases in the catalytic performance of the immobilized lipases and provide new insights regarding the role of brush chemistry on immobilized lipase stabilization. These findings open the door to significant improvements for lipase-based industrial biotransformations, and also have broad implications for improving the utility of other enzymes for biocatalysis, biosensing, and other applications.

3.3 Results and Discussion

3.2.1 Catalytic Performance of lipA Immobilized on PEGMA and PSBMA Brushes

To investigate the impact of polymer brush immobilization on lipA activity, we immobilized lipA on both PSBMA and PEGMA brushes. Polymer brushes composed of PEGMA or PSBMA were generated using surface-initiated atom transfer radical polymerization on 1 μm diameter silica particles functionalized with the initiator chloromethylphenyl trichlorosilane. For lipA immobilization, methacrylic acid N-hydroxysuccinimide (NHS) ester was added to the polymerization reactions at a molar ratio of 1:100 NHS-to-PEGMA or PSBMA. Inclusion of NHS

groups within the brush enabled covalent attachment of enzyme via primary amines on the enzyme's surface. The most likely sites for immobilization on the enzyme were, in addition to the N-terminus, Lys44, Lys61, Lys69, Lys88, Lys112, and Lys122, which have a solvent accessibility of ≥50%[47]. Additionally, because these sites were randomly distributed within lipA, the location of immobilization between individual lipA molecules was likely heterogeneous. Although statistically unlikely given the low density of NHS groups within the brush, it is also possible that some enzyme molecules were immobilized to the brush through more than one site. In addition to the site of covalent attachment, the enzyme may non-covalently interact with the brush through additional sites on the enzyme surface as a result of being entrapped by the brush. Because of the dynamic nature of these supports, the enzyme also presumably does not have a defined orientation of the enzyme relative to the underlying solid support. Additionally, based on a mass balance, the extent of enzyme loading was found to be 8 mg per g of PEGMA and PSBMA support, which represented a loading yield of 80%. Furthermore, after immobilization, the apparent specific activity of lipA on PSBMA (22.5 +/- 2.5 mole $mole^{-1}$ s^{-1}) and PEGMA (26.7 +/- 12.3 mole $mole^{-1}$ s^{-1}) was similar to that for soluble lipA (28.7 +/- 2.2 mole $mole^{-1}$ s^{-1}) at 20°C. The specific activity of the immobilized lipA was measured by monitoring the initial rate of the hydrolysis of resorufin butyrate.

Upon immobilization of lipA on the brush-modified particles, the temperature-dependent activity profile (i.e., specific activity versus temperature) of the immobilized enzyme was measured. Remarkably, immobilization of lipA on PSBMA-modified particles resulted in a dramatic 20˚C increase in the temperature optimum of the enzyme relative to that of soluble lipA (Figure 3-1). The specific activity of lipA at this optimal temperature (50°C) was more than 100-fold higher at this optimum relative to ambient temperature (i.e., 20°C). For comparison, the

enhancement in specific activity for soluble lipA at its temperature optimum (30°C) relative to 20°C was only two-fold. While lipA immobilized on PEGMA-modified particles also exhibited improved catalytic performance relative to soluble lipA, the improvements were not as dramatic. Specifically, immobilized on PEGMA-modified particles resulted in a 15°C increase in temperature optimum and only a 5-fold rate enhancement at this temperature relative to at 20°C. The performance enhancement due to immobilization on polymer brush-modified particles was presumably due to the stabilization of lipA at elevated temperatures.

An alternative hypothesis for the increase in activity at elevated temperatures is that mass transport of the substrate was differentially affected by temperature. This could potentially lead to changes in the local concentration of the substrate in the vicinity of the enzyme, thereby leading to changes in activity. To rule out this hypothesis, adsorption isotherms of the fluorescent product resorufin were measured on PEGMA and PSBMA brushes at 20°C and 50°C (Figure D-1). Notably, resorufin is chemically similar to the substrate resorufin butyrate and is fluorescent, enabling measurements of adsorbed quantity at an interface using attenuated total reflectance fluorescence. The amount of adsorbed resorufin was reduced for the PSBMA surface relative to PEGMA and, more importantly, the adsorption of resorufin decreased with increasing temperature on both surfaces. This indicated that neither the improved activity on PSBMA vs. PEGMA, nor the dramatic increase in activity with temperature on the PSBMA support, was related to changes in substrate concentration in the brush layer. Additionally, analysis of the Michaelis-Menten kinetics found that the apparent K_M for both soluble and immobilized enzymes were similar and less than the concentration of substrate used (Figure D-2). This demonstrated that the enzymes were near saturation for the activity measurements. Together, these experiments demonstrate that mass transport effects could not account for the differences in activity at elevated temperatures for lipA

immobilized on PEGMA and PSBMA, and that the dramatic increase in activity of lipA on PSBMA with increasing temperature is not the result of changes in mass transport with increasing temperature.

The activity enhancement of lipA immobilized on PSMBA-modified particles represents a large improvement in catalytic performance compared previous observations. While Rao and co-workers[45] obtained a 20°C increase in the temperature optimum of lipA using directed evolution, this improvement resulted in only a 5-fold increase in activity at this optimum relative to 25°C. A similar increase in activity was observed when CRL was covalently immobilized on poly(2-hydroxyethylmethacrylate-co-methacrylamido-phenylalanine) membranes as reported by Arica and co-workers[44]. However, in this case, only a 10°C increase in the temperature optimum was observed. Additionally, although ancestral sequence reconstruction has been used to generate stable enzyme variants, even with this approach, enhancements of activity of only 30-fold have been reported[46].

To develop insights into the mechanisms of activity enhancement, the kinetic stability (i.e., retention of activity as a function of time) of lipA immobilized on PSBMA and PEGMA-modified particles was measured at elevated temperature (i.e., 40°C). As shown in Figure 3-1b, although lipA immobilized on PEGMA-modified particles retained activity longer than soluble lipA, the improvement was only modest, with activity retention for approximately 1 h. However, lipA immobilized on PSBMA-modified particles retained 100% of its initial activity over 24 h, highlighting the remarkable stabilizing properties of the PSBMA brush. While both the PEGMA and PSBMA brushes were stabilizing, our findings underscore the impact of brush chemistry on the catalytic performance of lipA in nominally denaturing conditions.

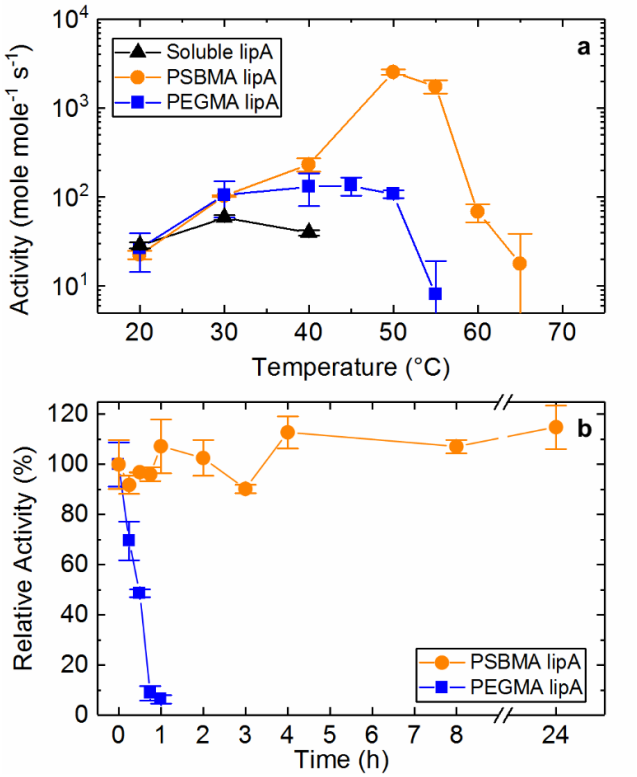

Figure 3-1: Temperature-dependent activity profiles of soluble and immobilized lipA . (a) Specific activity of lipA, expressed as the moles of product formed per second per mole of enzyme, for soluble lipA (black triangles), lipA immobilized on PEGMA-coated microparticles (blue squares), and lipA immobilized on PSBMA-coated microparticles (orange circles). The specific activity of the various forms of lipA was measured immediately at each temperature over the range from 20-65°C. (b) Relative activity retention of lipA immobilized on PEGMA (blue squares) and PSBMA (orange circles) functionalized microparticles upon incubation at 40 °C. The relative activity of immobilized enzyme was determined by normalizing the activity after incubation to the activity at time zero. The error bars represent a 95% confidence interval based on the standard error of three replicate experiments.

3.2.2 Conformational Stability of LipA Immobilized on PEGMA and PSBMA Brushes

Given the difference in stability of lipA immobilized on PEGMA and PSBMA brushes, we investigated the basis for the impact of brush chemistry on the stability of immobilized lipA using dynamic SM methods. SM-Förster resonance energy transfer (SM-FRET) imaging is particularly useful for measuring changes in enzyme structure as well as kinetics associated with unfolding and re-folding *in situ* in near-surface environments. In a recent example using SM-FRET imaging,

we previously demonstrated that mixed lipid bilayers stabilized nitroreductase through a chaperone-like mechanism[48].

Immobilized, FRET-labeled lipA molecules (between 153-4,702 for each experiment) were imaged via total internal flection fluorescent microscopy (TIRFM) using alternating laser excitation[49]. For SM-FRET experiments, lipA was site-specifically labeled through the incorporation of a unique cysteine (position 175) and p-azidophenylalanine (position 4) as described previously (Figure 3-2a)[50]. Donor and acceptor intensities were compiled into two-dimensional donor-acceptor intensity histograms (referred to as SM-FRET maps; see Figure 3-3 and Figure D-3) for all conditions[51]. These histograms exhibited two distinct populations, with either high acceptor and low donor intensity (high FRET) or vice versa (low FRET), and were attributed to folded and unfolded conformations, respectively. These populations were segmented in each histogram by identifying a dividing line between the two peaks that minimized the integrated probability under the line using a direct search algorithm[52]. Based on this dividing line, the temporal trajectories of individual lipA molecules were segmented into folded and unfolded time intervals as shown in Figure 3-2b.

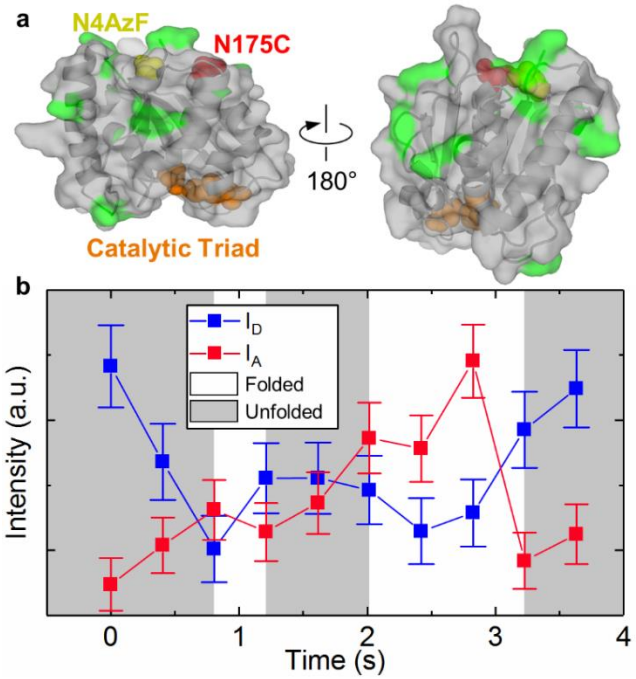

Figure 3-2: Determination of lipA conformation in SM-FRET experiments. (a) Crystal structure of lipA (PDB accession code: 1ISP) with primary amines highlighted in green, catalytic triad in orange, and donor and acceptor labeling sites in yellow and red, respectively. (b) Representative raw trajectory from SM-FRET imaging experiments showing changes in the donor (I_D; blue squares) and acceptor (I_A; red squares) intensities over time. The background shading indicates temporal intervals when the lipA molecule was folded (white) and unfolded (gray), respectively, as determined using quantitative criteria from the cumulative analysis of SM trajectories.

The results of SM-FRET experiments between 20-45°C showed that the retention of the folded conformation was significantly greater at elevated temperatures for lipA immobilized on PSBMA relative to PEGMA brushes. This can be seen qualitatively by comparing the SM-FRET maps as a function of temperature for the two different brush surfaces, which are shown in Figure 3-3. For lipA immobilized on PEGMA brushes, the enzyme remained mostly folded until 40°C at which temperature a significant decrease in the fraction of high FRET state observations was observed. Conversely, for lipA immobilized on PSBMA brushes, the fraction of observations in the folded state remained virtually unchanged over the entire temperature range, consistent with the retention of the native state of lipA. Differences in the fraction of observations in the high

FRET state on each surface for each temperature, which were quantified and expressed as folded fraction, are summarized in Figure 3-3m. Notably, at 45°C, the folded fractions on the PSBMA and PEGMA brush were 0.7 and 0.2, respectively, highlighting the difference in structural stability of lipA on the two brush surfaces. To determine if this difference in the structural stability of immobilized lipA extended beyond thermal denaturation, we also measured the stability of immobilized lipA to chemical denaturation by SM-FRET. Analysis of the FRET maps for immobilized lipA as a function of urea concentration also showed a greater stabilizing effect by PSBMA relative to PEGMA (Figure D-3). Amazingly, lipA immobilized on PSBMA was stable even in 8 M urea, and appeared to unfold in 8 M only after heating to 45°C. In contrast, the folded fraction of lipA immobilized on PEGMA decreased significantly at urea concentrations above 4M.

These findings suggested that the improved catalytic performance of immobilized lipA on PSBMA relative to PEGMA was the result of enhanced structural stability at elevated temperatures. To rule out the possibility that this effect was specific to the FRET mutant, we performed thermal denaturation studies using immobilized wild-type lipA, and saw very similar effects. Specifically, consistent with the results of SM-FRET experiments, the apparent melting temperature of wild-type lipA immobilized on PSBMA-modified particles was several degrees greater than that for wild-type lipA immobilized on PEGMA-modified particles (Figure D-4**)**. Details of the impact of brush chemistry on enzyme dynamics, which provided insight into this differential stability, are discussed in the following section.

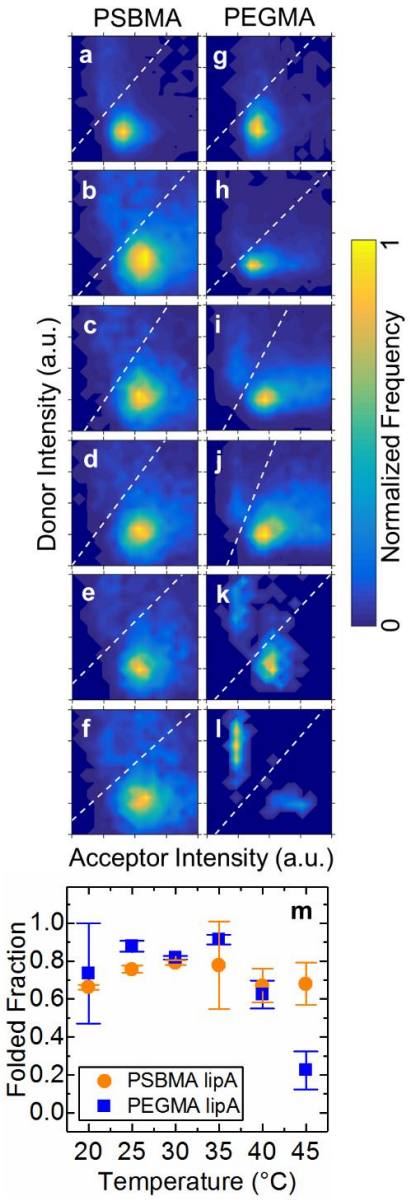

Figure 3-3: Thermal stability of immobilized lipA from SM-FRET experiments. (a-l) SM-FRET maps for lipA as a function of temperature and support chemistry with dashed white lines indicating the threshold used to distinguish folded from unfolded observations. The left column panels (a-f) represent lipA immobilized on PSBMA at (a) 20°C (2,930 trajectories), (b) 25°C (4,702 trajectories), (c) 30°C (3,055 trajectories), (d) 35°C (3,192 trajectories), (e) 40°C (1,633 trajectories), (f) 45°C (2,099 trajectories). The right column panels (g-l) represent lipA immobilized on PEGMA at (g) 20°C (1,280 trajectories), (h) 25°C (413 trajectories), (i) 30°C (866 trajectories), (j) 35°C (793 trajectories), (k) 40°C (153 trajectories), (l) 45°C (411 trajectories). (m) Folded fraction of lipA immobilized on PEGMA (blue squares) and PSBMA (orange circles) as determined from quantitative analysis of the SM-FRET maps in panels a-l. Error bars

represent the standard error of folded fraction, which was estimated using jackknife resampling with replacement of trajectories for each condition.

3.2.3 Conformational Dynamics of LipA Immobilized on PEGMA and PSBMA Brushes

To further elucidate the basis for the impact of brush chemistry on the stability of lipA on the brushes, we analyzed the dynamics of lipA immobilized on PEGMA and PSBMA brushes. From the SM-FRET trajectories, the apparent rate constants associated with unfolding (k_u) and re-folding (k_f) of immobilized lipA on PEGMA and PSBMA brushes were quantified from the analysis the distributions of the folded and unfolded state dwell times. Notably, the state dwell times represent the time spent in a given conformation before undergoing a conformational transition. Changes in FRET state were considered structural transitions if the donor-intensity pair crossed the threshold on the FRET map by a value greater than the uncertainty in the quantified donor and acceptor intensities. When state transitions are rare (e.g., in strongly denaturing conditions where most of the observations are unfolded), a large fraction of the molecules may photobleach prior to changing states. Therefore, we employed a maximum-likelihood approach to determine k_u and k_f, which incorporated a probability of changing state and a probability of bleaching that accounted for all SM observations, including trajectories that did not exhibit a transition. Transition probabilities were fit to a beta distribution to account for continuous heterogeneity of the probabilities of a transition in the case that k_u and k_f could not be modeled by a single first-order process or a superposition thereof, as described in detail by Kienle et al.[51]

Figure 3-4 shows the values of k_u and k_f as a function of temperature for immobilized lipA on PSBMA and PEGMA brushes, respectively. These plots are analogous to Chevron plots for ensemble protein folding and unfolding experiments, where the folding and unfolding rate

constants as a function of denaturant are plotted together on semilogarithmic axes[53]. Interestingly, while k_u and k_f were relatively constant with temperature for immobilized lipA on PSBMA, the rate constants changed systematically with temperature for lipA immobilized on PEGMA (except at the lowest temperatures). Specifically, for lipA immobilized on PEGMA, k_u systematically increased with temperature (except at the lowest temperatures) while k_f decreased significantly with increasing temperature. These observations correlated with the difference in structural stability for immobilized lipA on PSBMA and PEGMA brushes described above. Specifically, they suggest that the retention of folded lipA immobilized on PSBMA relative to PEGMA at elevated temperatures was due both to a reduction in unfolding (i.e., stabilization of the folded state) and the facilitation of re-folding of denatured lipA molecules by PSBMA brushes.

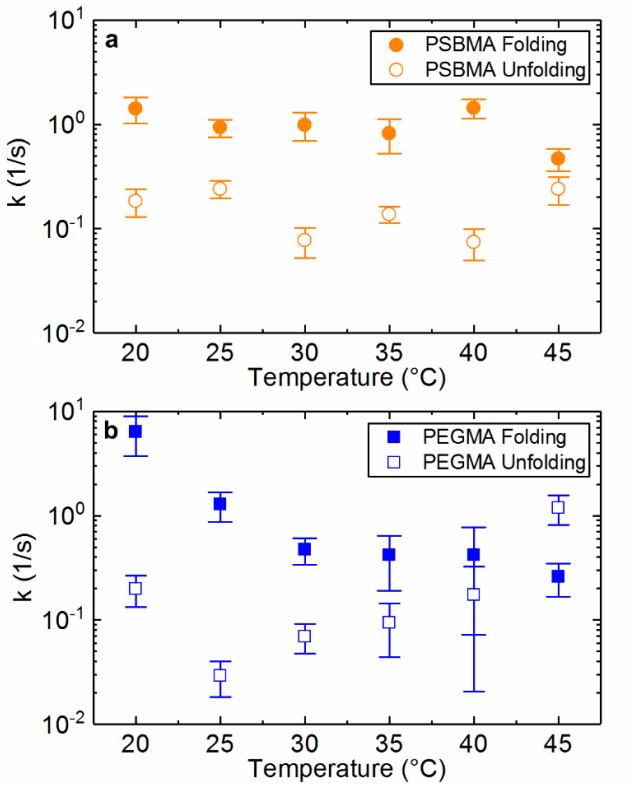

Figure 3-4: Equilibrium rate constants for folding (closed symbols) and unfolding (open symbols) of lipA immobilized on (a) PSBMA and (b) PEGMA as a function of temperature from SM observations. Folding (k_f) and unfolding (k_u) rate constants represent maximum likelihood estimates, which account for the probabilities associated with conformational state changes as well as photophysical effects (i.e., bleaching). Error bars represent the standard error of the rate constant, which were estimated using jackknife resampling with replacement of trajectories for each condition.

In light of the findings, it is interesting to speculate on the physical origin of the differential stability of lipA immobilized to PSBMA and PEGMA supports. One hypothesis is related to differences in spatial heterogeneity between the different types of brushes. Specifically, using super-resolution fluorescence mapping of PEG brushes using a solvatochromic fluorophore, we have previously shown that PEG brushes may exhibit spatially heterogeneous hydrophobicity, including highly hydrophobic local regions within the brush layer[54]. The emergence of such heterogeneity in local hydrophobicity is presumed to result from an increase in local interactions between PEG chains, which leads to the exclusion of water[55]. Because unfolded lipA may interact

strongly with these niches, their presence may promote unfolding and inhibit the re-folding of denatured immobilized lipA molecules. PSBMA brushes are believed to be more hydrophilic, due to the uniformly hydrophilic nature of sulfobetaine (unlike ethylene glycol, which has significant hydrophobic character). Further supporting this hypothesis, we previously reported a correlation between the presence of such niches and increased unfolding of fibronectin on PEG brushes[56]. This hypothesis is also supported by Eyring analysis of the temperature dependence of k_u. Interestingly, the larger temperature dependence of k_u on PEGMA relative to PSBMA suggests the free energy barrier for unfolding had a larger entropic component on PSBMA. While somewhat speculative, the lower hydration of PEGMA may reduce the entropic penalty associated with exposing the hydrophobic core of lipA upon unfolding since less water is present (i.e., smaller hydrophobic effect). Conversely, due to the strong hydration of PSBMA brushes, the increase in water may increase this entropic penalty.

3.2.4 Catalytic Performance of Immobilized RML, CRL, and CALB

Our results show that the catalytic performance of lipA immobilized on PSBMA and PEGMA brushes was strongly dependent on the underlying chemical details of the brush surface. To determine if this dependence is general or enzyme specific, the impact of brush chemistry on the catalytic performance of immobilized RML, CRL, and CALB was also determined. Notably, RML, CRL, and CALB are all applied in industrial biocatalysis for food modification[57], fine chemical synthesis[58], and biofuel production[59], among other applications[60]. For these studies, RML, CRL, and CALB were immobilized on PSBMA and PEGMA-modified particles using the same immobilization chemistry as for lipA. Enzyme loading was found to be 1.5 mg/g of particles for RML and 0.1 mg/g particles for CRL and CALB, representing immobilization yields of 90% for all three enzymes. Analysis of the temperature-dependent activity profiles for the three

immobilized lipases (and their soluble counterparts) indicated that the dependence of catalytic performance on brush chemistry was strongly enzyme specific. For RML, the specific activity at all temperatures between 20-70°C was significantly greater when immobilized on PSBMA compared to on PEGMA-immobilized RML or soluble RML (Figure 3-5a). The increase in specific activity at upon immobilization, commonly referred to as interfacial activation, is often attributed to stabilization of an open conformation of the active site and a neighboring amphiphilic loop, commonly referred to as a lid[31–33]. Similar to the case of lipA, there was a significant (~10°C) increase in the temperature optimum for RML immobilized on PSBMA compared to soluble RML. For CRL, the temperature optimum when immobilized on PSBMA was similar as that for soluble CRL; however, like RML, the specific activity at all temperatures was increased compared to soluble CRL (Figure 3-5b). Like RML, CRL also exhibits an amphiphilic lid domain and an increase in activity upon immobilization is typically ascribed to stabilization of the open, more active form of the enzyme[23,61,62]. Notably, CRL immobilized on PEGMA had a lower temperature optimum than either PSMBA-immobilized or soluble CRL, suggesting that PEGMA destabilized CRL. Conversely, in the case of CALB, the apparent temperature optimum of PEGMA-immobilized CALB was significantly greater than PSBMA-immobilized or soluble CALB (Figure 3-5c). Moreover, even though the specific activity of immobilized CALB on PEGMA and PSBMA was lower than that of soluble CALB below 50°C, the highest specific activity over the temperature range studies was observed for CALB immobilized on PEGMA at 80 °C. It is also interesting that at 80 °C (the highest temperature employed due to instrument limitations), the specific activity for CALB immobilized on PEGMA appeared to still be increasing. To evaluate any potential impact of mass transport, Michaelis-Menten kinetics were measured for soluble RML, CRL, and CALB (Figure D-5). In the case of RML and CRL, the substrate concentration

employed (10 μM) was greater than the measured K_M, indicating that mass transport effects could, at most, account for a two-fold change in activity. However, for CALB, we cannot rule out mass transport effects for the large increase in activity with increasing temperature on the PEGMA support since its apparent K_M was greater than the substrate concentration.

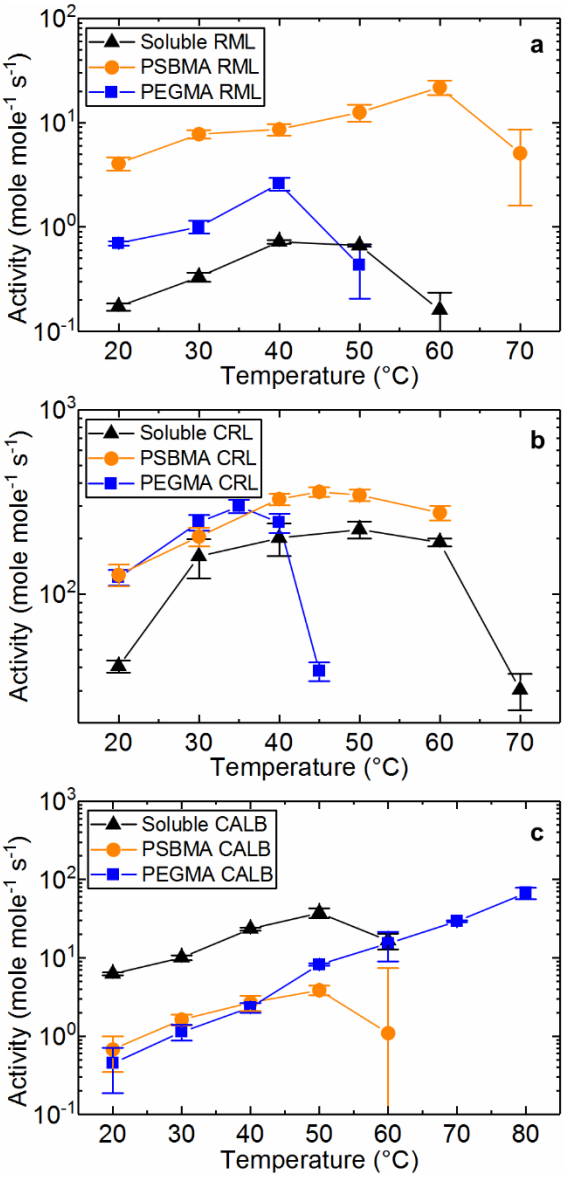

Figure 3-5: Temperature-dependent activity profiles of soluble and immobilized forms of lipases from (a) *Rhizomucor miehei* lipase (RML), (b) *Candida rugosa* lipase (CRL), and (c) *Candida antarctica* lipase B (CALB). The temperature-dependent activity profiles for the soluble forms of each enzyme are shown as

black triangles while the temperature-dependent activity profiles for each enzyme immobilized on PEGMA and PSBMA are shown as blue squares and orange circles, respectively. The error bars represent a 95% confidence interval from the standard error of three replicate experiments.

These results demonstrate that the performance of immobilized enzymes is specific to both the enzyme and the support chemistry. While both lipA and RML were more stable on PSBMA than in solution, both CRL and CALB were not stabilized by PSBMA. Conversely, CALB apparently stabilized upon immobilization to the more hydrophobic PEGMA support, which could be due to the fact that CALB has a relatively hydrophobic surface; a large fraction of solvent accessible surface area is occupied by hydrophobic residues as calculated by the VADAR (Volume, Area, Dihedral Angle Reporter) web-based structural analysis program[63]. Notably, the specific activity of both lidded lipases used (RML and CRL) increased significantly upon immobilization, indicative of interfacial activation typically ascribed to stabilization of the open, more active conformation of these enzymes[62,31]. Additionally, because the stability and activity of monomeric and multimeric lipases may differ, it is possible that some of the differences observed on the two supports may be due to the formation of multimeric species during immobilization (i.e., dimers, trimers, etc.) [64]. Conversely, CALB lost significant activity upon immobilization, which may be due to the three lysine residues within 15 Å the active site (K136, K208, and K308), which, if involved in covalent immobilization to the brush, could limit substrate accessibility, thereby reducing specific activity[65].

3.4 Conclusions

We observed a large enhancement in the catalytic performance of the industrially relevant enzyme lipA through its immobilization on PSBMA brushes. This enhancement is an order of magnitude greater than previously observed for lipase immobilized on any surface, and, to our

knowledge, represents the largest enhancement ever reported for any enzyme by immobilization to a solid support material. Using SM methods, we demonstrated that the dependence of this enhancement on brush chemistry arose from differences in conformational dynamics of the immobilized lipA. These insights were enabled by the unique advantages of SM methods, which permitted the structure and dynamics of immobilized lipA to be characterized independently *in situ*. The dependence on brush chemistry was strongly enzyme specific, highlighting the importance of surface chemistry in mediating the protein-brush interface. Future studies will be necessary to elucidate the molecular details of the connection between brush chemistry and enzyme activation, which may also be influenced by the location of enzyme attachment to the brush. The enormous improvement in lipase activation reported here may enable transformational advances in the use of lipases for industrial biotransformations. Moreover, the mechanisms of stabilization and activation reported here have important implications extending to novel materials and interfaces for the immobilization of enzymes for diverse biocatalysis and biosensing applications.

3.5 Methods

3.5.1 Surface Preparation, Functionalization, and Characterization

Silica particles (1 μm diameter) for ensemble activity and stability measurements were purchased from NanoCym and cleaned by UV-ozone for 1 h before functionalization. Two-inch fused silica wafers (Mark Optics) for SM imaging and two-inch silicon wafers with native oxide coating (Wafer Pro) were cleaned in warm piranha solution (30% v/v hydrogen peroxide, 70% sulfuric acid) for 1 h, rinsed with water, dried under nitrogen, and subsequently cleaned for 1 h with UV-ozone prior to use. Particles and wafers were functionalized with initiator chloromethylphenyl trichlorosilane (Gelest) by submersion in a solution of 0.01% (v/v) of CMPS

in toluene for 45 min, serially rinsed with toluene, isopropanol, and water, and dried in a vacuum desiccator.

Surface-initiated atom transfer radical polymerization (siATRP) was used to grow polymer brushes from fused silica and silicon wafers using the protocol from Guo et. al[66]. Poly(ethylene glycol) methyl ether methacrylate (EGMA, M_n=300), [2-(methacryloyloxy)ethyl]dimethyl-(3-sulfopropyl)ammonium hydroxide (SBMA), methacrylic acid N-hydroxysuccinimide ester (MA-NHS), 2,2'-bipyridine (bpy), copper (I) chloride, copper (II) chloride, anhydrous dimethylformamide (DMF) and anhydrous methanol were purchased from Sigma-Aldrich and used as received. A 100:1:5:2:0.2 molar ratio of monomer (EGMA or SBMA), MA-NHS, bpy, copper (I) chloride, and copper (II) chloride was used for surface-initiated atom transfer radical polymerization with either anhydrous DMF (for EGMA) or anhydrous methanol (for SBMA) as the solvent. Polymerizations were performed in a 3-inch-wide mouth jar sealed with a septum. Monomer solutions with CMPS functionalized wafers or particles were degassed by bubbling nitrogen for 3 h before adding copper (I) chloride under nitrogen. Polymerizations proceeded at room temperature for 24 h under positive nitrogen pressure to prevent oxygen ingress and subsequently rinsed with warm, anhydrous solvent and dried in a vacuum desiccator.

Flat surfaces were characterized by water contact angle goniometry and variable angle ellipsometry to confirm functionalization with the silane initiator and subsequent polymerization. Static water contact angles were measured on a custom-built goniometer, and thicknesses were measured using variable-angle spectroscopic ellipsometer (VASE-VB-250). Silica functionalized with CMPS had a contact angle of 67° +/- 3° and a thickness of 0.8 +/- 0.4 nm, consistent with monolayer formation. Surfaces functionalized with PEGMA had a contact angle of 58° +/- 3° and

a dry thickness of 17.1 +/- 0.7 nm while those functionalized with PSBMA had a contact angle less than 5° and a dry thickness 17.5 +/- 3.4 nm.

3.5.2 Cloning, Expression, and Purification of lipA

The pet21b vector containing the gene lipA from *Bacillus subtilis* with a C-terminal polyhistidine tag was mutated at amino acid positions 4 and 175 for FRET-labeling. These residues were specifically mutated to an amber stop codon (position 4) and cysteine (position 175) using the quikchange mutagenesis kit (Agilent). The primers for the N175C and N4AzF mutations were 5'-GTCAACAGCCTGATTAAAGAAGGGCTGTGCGGCGGGGGCCAGAATACGAATCACCACC -3' and 5'-GAAGGAGATATACATATGGCTGAACACTAGCCAGTCGTTATGGTTCACGGTATTGGAGG-3', respectively, and both mutations were confirmed via sequencing (Integrated DNA Technologies). Wild-type and mutant lipA were co-transformed in BL21 (DE3) *Escherichia coli* with the pDule2 pCNF RS plasmid. Transformed cells were plated on agar containing spectinomycin (50 μg/mL) and ampicillin (50 μg/mL) and subsequently expressed and purified using the protocol developed for this non-natural amino acid system[67].

After expression, cells were harvested by centrifugation at 4,000 x g for 15 min, re-suspended in 50 mM sodium phosphate, pH 7.5, 100 mM NaCl, 5 mM imidazole, and 8 M urea, and lysed via sonication. The cell lysate was loaded on a nickel column (Biorad) and eluted in 50 mM sodium phosphate, pH 7.5, 100 mM NaCl, and 8 M urea with 250 mM imidazole. Purified lipA was refolded by rapid dilution (20-fold by volume) into 50 mM sodium phosphate, pH 7.50, before de-salting with a Zeba spin column with a 7K MWCO (Thermo Fisher) with 50 mM sodium

phosphate, pH 7.5. To prevent degradation of the aryl-azide substituent, the lipA containing the N4AzF was not exposed to UV light during or after purification.

3.5.3 Site-Specific Labeling of lipA

Following purification, mutant lipA was site-specifically labeled with fluorophores in 50 mM sodium phosphate, pH 7.5, with 8 M urea. Donor labeling with Alexa Fluor 555 DBCO (Life Technologies) was performed with a 5-fold molar excess of fluorophore-to-enzyme for 4 h at room temperature. Subsequently, a 5-fold molar excess of TCEP was used to reduce any intermolecular disulfide bonds for 30 min, followed by the addition of a 5-fold molar excess of acceptor, Alexa Fluor 647-maleimide (Life Technologies). Labeled lipA was refolded by rapid dilution (20-fold by volume) in 50 mM sodium phosphate, pH 7.5, and excess dye was removed by repetitive purification (i.e., 3 serial washes) using a Zeba spin column with a 7K MWCO (Thermo Fisher). Ensemble solution FRET as well as tryptophan fluorescence experiments confirmed that the intrinsic stability of lipA was unaffected by labeling, and that the denaturation of lipA resulted in a decrease in FRET (Figure D-6). Additionally, activity assays further indicated that mutagenesis did not perturb the activity of the lipA construct used for SM-FRET studies (Figure D-6).

3.5.4 Enzyme Immobilization

LipA was immobilized on functionalized microparticles by reconstituting 100 mg dry particles in 1 mL of a solution containing $5x10^{-5}$ M wild-type lipA in 50 mM sodium phosphate, pH 7.5, for 24 h at room temperature with gentle mixing to prevent particle sedimentation. After immobilization, particles were sedimented at 1000 x g for 2 min. The residual activity of the supernatant was used to estimate the concentration of unreacted enzyme (i.e., enzyme remaining in solution), and, from a mass balance, the concentration of the enzyme immobilized on particles

was estimated. This loading was consistent with monolayer coverage based on the two-dimensional projected area of lipA from its crystal structure[68]. Supports were serially washed by re-suspension in buffer and sedimented five additional times after which no residual activity was detected. For SM experiments, FRET-labeled lipA was added at a concentration of 1.0×10^{-10} M in the presence of the same concentration of wild-type lipA for immobilization and thoroughly rinsed with buffer before imaging to remove any unreacted enzyme. Surfaces and particles were maintained in contact with buffer after immobilization to prevent any effects of de-wetting on the immobilized enzyme.

For the immobilization of RML, CRL, and CALB, which were purchased from Sigma-Aldrich, the enzymes were dissolved and dialyzed against 50 mM sodium phosphate, pH 7.5 for 24 h at 4°C and passed through a 0.22 μm filter before immobilization. The concentration of RML, CRL, and CALB after dialysis was estimated by densitometry on SDS-PAGE gels using a purified recombinant GFP sample of known concentration as a standard (Figure D-7). Enzyme loading after immobilization was determined as described for wild-type lipA and was 1.5 mg/g of particles for RML and 0.1 mg/g particles for CRL and CALB.

3.5.5 Enzyme Activity

Activity measurements for all lipases were measured with 10 μM of the fluorogenic substrate resorufin butyrate in 50 mM sodium phosphate, pH 7.5 in a temperature-controlled cuvette with mixing. Specific activity was determined from the initial rate of the hydrolysis reaction and expressed on a mole product per mole enzyme per second basis (i.e. turnover frequency). The background hydrolysis was subtracted using identical reaction conditions in the absence of enzyme. Standard curves of purified resorufin were used to determine product concentration from fluorescence intensity.

3.5.6 SM-FRET Imaging and Analysis

Functionalized wafers were installed in a custom-built flow cell and imaged on a homebuilt, prism-based TIRF microscope based on the Nikon TE-2000 platform with a 60x water immersion objective. Emission from donor and acceptor fluorophores was separated using an optosplit III (Cairn Research) and a dichroic mirror with a nominal separation wavelength of 610 nm (model T610LPXR, Chroma). The donor signal was further cleaned with a 585 nm bandpass filter with a spectral width of 29 nm (Semrock) and the acceptor was cleaned with a 685 nm bandpass filter with a spectral width of 40 nm (Semrock). Both channels were projected onto different regions of a Cascade II: 1024 EMCCD camera (Photometrics) with an acquisition time of 200 ms per exposure.

Surfaces were imaged using alternating laser excitation with both a 50 mW 532 nm laser (Cobolt, Samba) and a 50 mW 640 nm laser (Crystalaser). Details of the imaging processing and analysis are described in detail by Marruecos and co-workers[54]. Alternating frames comprised images of either donor excited or acceptor excited frames, molecules were excluded from the analysis if they lacked a functional acceptor. Furthermore, SM trajectories were truncated at the moment of acceptor photobleaching as measured by the excitation with the 640 nm laser.

3.5.7 Estimation of Folding and Unfolding Rate

The folding and unfolding rates were estimated using a previously described statistical model, which account for heterogeneity in the rates between enzymes. This model accounted for populations where the folding and unfolding rates were broadly and continuously distributed and could not be adequately modeled as a homogeneous population or as multiple discrete populations. Briefly, the enzyme trajectories were modeled as a Markov Chain, in which the enzyme could take

on a folded state, an unfolded state, or a photobleached state, and the probability of transitions from folded to unfolded and vice-versa varied between enzyme molecules according to a beta-distribution. Maximum-likelihood fitting was used to estimate the parameters describing the beta-distributed folding (a_f and b_f) and unfolding (a_u and b_u) probabilities with the likelihood function,

$$LF(N|a_f, b_f, a_u, b_u) = \prod_k \left[\frac{\mathrm{B}(a_f+N_{uf,k}, b_f+N_{uu,k})\mathrm{B}(a_u+N_{fu,k}, b_u+N_{ff,k})}{\mathrm{B}(a_f,b_f)\mathrm{B}(a_u,b_u)} p_b^{N_{b,k}} (1-p_b)^{N_{uu,k}+N_{uf,k}+N_{ff,k}+N_{fu,k}} \right]$$

where B is the beta function, N_{uf}, N_{uu}, N_{fu}, N_{ff}, and N_b are the total number of times an object folds, remains unfolded, unfolds, or remains folded between frames, respectively, p_b is the probability of photobleaching at any given frame (which is determined independently using the trajectory durations) and the subscript *k* indicates the trajectory index. From these parameters, the average folding and unfolding rate constants could be estimated as $k_f = -\left(\psi(b_f) - \psi(a_f + b_f)\right)/\tau$ and $k_u = -\left(\psi(b_u) - \psi(a_u + b_u)\right)/$, respectively, where τ is the frame acquisition time and ψ is the digamma function.

3.6 References

(1) Ávila, S. N. S.; Gutarra, M. L. E.; Fernandez-Lafuente, R.; Cavalcanti, E. D. C.; Freire, D. M. G. Multipurpose Fixed-Bed Bioreactor to Simplify Lipase Production by Solid-State Fermentation and Application in Biocatalysis. *Biochem. Eng. J.* **2019**, *144*, 1–7.

(2) Bornscheuer, U. T.; Huisman, G. W.; Kazlauskas, R. J.; Lutz, S.; Moore, J. C.; Robins, K. Engineering the Third Wave of Biocatalysis. *Nature* **2012**, *485*, 185–194.

(3) Schmid, A.; Dordick, J. S.; Hauer, B.; Kiener, A.; Wubbolt, M.; Witholt, B. Industrial Biocatalysis Today and Tomorrow. *Nature* **2001**, *409*, 258–268.

(4) DiCosimo, R.; McAuliffe, J.; Poulose, A. J.; Bohlmann, G. Industrial Use of Immobilized Enzymes. *Chem. Soc. Rev.* **2013**, *42*, 6437–6474.

(5) De Godoy Daiha, K.; Angeli, R.; De Oliveira, S. D.; Almeida, R. V. Are Lipases Still Important Biocatalysts? A Study of Scientific Publications and Patents for Technological Forecasting. *PLoS One* **2015**, *10*, 1–20.

(6) Klibanov, A. M. Improving Enzymes by Using Them in Organic Solvents. *Nature* **2001**, *409*, 241–246.

(7) Gotor-Fernández, V.; Brieva, R.; Gotor, V. Lipases: Useful Biocatalysts for the Preparation of Pharmaceuticals. *J. Mol. Catal. B Enzym.* **2006**, *40*, 111–120.

(8) Mustranta, A. Use of Lipases in the Resolution of Racemic Ibuprofen. *Appl. Microbiol. Biotechnol.* **1992**, *38*, 61–66.

(9) Jacobsen, E. E.; Hoff, B. H.; Moen, A. R.; Anthonsen, T. Enantioselective Enzymatic Preparation of Chiral Glutaric Monocarboxylic Acids and Amides. *J. Mol. Catal. B Enzym.* **2003**, *21*, 55–58.
(10) Dong, H. P.; Wang, Y. J.; Zheng, Y. G. Enantioselective Hydrolysis of Diethyl 3-Hydroxyglutarate to Ethyl (S)-3-Hydroxyglutarate by Immobilized *Candida Antarctica* Lipase B. *J. Mol. Catal. B Enzym.* **2010**, *66*, 90–94.
(11) Shimada, Y.; Watanabe, Y.; Samukawa, T.; Sugihara, A.; Noda, H.; Fukuda, H.; Tominaga, Y. Conversion of Vegetable Oil to Biodiesel Using Immobilized *Candida Antarctica* Lipase. *J. Am. Oil Chem. Soc.* **1999**, *76*, 789–793.
(12) Fernández-Lorente, G.; Terreni, M.; Mateo, C.; Bastida, A.; Fernández-Lafuente, R.; Dalmases, P.; Huguet, J.; Guisán, J. M. Modulation of Lipase Properties in Macro-Aqueous Systems by Controlled Enzyme Immobilization: Enantioselective Hydrolysis of a Chiral Ester by Immobilized Pseudomonas Lipase. *Enzyme Microb. Technol.* **2001**, *28*, 389–396.
(13) Palomo, J. M.; Segura, R. L.; Fernandez-Lorente, G.; Guisán, J. M.; Fernandez-Lafuente, R. Enzymatic Resolution of (±)-Glycidyl Butyrate in Aqueous Media. Strong Modulation of the Properties of the Lipase from *Rhizopus Oryzae* via Immobilization Techniques. *Tetrahedron Asymmetry* **2004**, *15*, 1157–1161.
(14) Vorlova, S.; Bornscheuer, U. T.; Gatfield, I.; Hilmer, J.; Bertram, H.; Schmid, D. Enantioselective Hydrolysis of d,l-Menthyl Benzoate. *Adv. Synth. Catal.* **2002**, *344*, 1152–1155.
(15) Hasan, F.; Shah, A. A.; Hameed, A. Industrial Applications of Microbial Lipases. *Enzyme Microb. Technol.* **2006**, *39*, 235–251.
(16) Schmid, R. D.; Verger, R. Lipases: Interfacial Enzymes with Attractive Applications. *Angew. Chemie Int. Ed.* **1998**, *37*, 1608–1633.
(17) Taverna, D. M.; Goldstein, R. A. Why Are Proteins Marginally Stable? *Proteins Struct. Funct. Genet.* **2002**, *46*, 105–109.
(18) Adams, M. W. W.; Perler, F. B.; Kelly, R. M. Extremozymes: Expanding the Limits of Biocatalysis. *Nature Biotechnology*. **1995**, *13*, 662–668.
(19) Zamost, B. L.; Nielsen, H. K.; Starnes, R. L. Thermostable Enzymes for Industrial Applications. *Journal of Industrial Microbiology*. **1991**, *8*, 71–81.
(20) Haki, G. D.; Rakshit, S. K. Developments in Industrially Important Thermostable Enzymes: A Review. *Bioresour. Technol.* **2003**, *89*, 17–34.
(21) Mateo, C.; Palomo, J. M.; Fernandez-Lorente, G.; Guisan, J. M.; Fernandez-Lafuente, R. Improvement of Enzyme Activity, Stability and Selectivity via Immobilization Techniques. *Enzyme Microb. Technol.* **2007**, *40*, 1451–1463.
(22) Rodrigues, R. C.; Ortiz, C.; Berenguer-Murcia, Á.; Torres, R.; Fernández-Lafuente, R. Modifying Enzyme Activity and Selectivity by Immobilization. *Chem. Soc. Rev.* **2013**, *42*, 6290–6307.
(23) Fernández-Lorente, G.; Palomo, J. M.; Cabrera, Z.; Guisán, J. M.; Fernández-Lafuente, R. Specificity Enhancement towards Hydrophobic Substrates by Immobilization of Lipases by Interfacial Activation on Hydrophobic Supports. *Enzyme Microb. Technol.* **2007**, *41*, 565–569.
(24) Palomo, J. M.; Fernandez-Lorente, G.; Mateo, C.; Ortiz, C.; Fernandez-Lafuente, R.; Guisan, J. M. Modulation of the Enantioselectivity of Lipases via Controlled Immobilization and Medium Engineering: Hydrolytic Resolution of Mandelic Acid Esters.

Enzyme Microb. Technol. **2002**, *31*, 775–783.
(25) Barbosa, O.; Torres, R.; Ortiz, C.; Fernandez-Lafuente, R. Versatility of Glutaraldehyde to Immobilize Lipases: Effect of the Immobilization Protocol on the Properties of Lipase B from *Candida Antarctica*. *Process Biochem.* **2012**, *47*, 1220–1227.
(26) Almeida, R. V.; Cunha, A. G.; Manoel, E. A.; da Silva, A. A. T.; Pinto, J. C.; Freire, D. M. G.; Simas, A. B. C.; Besteti, M. D.; Fernandez-Lafuente, R. Preparation of Core–shell Polymer Supports to Immobilize Lipase B from *Candida Antarctica*. *J. Mol. Catal. B Enzym.* **2013**, *100*, 59–67.
(27) Palomo, J. M.; Ortiz, C.; Fuentes, M.; Fernandez-Lorente, G.; Guisan, J. M.; Fernandez-Lafuente, R. Use of Immobilized Lipases for Lipase Purification via Specific Lipase-Lipase Interactions. *J. Chromatogr. A* **2004**, *1038*, 267–273.
(28) Cabrera, Z.; Fernandez-Lorente, G.; Fernandez-Lafuente, R.; Palomo, J. M.; Guisan, J. M. Novozym 435 Displays Very Different Selectivity Compared to Lipase from *Candida Antarctica* B Adsorbed on Other Hydrophobic Supports. *J. Mol. Catal. B Enzym.* **2009**, *57*, 171–176.
(29) Arroyo, M.; Sánchez-Montero, J. M.; Sinisterra, J. V. Thermal Stabilization of Immobilized Lipase B from *Candida Antarctica* on Different Supports: Effect of Water Activity on Enzymatic Activity in Organic Media. *Enzyme Microb. Technol.* **1999**, *24*, 3–12.
(30) Palomo, J. M.; Muoz, G.; Fernández-Lorente, G.; Mateo, C.; Fernández-Lafuente, R.; Guisán, J. M. Interfacial Adsorption of Lipases on Very Hydrophobic Support (Octadecyl-Sepabeads): Immobilization, Hyperactivation and Stabilization of the Open Form of Lipases. *J. Mol. Catal. B Enzym.* **2002**, *19*, 279–286.
(31) Brzozowski, A. M.; Derewenda, U.; Derewenda, Z. S.; Dodson, G. G.; Lawson, D. M.; Turkenburg, J. P.; Bjorkling, F.; Huge-Jensen, B.; Patkar, S. A.; Thim, L. A Model for Interfacial Activation in Lipases from the Structure of a Fungal Lipase-Inhibitor Complex. *Lett. to Nat.* **1991**, *351*, 491–494.
(32) Derewenda, Z. S.; Derewenda, U.; Dodson, G. G. The Crystal and Molecular Structure of the *Rhizomucor Miehei* Triacylglyceride Lipase at 1.9 Å Resolution. *J. Mol. Biol.* **1992**, *227*, 818–839.
(33) Pleiss, J.; Fischer, M.; Schmid, R. D. Anatomy of Lipase Binding Sites: The Scissile Fatty Acid Binding Site. *Chem. Phys. Lipids* **1998**, *93*, 67–80.
(34) Manoel, E. A.; dos Santos, J. C. S.; Freire, D. M. G.; Rueda, N.; Fernandez-Lafuente, R. Immobilization of Lipases on Hydrophobic Supports Involves the Open Form of the Enzyme. *Enzyme Microb. Technol.* **2015**, *71*, 53–57.
(35) Jiang, H.; Xu, F. J. Biomolecule-Functionalized Polymer Brushes. *Chem. Soc. Rev.* **2013**, *42*, 3394–3426.
(36) Wilson, C. J.; Clegg, R. E.; Leavesley, D. I.; Pearcy, M. J. Mediation of Biomaterial–Cell Interactions by Adsorbed Proteins: A Review. *Tissue Eng.* **2005**, *11*, 1–18.
(37) Qi, H.; Du, Y.; Hu, G.; Zhang, L. Poly(Carboxybetaine Methacrylate)-Functionalized Magnetic Composite Particles: A Biofriendly Support for Lipase Immobilization. *Int. J. Biol. Macromol.* **2018**, *107*, 2660–2666.
(38) Stuart, M. A. C.; Huck, W. T. S.; Genzer, J.; Müller, M.; Ober, C.; Stamm, M.; Sukhorukov, G. B.; Szleifer, I.; Tsukruk, V. V.; Urban, M.; Winnik, F.; Zauscher, S.; Luzinov, I.; Minko, S. Emerging Applications of Stimuli-Responsive Polymer Materials. *Nat. Mater.* **2010**, *9*, 101–113.

(39) Haag, R.; Neffe, A. T.; Wischke, C.; Ballauff, M.; Lendlein, A.; Dzubiella, J.; Becherer, T.; Angioletti-Uberti, S.; Wei, Q. Protein Interactions with Polymer Coatings and Biomaterials. *Angew. Chemie Int. Ed.* **2014**, *53*, 8004–8031.
(40) Gunkel, G.; Huck, W. T. S. Cooperative Adsorption of Lipoprotein Phospholipids, Triglycerides, and Cholesteryl Esters Are a Key Factor in Nonspecific Adsorption from Blood Plasma to Antifouling Polymer Surfaces. *J. Am. Chem. Soc.* **2013**, *135*, 7047–7052.
(41) Jiang, S.; Cao, Z. Ultralow-Fouling, Functionalizable, and Hydrolyzable Zwitterionic Materials and Their Derivatives for Biological Applications. *Adv. Mater.* **2010**, *22*, 920–932.
(42) Zdarta, J.; Klapiszewski, L.; Jedrzak, A.; Nowicki, M.; Moszynski, D.; Jesionowski, T. Lipase B from *Candida Antarctica* Immobilized on a Silica-Lignin Matrix as a Stable and Reusable Biocatalytic System. *Catalysts* **2016**, *7*, 1–21.
(43) Niu, W.; Li, Z.; Zhang, D.; Yu, M.; Tan, T. Improved Thermostability and the Optimum Temperature of *Rhizopus Arrhizus* Lipase by Directed Evolution. *J. Mol. Catal. B Enzym.* **2006**, *43*, 33–39.
(44) Bayramoğlu, G.; Kaçar, Y.; Denizli, A.; Yakup Arica, M. Covalent Immobilization of Lipase onto Hydrophobic Group Incorporated Poly(2-Hydroxyethyl Methacrylate) Based Hydrophilic Membrane Matrix. *J. Food Eng.* **2002**, *52*, 367–374.
(45) Ahmad, S.; Kamal, M. Z.; Sankaranarayanan, R.; Rao, N. M. Thermostable *Bacillus Subtilis* Lipases: In Vitro Evolution and Structural Insight. *J. Mol. Biol.* **2008**, *381*, 324–340.
(46) Gumulya, Y.; Baek, J.-M.; Wun, S.-J.; Thomson, R. E. S.; Harris, K. L.; Hunter, D. J. B.; Behrendorff, J. B. Y. H.; Kulig, J.; Zheng, S.; Wu, X.; Wu, B.; Stok, J. E.; De Voss, J. J.; Schenk, G.; Jurva, U.; Andersson, S.; Isin, E. M.; Bodén, M.; Guddat, L.; Gillam, M. J. Engineering Highly Functional Thermostable Proteins Using Ancestral Sequence Reconstruction. *Nat. Catal.* **2018**, *1*, 878–888.
(47) Chado, G. R.; Holland, E. N.; Tice, A. K.; Stoykovich, M. P.; Kaar, J. L. Exploiting the Benefits of Homogeneous and Heterogeneous Biocatalysis: Tuning the Molecular Interaction of Enzymes with Solvents via Polymer Modification. *ACS Catal.* **2018**, *8*, 11579–11588.
(48) Sosa, A. F. C.; Kienle, D. F.; Falatach, R. M.; Flanagan, J.; Kaar, J. L.; Schwartz, D. K. Stabilization of Immobilized Enzymes via the Chaperone- like Activity of Mixed Lipid Bilayers. *ACS Appl. Mater. Interfaces* **2018**, *10*, 19504–19513.
(49) Hohlbein, J.; Craggs, T. D.; Cordes, T. Alternating-Laser Excitation: Single-Molecule FRET and Beyond. *Chem. Soc. Rev.* **2014**, *43*, 1156–1171.
(50) Weltz, J. S.; Schwartz, D. K.; Kaar, J. L. Surface-Mediated Protein Unfolding as a Search Process for Denaturing Sites. *ACS Nano* **2015**, *10*, 730–738.
(51) Kienle, D. F.; Falatach, R. M.; Kaar, J. L.; Schwartz, D. K. Correlating Structural and Functional Heterogeneity of Immobilized Enzymes. *ACS Nano* **2018**, *12*, 8091–8103.
(52) Lewis, R. M.; Torczon, V.; Trosset, M. W. Direct Search Methods : Then and Now. *J. Comput. Appl. Math.* **2000**, *124*, 191–207.
(53) Gianni, S.; Guydosh, N. R.; Khan, F.; Caldas, T. D.; Mayor, U.; White, G. W. N.; DeMarco, M. L.; Daggett, V.; Fersht, A. R. Unifying Features in Protein-Folding Mechanisms. *Proc. Natl. Acad. Sci.* **2003**, *100*, 13286–13291.
(54) Faulón Marruecos, D.; Kienle, D. F.; Kaar, J. L.; Schwartz, D. K. Grafting Density Impacts Local Nanoscale Hydrophobicity in Poly(Ethylene Glycol) Brushes. *ACS Macro*

Lett. **2018**, *7*, 498–503.
(55) Unsworth, L. D.; Sheardown, H.; Brash, J. L. Protein-Resistant Poly(Ethylene Oxide)-Grafted Surfaces: Chain Density-Dependent Multiple Mechanisms of Action. *Langmuir* **2008**, *24*, 1924–1929.
(56) Faulón Marruecos, D.; Kastantin, M.; Schwartz, D. K.; Kaar, J. L. Dense Poly(Ethylene Glycol) Brushes Reduce Adsorption and Stabilize the Unfolded Conformation of Fibronectin. *Biomacromolecules* **2016**, *17*, 1017–1025.
(57) Rodrigues, R. C.; Fernandez-Lafuente, R. Lipase from Rhizomucor Miehei as a Biocatalyst in Fats and Oils Modification. *J. Mol. Catal. B Enzym.* **2010**, *66*, 15–32.
(58) Benjamin, S.; Pandey, A. *Candida Rugosa* Lipases: Molecular Biology and Versatility in Biotechnology. *Yeast* **1998**, *14*, 1069–1087.
(59) Kirk, O.; Christensen, M. W. Lipases from *Candida Antarctica*: Unique Biocatalysts from a Unique Origin. *Org. Process Res. Dev.* **2002**, *6*, 446–451.
(60) Villeneuve, P.; Muderhwa, J. M.; Graille, J.; Haas, M. J. Customizing Lipases for Biocatalysis: A Survey of Chemical, Physical and Molecular Biological Approaches. *J. Mol. Catal. - B Enzym.* **2000**, *9*, 113–148.
(61) Grochulski, P.; Li, Y.; Schrag, J. D.; Cygler, M. Two Conformational States of *Candida Rugosa* Lipase. *Protein Sci.* **1994**, *3*, 82–91.
(62) Grochulski, P.; Li, Y.; Schrag, J. D.; Bouthillier, F.; Smith, P.; Harrison, D.; Rubin, B.; Cygler, M. Insights into Interfacial Activation from an Open Structure of *Candida Rugosa* Lipase. *J. Biol. Chem.* **1993**, *268*, 12843–12847.
(63) Willard, L.; Ranjan, A.; Zhang, H.; Monzavi, H.; Boyko, R. F.; Sykes, B. D.; Wishart, D. S. VADAR: A Web Server for Quantitative Evaluation of Protein Structure Quality. *Nucleic Acids Res.* **2003**, *31*, 3316–3319.
(64) Fuentes, M.; Mateo, C.; Guisan, J. M.; Fernández-Lafuente, R.; Palomo, J. M.; Fernández-Lorente, G. General Trend of Lipase to Self-Assemble Giving Bimolecular Aggregates Greatly Modifies the Enzyme Functionality. *Biomacromolecules* **2003**, *4*, 1–6.
(65) Uppenberg, J.; Hansen, M. T.; Patkar, S.; Jones, T. A. The Sequence, Crystal Structure Determination and Refinement of Two Crystal Forms of Lipase B from *Candida Antarctica*. *Structure* **1994**, *15*, 293–308.
(66) Guo, S.; Jańczewski, D.; Zhu, X.; Quintana, R.; He, T.; Neoh, K. G. Surface Charge Control for Zwitterionic Polymer Brushes: Tailoring Surface Properties to Antifouling Applications. *J. Colloid Interface Sci.* **2015**, *452*, 43–53.
(67) Peeler, J. C.; Mehl, R. A. Site-Specific Incorporation of Unnatural Amino Acids as Probes for Protein Conformational Changes. In *Unnatural Amino Acids: Methods and Protocols*; Pollegioni, L., Servi, S., Eds.; Methods in Molecular Biology; Humana Press: Totowa, NJ, 2012; Vol. 794, pp 125–134.
(68) Kawasaki, K.; Kondo, H.; Suzuki, M.; Ohgiya, S.; Tsuda, S. Alternate Conformations Observed in Catalytic Serine of *Bacillus Subtilis* Lipase Determined at 1.3 Å Resolution. *Acta Crystallogr. Sect. D Biol. Crystallogr.* **2002**, *58*, 1168–1174.

Chapter 4 Reduced Enzyme Dynamics upon Multipoint Covalent Immobilization Leads to Stability-Activity Tradeoff

4.1 Abstract

The successful incorporation of enzymes into materials through multipoint covalent immobilization (MPCI) has served as the foundation for numerous advances in diverse fields, including biocatalysis, biosensing, and chemical weapons defense. Despite this success, a mechanistic understanding of the impact of this approach on enzyme stability has remained elusive, which is critical for realizing the full potential of MPCI. Here, we showed that the stabilization of lipase upon MPCI to polymer brush surfaces resulted from the rigidification of the enzyme with an increase in the number of enzyme-brush attachments. This was evident by a 10-fold decrease in the rates of enzyme unfolding and re-folding as well as a reduction of the intrinsic fluctuations of the folded and unfolded states, which was measured by single-molecule (SM) Förster Resonance Energy Transfer imaging. Moreover, our results illuminated an important tradeoff between stability and activity as a function of this decrease in structural dynamics of the immobilized lipase. Notably, as the thermal stability of lipase increased, as indicated by the temperature optimum for activity of the enzyme, the specific activity of lipase decreased. This decrease in activity was attributed to a reduction in the essential motions of the folded state that are required for catalytic turnover of substrate. These results provide direct evidence of this effect, which has long been a matter of speculation. Furthermore, our findings suggest that the retention of activity and stabilization of an enzyme may be balanced by tuning the extent of enzyme attachment.

4.2 Introduction

Beginning with the pioneering work by Klibanov, Halling, Russell, and others on the preparation and use of immobilized enzymes, there has been considerable interest in combining enzymes with materials[1–5]. Of specific interest has been incorporating proteins into or on materials to impart materials with biological activity as well as to enhance enzyme properties (e.g., stability, activity, and even substrate specificity)[6–9]. Examples include the creation of protein and enzyme-containing films and coatings that capture antigens[10–12], resist contamination and fouling[13–15], detoxify organophosphorus nerve agents[16–18], and catalyze industrial chemical transformations[19–21]. Chemical modification and immobilization have also proven useful for the "ruggedization" of enzymes in extreme environments, including non-aqueous media[22–24]. However, despite such efforts, we lack the mechanistic understanding of how various conjugation approaches impact enzyme structure and function[25–27]. This lack of understanding, in turn, prohibits the rational design of enzyme-containing supramolecular structures and assemblies.

One approach for the conjugation of enzymes to materials that has met with practical success involves multipoint covalent immobilization (MPCI)[28–30]. This approach generally entails the covalent coupling of multiple reactive groups on the surface of the enzyme with functional groups either in or on the immobilization support. Notably, the formation of multiple linkages between the enzyme and immobilization support ensures retention of the enzyme (i.e., prevents leaching)[31–33] and has been shown to lead to exceptional enhancements in stability against denaturation by organic solvents[34], elevated temperatures[35], surfactants[36], and other environmental pressures[37]. It has been proposed that this enhancement in stability is due to a restriction in the mobility of the enzyme, which, in turn, suppresses unfolding[38–40]. However, in the absence of biophysical methods to characterize the impact of MPCI on enzyme dynamics, the mechanistic understanding for this stabilizing effect remains elusive. Specifically, to understand this

mechanism, it is necessary to determine how varying the number of attachments impacts enzyme structure and dynamics. Moreover, given that changes in enzyme dynamics may adversely impact enzyme activity[41–43], it is plausible that there is an inherent balance between increased stability and decreasing activity that is dependent on the number of covalent attachments.

In recent work, we demonstrated the potential of single-molecule (SM) methods based on intramolecular Förster resonance energy transfer (FRET) to directly characterize the structural dynamics of enzymes immobilized to polymer brushes as well as lipid bilayers[44,45]. These methods, which involve measuring dynamic changes in FRET, molecule-by-molecule, via wide-field total internal reflection fluorescence (TIRF) imaging, enable the observation of unfolding and re-folding of individual enzymes. From these conformational transitions, the rates associated with unfolding and re-folding may be quantified for 10^3-10^5 molecules per experiment[46]. In addition to quantifying the rates associated with conformational transitions, structural fluctuations within a given conformational state may be resolved. For example, dynamic fluctuations of the folded and unfolded states are, in principle, determined by analyzing the variability of the FRET signature for each state[47–49]. Importantly, while these methods lack the temporal resolution to observe ultrafast dynamics, including side-chain rotation, loop motions, and tumbling, analysis of variability in FRET can provide information about large collective motions (e.g., domain motions)[41]. As such, such methods offer tremendous potential for elucidating the impact of immobilization within materials on enzyme dynamics as well as on structural stability.

In this work, we investigated the stabilization of the *Bacillus subtilis* lipase A (lipA), an industrially important enzyme[50,51], by MPCI to polymer brushes composed of poly(sulfobetaine methacrylate) (PSBMA). While varying the number of covalent tethers between lipA and the brush layer, the impact of attachment number on the temperature dependence of the activity and stability

of lipA was determined. Additionally, SM-FRET analysis was used to paint a comprehensive picture of the collective structural dynamics of lipA (i.e., the unfolding and re-folding rates as well as the structural dynamics of the folded and unfolded states) as a function of number of covalent interactions. By providing information about the correlation of dynamics and crosslinking, these findings provided unique insights into the mechanism of enzyme stabilization via MPCI. Furthermore, these results demonstrate an intrinsic trade-off between stabilization and the loss of activity due to a decrease in enzyme flexibility. Such findings suggest there may be an optimum number of attachments that enhance stability while minimizing the loss of activity, which is crucial for improving enzyme utility.

4.3 Results

4.3.1 Immobilization of LipA to PSBMA Brush-Modified Particles

To investigate the impact of the number of attachments on the stability of the immobilized enzyme, PSBMA brushes containing methacrylic acid *N*-hydroxysuccinimide ester (NHS) were synthesized on 1 μm silica particles. Using surface-initiated atom transfer radical polymerization, the brushes were grown with a 1%, 5%, or 10% molar ratio of NHS-to-sulfobetaine methacrylate in the reaction feed. LipA was subsequently immobilized within the brush layer via reaction between primary amines on the enzyme surface and the NHS groups within the brush layer. With up to 12 primary amines on the surface of lipA that may react, a single enzyme molecule may be immobilized at multiple sites on the enzyme's surface (Figure 4-1a)[52]. The amount of lipA immobilized on the brush surfaces was consistent with monolayer coverage (8 mg enzyme per g silica support, Figure E-1) and was independent of the molar ratio of NHS-to-sulfobetaine methacrylate within the brush.

By varying the molar ratio of NHS-to-sulfobetaine methacrylate within the brush, the extent of MPCI of lipA to the brush layer was controlled. This was confirmed via titrating the number of residual amines on the enzyme surface that did not react with NHS groups within the brush layer with fluorescamine. As expected, the average number of covalent attachments per enzyme molecule ($\bar{n}$), which was determined from the difference in the number of free amines for the soluble and immobilized enzyme, increased with increasing NHS concentration in the brush (Figure 4-1b). Specifically, the value of $\bar{n}$ for supports synthesized with 1%, 5%, and 10% NHS was 1.1, 2.1, and 4.8, respectively. Given the non-site-specific nature of the immobilization reaction and the random distribution of amine groups on the surface of lipA, it is expected that the immobilization was heterogeneous with respect to the number and location of cross-linking sites. As such, the orientation of lipA relative to the brush surface likely varied between enzyme molecules even within the same brush surface. The orientation of individual immobilized lipA molecules may also be influenced by the dynamic nature of the brush layer, which stems from the mobility of the polymer chains when hydrated. Notably, although randomly distributed over the surface of lipA, none of the primary amines that may participate in the immobilization reaction are within 1.5 nm of the active site of the enzyme.

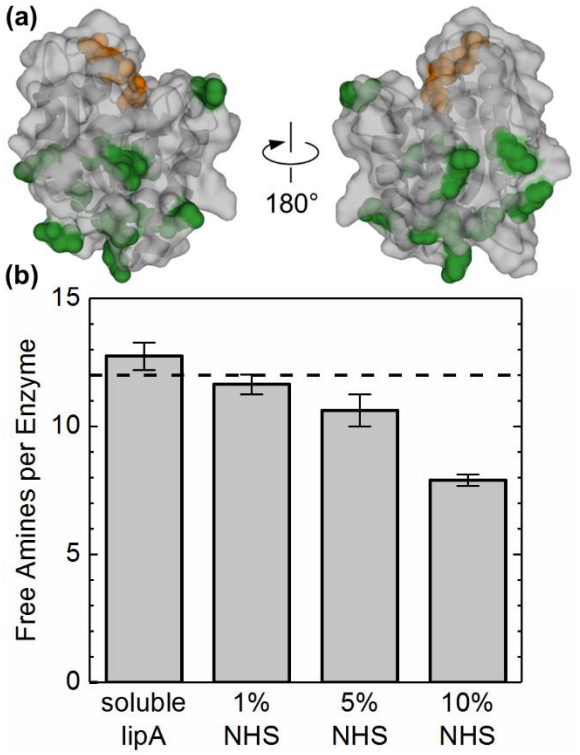

Figure 4-1: Extent of MPCI of lipA on silica particles functionalized with PSBMA brushes. (a) Structure of lipA (PDB ID: 1ISP) showing the possible sites of immobilization as well as the active site. The ε-amine of lysines and the N-terminal amine, which represent potential sites for covalent attachment, are colored green. Additionally, the catalytic triad in the active site is colored orange. (b) The number of primary amines per enzyme for soluble and immobilized lipA determined by titration with fluorescamine. The difference between the number of amines in the soluble enzyme and the remaining amines after immobilization to the brush surfaces with varying concentration of NHS groups indicated the number of covalent attachments per enzyme. The dashed line represents the number of theoretical primary amines per enzyme molecule (12) based on the sequence of lipA. Error bars represent the standard deviation from three independent measurements.

4.3.2 Immobilized LipA Stability on PSBMA Brush-Modified Particles

The stability of immobilized lipA as a function of the number of attachment sites was characterized by measuring the temperature-dependence of immobilized lipA activity. The hydrolytic activity of immobilized lipA as well as soluble lipA was assayed over a broad temperature range using resorufin butyrate as the substrate. As shown in Figure 4-2a, a systematic increase in the temperature optimum for immobilized lipA was observed with increasing $\bar{n}$,

suggesting increased stability. Notably, the temperature optimum increased from 50°C to 55°C to 70°C as $\bar{n}$ increased from 1.1 to 2.1 to 4.8. For comparison, the temperature optimum for soluble lipA was only 30°C. Additionally, at the optimum temperature, the specific activity of immobilized lipA was 20-fold higher than for soluble lipA for all three values of $\bar{n}$. This increase was consistent with results from our previous studies in which lipA was immobilized to PSBMA as well as poly(poly(ethylene glycol) methacrylate) brushes without controlling $\bar{n}$.[44] As a further measure of stability, the retention of immobilized and soluble activity as a function of time when incubated at 50ºC was also measured. As with the temperature optimum, the retention of activity increased systematically with $\bar{n}$ (Figure 4-2b). Specifically, as $\bar{n}$ increased, the activity of immobilized lipA was retained for longer times, which also indicated enhanced stability. Remarkably, for the brush surface with $\bar{n}$ = 4.8, the enzyme retained approximately 90% of its initial activity after 24 h. This was especially impressive given that soluble lipA was inactivated immediately (i.e., within the first minute) at this temperature. To the best of our knowledge, this represents the first time that the stability of an immobilized enzyme has been directly measured as a function of the number of attachment sites.

In addition to showing the impact of number of attachment sites on stability, our results reveal an interesting tradeoff between stability and activity for immobilized lipA. Specifically, as the stability of immobilized lipA increased with increasing $\bar{n}$, the specific activity of immobilized lipA decreased. This was particularly evident by comparing the specific activity of lipA immobilized on the different brush surfaces in Figure 4-2a between 40°C and 50°C. As can be seen within this range, the specific activity of immobilized lipA was greatest for the brush surface on which the lipA had the lowest temperature optimum. Conversely, the specific activity of immobilized lipA was the lowest for the brush surface on which lipA had the highest temperature

optimum. Such a tradeoff between stability and activity with increasing $\bar{n}$ may be attributed to a decrease in conformational dynamics of the immobilized enzyme. For example, a decrease in conformational dynamics may make the enzyme more resistant to unfolding yet prevent the full range and scope of motions required for catalytic turnover of the substrate. A similar explanation is often used to explain how mutations that improve stability are often detrimental to activity in enzymes that are naturally evolved or engineered[53–55]. Although the reduced activity could also be associated with increased unfolding of lipA, the average folded fraction of immobilized lipA was the same for all values of $\bar{n}$ as discussed below. Moreover, we confirmed that differences in mass transport effects over the range of $\bar{n}$ employed was negligible by measuring the apparent Michaelis constant (i.e., K_M) for lipA immobilized each support (Figure E-2).

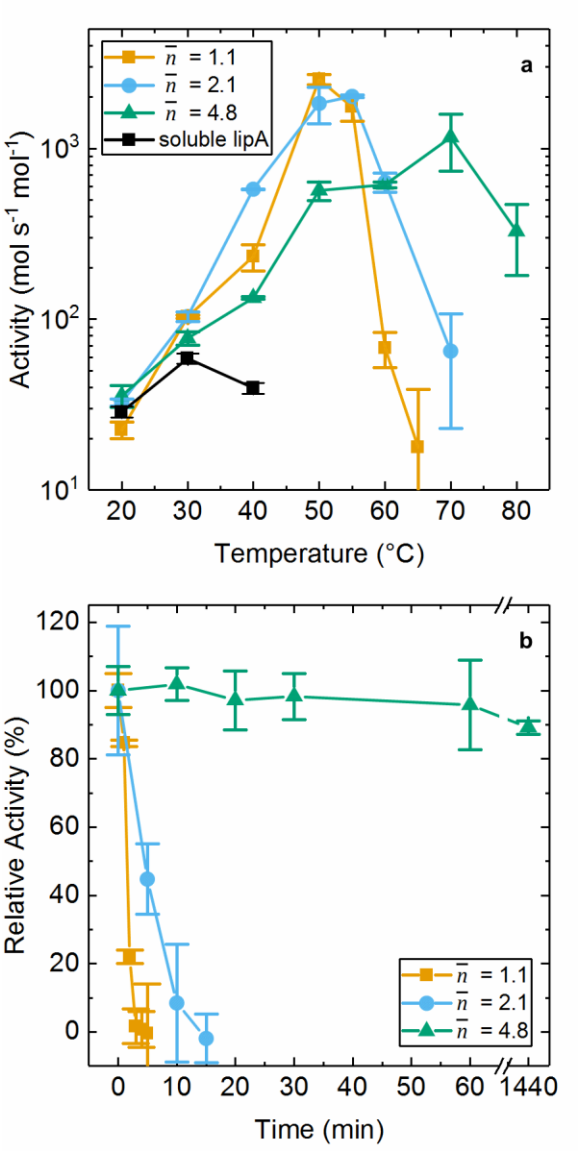

Figure 4-2: Impact of the number of attachments per enzyme molecule on (a) the temperature dependence of lipA activity and (b) the retention of lipA activity at 50°C. The temperature dependence and retention of lipA activity were measured for $\bar{n}$ = 1.1 (yellow squares), $\bar{n}$ = 2.1 (blue circles), and $\bar{n}$ = 4.8 (green triangles), where $\bar{n}$ represents the average number of attachment sites per enzyme. For temperature dependence measurements, activity is expressed as moles of product formed per second per mole of enzyme. Additionally, relative activity was determined by normalizing the activity after incubation to the activity at time zero. Error bars represent the standard deviation of the mean from three independent measurements.

4.3.3 Immobilized LipA Unfolding and Re-folding Kinetics

To elucidate the basis for the apparent stabilization as well as loss of activity of immobilized lipA with increasing $\bar{n}$, the *in situ* dynamics of immobilized lipA was measured by SM-FRET imaging. As a technique for studying the dynamics of proteins, including enzymes, on surfaces, SM-FRET imaging is extremely powerful as recently demonstrated in numerous reports[47–49]. We have previously showed that SM-FRET imaging can be used to quantify the kinetics of unfolding and re-folding of enzymes immobilized to various types of surfaces[44–46]. Notably, the quantification of unfolding and re-folding rates has been instrumental in uncovering the mechanisms by which immobilization to various types of surfaces impacts enzyme stability. Through quantifying these rates, we recently demonstrated how the stability of immobilized lipA on polymer brushes can be affected by the underlying brush chemistry[44].

For SM-FRET analysis of the dynamics of immobilized lipA, a lipA construct that was previously engineered to permit site-specific donor and acceptor labeling was used. In addition to the sensitivity of the FRET signal of this construct to lipA structure, this construct has similar activity and stability to wild-type lipA[44]. Polymer brushes were prepared for SM imaging on fused silica wafers using the same immobilization chemistry for the FRET-labeled construct as described above for the immobilization of lipA on silica particles. Monolayer coverage of the enzyme was maintained by immobilizing 10^{-10} M FRET-labeled lipA with 5.0×10^{-10} M wild-type lipA. Upon immobilization of FRET-labeled lipA, enzyme molecules on the brush surface were illuminated by alternative laser excitation, enabling unambiguous identification of properly labeled molecules and of acceptor photobleaching events[56]. Temporal trajectories of the donor and acceptor intensities for each molecule were collected and segmented based on folding state (i.e., folded or unfolded). The folding state of each molecule at any given time was determined from quantitative

analysis of the distribution of donor and acceptor intensities for every observation in every trajectory. Figure E-3 shows the distributions of donor and acceptor intensities for each immobilization condition (i.e., $\bar{n}$ = 1.1, 2.1, and 4.8) at 20ºC and 45ºC in which two distinct states are observed; a high-FRET state with high acceptor and low donor emission, which corresponds to a compact, folded state, and a low-FRET state with low acceptor and high donor emission, which corresponds to an unfolded state. The Table E-1 shows the number of trajectories collected for each immobilization condition, which ranged between 1645 and 2930.

As expected, the magnitude of the conformational dynamics of immobilized lipA decreased significantly with increasing $\bar{n}$, which is consistent with an increase in the rigidification of the immobilized enzyme. This was evident by a reduction in the fraction of immobilized lipA molecules that underwent an unfolding or re-folding transition prior to photobleaching as $\bar{n}$ increased (Figure 4-3a). As $\bar{n}$ increased from 1.1 to 4.8, the fraction of immobilized lipA molecules that underwent a conformation transition decreased from 16.3% to 6.0%, respectively. Moreover, similar trends with $\bar{n}$ were observed in the analysis of the unfolding (k_u) and re-folding (k_f) rate constants for immobilized lipA (Figure 4-3b). The values of k_u and k_f were estimated from a Markov chain model of every observation in each trajectory collected, which accounted for changes in folding state as well as heterogeneity between molecules, as described previously[46]. Specifically, k_u decreased from 0.19 s^{-1} to 0.03 s^{-1} while k_f decreased from 1.4 s^{-1} to 0.05 s^{-1} over the range of $\bar{n}$ characterized. Such a decrease in k_u with $\bar{n}$ indicates the apparent stabilization of lipA was at least in part due to an increase in the kinetic barrier associated with unfolding (i.e., folded molecules are kinetically trapped in their native state). Although the decrease in k_f with $\bar{n}$ indicates that unfolded molecules also re-folded more slowly, this effect was presumably offset by the reduction in k_u. Notably, the adverse impact of $\bar{n}$ on k_f has potentially important implications

in attempting to re-nature an immobilized enzyme after unfolding. Furthermore, it was interesting that the greatest difference in k_u and k_f occurred between $\bar{n}$ values of 1.1 and 2.1. This suggests that the addition of a second covalent linkage had a much greater impact on conformational dynamics relative to the addition of subsequent linkages.

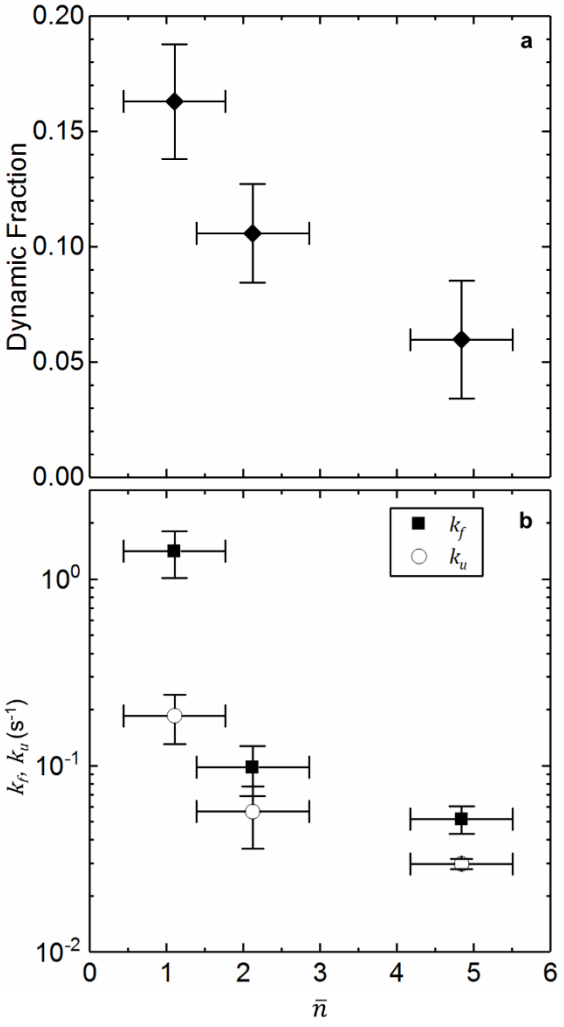

Figure 4-3: SM dynamics of lipA unfolding and re-folding at 20ºC. (a) Fraction of immobilized lipA molecules that underwent an unfolding or re-folding transition before photobleaching as a function of $\bar{n}$. (b) Rate constants for unfolding (k_u, open circles) and re-folding (k_f, solid squares) of immobilized lipA based on maximum likelihood estimation of conformational dynamics from SM trajectories. Y-axis error bars represent the standard error, which were estimated using jackknife re-sampling with replacement of trajectories for each condition. X-axis error bars represent standard deviation from propagated errors of the data in Figure 4-1.

4.3.4 Structural Fluctuations of Immobilized LipA

The impact of $\bar{n}$ on the dynamics of immobilized lipA was further examined by quantifying the structural fluctuations of the folded and unfolded states from SM-FRET trajectories. Such fluctuations differ from large scale conformational transitions (e.g., unfolding or re-folding) in that they represent microscopic motions within a given conformational state. Motions within the folded state may be particularly critical for an enzyme given their frequent role in substrate binding as well as the catalytic mechanism of many enzymes[41–43]. Additionally, the loss of entropy of the folded state due to the restriction of such motions can negatively impact enzyme stability if greater than the entropy loss of the unfolded state[57]. These intrinsic motions were quantified by characterizing deviations in the relative fluorophore-to-fluorophore distance, $d = \left(\frac{I_D}{I_A}\right)^{\frac{1}{6}}$, for SM-FRET trajectories of molecules that were always folded or always unfolded, where I_D and I_A represent the instantaneous intensity in the donor and acceptor channels, respectively. A dimensionless parameter, d is proportional to the distance between fluorophores by the Förster radius, R_0, which is ~5.1 nm for the donor (Alexa Fluor 555) and acceptor (Alexa Fluor 647) pair with unhindered rotation in water. The dynamics of fluorophore rotation were assumed to be isotropic and sufficiently averaged over the acquisition time of each observation, in accordance with recent SM measurements of fluorophore anisotropy in similar polymer brush environments[58]. Additionally, given the acquisition time of our measurements, we were unable to measure fluctuations in d on timescales of less than 200 ms. However, the sampling of dynamics at the timescale measured here provided a relative measure of the effect of $\bar{n}$ on the magnitude of structural fluctuations. As an example of the type of dynamics measured here, the fluctuations in

I_D and I_A for a molecule of immobilized lipA that is always folded is shown in Figure 4-4a. The fluctuations in instantaneous I_D and I_A were used to generate the distribution of d-values for each trajectory from which the root-mean-square deviation (RMSD) of d was determined (Figure 4-4b and c).

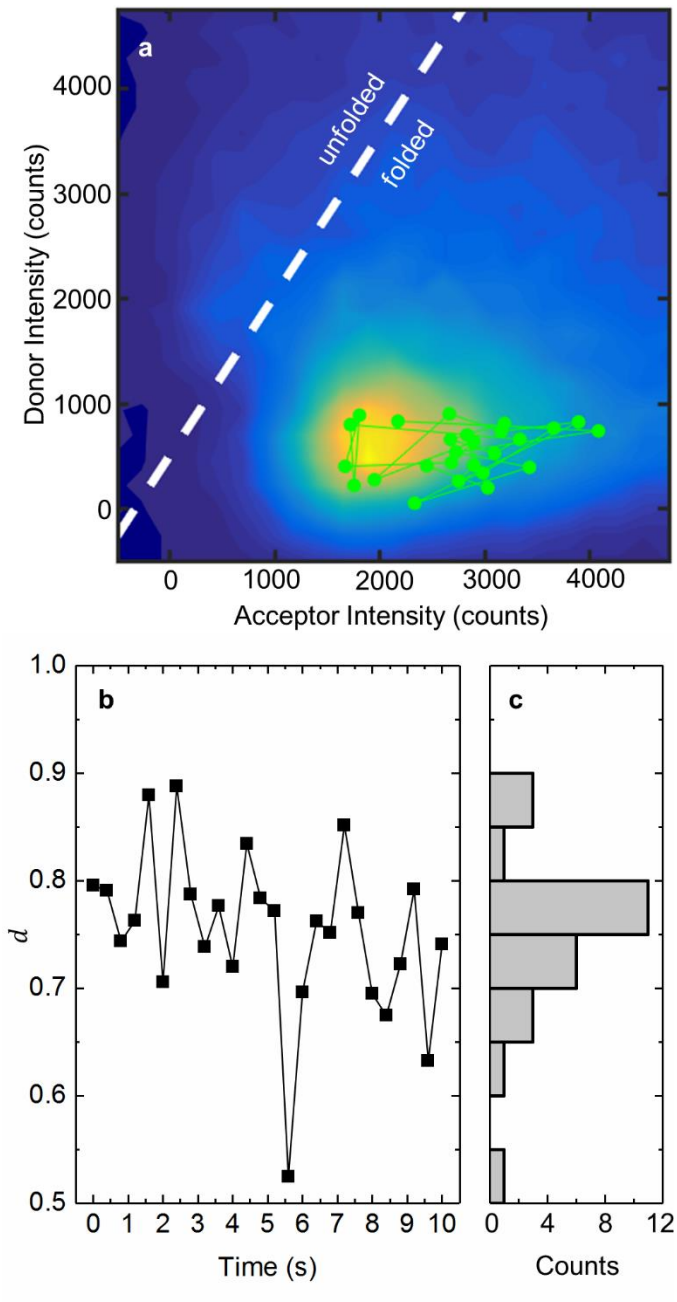

Figure 4-4: Analysis of the structural fluctuations of immobilized lipA by SM-FRET. (a) Two-dimensional donor-acceptor intensity histogram of all SM-FRET observations of immobilized lipA for a given condition. Representative time series of donor and acceptor intensities for a folded, immobilized lipA molecule. (b) Corresponding d-value timeseries for the same trajectory. (c) The distribution of d-values for this representative trajectory. From this distribution, the RMSD in d were calculated for this trajectory.

To determine the impact of $\bar{n}$ on the folded and unfolded state dynamics of immobilized lipA, the distributions of RMSD of d for always folded and unfolded trajectories were analyzed. Figure E-4 shows the distribution of the RMSD of d for each state for different values of $\bar{n}$ at 20ºC and 45ºC for 117 – 706 trajectories (see Table E-2 for details of the number of trajectories analyzed for each surface and temperature). Importantly, as apparent in the distribution of the compiled trajectories, the values of the observed RMSD of d were generally greater than that expected based on the uncertainties in I_D and I_A (Figure E-4). Analysis of the distributions clearly showed that, as $\bar{n}$ increased, the intrinsic microscopic dynamics of the folded and unfolded states decreased at both temperatures. This was evident by comparing the median of the distributions of the RMSD of d of both states as a function of $\bar{n}$ (Figure 4-5a and b). For the folded state, the median RMSD of d decreased from 0.124 to 0.073 at 45 ºC and from 0.088 to 0.058 at 20 ºC as $\bar{n}$ increased from 1.1 to 4.8. For the unfolded state, the median RMSD of d decreased from 0.190 to 0.129 at 45 ºC and from 0.199 to 0.103 at 20 ºC, over the same range of $\bar{n}$. The decrease in median RMSD of d for both states with $\bar{n}$ was consistent with the rigidification of lipA based on the impact of $\bar{n}$ on k_u and k_f. Additionally, as for k_u and k_f, the change in the median RMSD of d for both states (at both temperatures) was the greatest as $\bar{n}$ increased from 1.1 to 2.1. This finding further underscores the impact of a second covalent linkage on enzyme dynamics relative to subsequent linkages.

While the dynamics discussed in the previous section explain the change in lipA stability with $\bar{n}$, the dynamics discussed here explain the change in lipA activity with $\bar{n}$. Specifically, the reduction in the intrinsic dynamics of the folded as a function of $\bar{n}$ explain how increasing $\bar{n}$ can lead to a loss of activity as observed previously (Figure 4-1). This represents, as far as the authors are aware, the first direct observation of immobilized enzyme dynamics and the effects of dynamics on activity, which was made possible through SM methods.

To confirm that the loss of apparent activity as a function of $\bar{n}$ was not due to changes in structural stability, the steady-state fraction of folded lipA molecules for all values of $\bar{n}$ between 20 ºC and 45 ºC was analyzed (Figure E-5). Notably, the steady-state fraction of folded lipA over this temperature range was constant, suggesting the extent of unfolding of lipA for all conditions was virtually the same. Moreover, although the magnitude of the decrease in RMSD of d with increasing $\bar{n}$ was similar for both the folded and unfolded state, the decrease in conformational entropy of the unfolded state was presumably greater than that for the folded state. Therefore, the apparent reduction in intrinsic dynamics likely also contributed to an increase in the thermodynamic stability of the immobilized enzyme. Although not explored here, the extent of the thermodynamic stabilization of lipA as a result of this effect may be determined using molecular dynamics simulations.

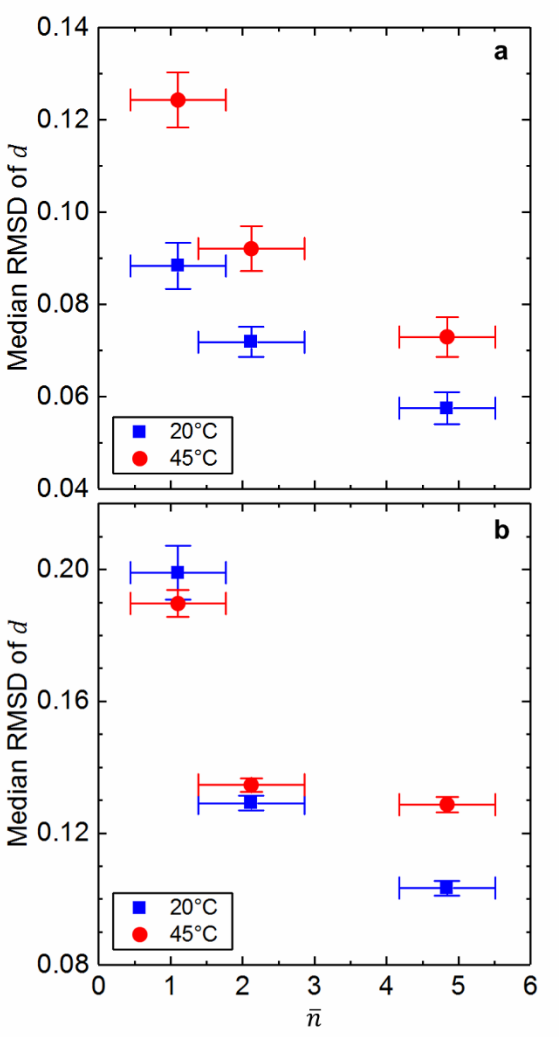

Figure 4-5: Thermal fluctuations of the (a) folded and (b) unfolded states of immobilized lipA as a function of $\bar{n}$ at 20ºC (blue squares) and 45ºC (red circles). The thermal fluctuations of each trajectory were determined from the root-mean-square deviation (RMSD) of the dimensionless distance parameter, d, which represents the relative fluorophore-to-fluorophore separation. The median RMSD of d was calculated from the distributions of RMSDs for a given condition. Y-axis error bars represent the standard deviation of the median RMSD obtained from 1000 bootstrap samples of the RMSD of d distributions. X-axis error bars represent the propagated error of $\bar{n}$ from the data in Figure 4-1b.

To complement the analysis of the RMSD of d, the Hookean spring constant distributions were calculated for each folded and unfolded trajectory of immobilized lipA (Figure E-6). This analysis was intended to provide a more physical interpretation of the impact of $\bar{n}$ on the dynamics of the folded and unfolded states by quantifying rigidity of the enzyme. Spring constants were

calculated at 20 ºC based on equipartition assuming a quadratic potential energy well, $\frac{1}{2}k_{spring}\langle x^2\rangle = \frac{1}{2}k_B T$, where k_{spring} is the spring constant, $\langle x^2\rangle$ is the second moment of distance fluctuations obtained by multiplying d values by R_0 (5.1 nm), k_B is the Boltzmann constant, and T is the temperature. This calculation was analogous to the determination of the stiffness of an optical trap or an atomic force microscope cantilever, except that the dynamics of proteins at these temperatures were likely not purely harmonic and, therefore, this represents an approximation of apparent stiffness[59–61]. As expected from rigidification, the median spring constant of the calculated distributions increased from 27 to 55 mN/m for the folded state and from 10 to 17 mN/m for the unfolded state with increasing $\bar{n}$ (**Figure 6**). Interestingly, the folded state stiffness appeared linear with increasing $\bar{n}$ while the unfolded state stiffness was nonlinear, with no significant increase between $\bar{n}$ = 1.1 and $\bar{n}$ = 2.1. Notably, the spring constants measured here were lower than those obtained from neutron scattering of hydrated protein powders (~0.1 N/m)[60] as well as crystallographic experiments (~1 N/m)[62]. This is perhaps not surprising given the difference in local environment of the protein when immobilized in a brush compared to in a powder or crystal.

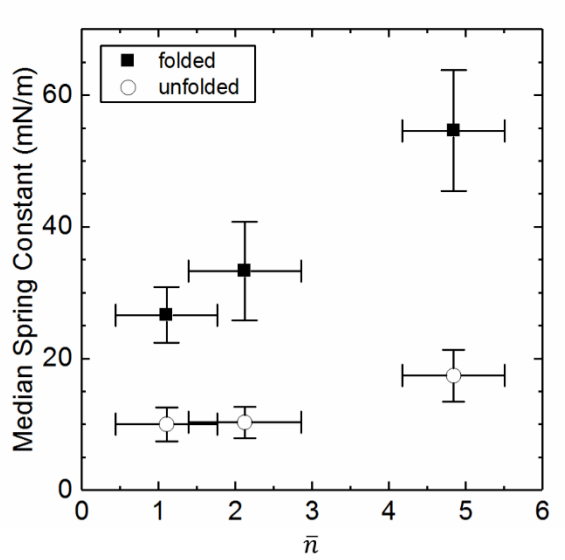

Figure 4-6: Estimated Hookean spring constants for folded (black squares) and unfolded (open circles) lipA from SM structural dynamics as a function of $\bar{n}$ at 20ºC. The Hookean spring constants for the folded and unfolded states are expressed as millinewtons per meter. Y-axis error bars represent the standard error from 1000 bootstrap samples of the underlying distribution of spring constants for each condition. X-axis error bars represent the propagated error of $\bar{n}$ from the data in Figure 4-1.

4.4 Conclusions

By combining stability assays with SM measurements of immobilized enzyme dynamics, we uncovered the mechanistic basis for the stabilization of lipA by MPCI. Our results showed that, as the number of enzyme-brush attachments increased, the stability of lipA increased, which directly correlated with the rigidification of the enzyme. The direct measurement of enzyme rigidification was enabled using dynamic SM-FRET methods, which permitted the *in situ* measurement of immobilized enzyme dynamics. Through SM-FRET imaging, we showed that the rates of enzyme unfolding and re-folding as well as the intrinsic fluctuations of the folded and unfolded states decreased as the number of enzyme-brush attachments increased. While elucidating this effect, our results shed light on the tradeoff between activity and stability of immobilized lipA, which has important practical implications. Notably, as stability increased, the

specific activity of the enzyme decreased, which could be attributed to the loss of intrinsic dynamics of the folded state. This suggests there is an optimum number of attachments for both the preservation of activity and the enhancement of stability, which may be enzyme-dependent. Importantly, although polymer brush surfaces were used in this study as the immobilization support, these findings may presumably be extended to other types of immobilization supports, including polymer coatings, foams, and hydrogels, where the enzyme may be directly reacted into the polymer network via MPCI (e.g., by including the enzyme as a monomer in the polymerization reaction). Such understanding may ultimately impact a myriad of fields where the marriage of enzymes and materials is beneficial, including biocatalysis, drug delivery, biosensing, and in medical devices.

4.6 Methods

4.6.1 Preparation and Immobilization of LipA on PSBMA Brushes

Polymer brush supports for lipA immobilization were prepared via surface-initiated atom transfer radical polymerization as described previously. Briefly, either silica particles (1 μm diameter, Nanocym) or fused silica wafers (2 in) were initially cleaned and functionalized with a monolayer of chloromethylphenyltrichlorosilane. For the polymerization reaction, a 100-x:x:5:2:0.2 molar ratio of [2-(methacryloyloxy)ethyl]dimethyl-(3-sulfopropyl)-ammonium hydroxide (sulfobetaine methacrylate), methacrylic acid *N*-hydroxysuccinimide ester (NHS), 2,2′-bipyridine, copper (I) chloride, and copper (II) chloride was used, where x was 1, 5, or 10 for the 1% NHS, 5% NHS, and 10% NHS conditions, respectively, and trifluoroethanol was used as the solvent. For ellipsometry measurements to determine brush thickness, silicon wafers with native

oxide coatings were used. Modification of flat surfaces was further confirmed via sessile drop contact angle goniometry. All surfaces exhibited a water contact angle less than 10º and a dry thickness between 16 and 22 nm (Figure E-7) as measured using ellipsometry. For the particle system, the average number of covalent attachments per enzyme was determined with fluorescamine. A calibration curve (Figure E-8) correlating the concentration of amines with measured fluorescence was generated using purified lysine standards (Research Products International, Inc.) and measured with a plate reader with fluorescence (Infinite M Plex, Tecan) by measuring fluorescence emission at 470 nm with excitation at 365 nm.

For ensemble activity measurements and quantification of enzyme loading, lipA was immobilized to the brush surfaces via incubating wild-type lipA ($5x10^{-5}$ M) with 100 mg of dry, functionalized particles in 1 mL of 50 mM sodium phosphate buffer (pH 7.5) for 24 h at room temperature. Particles were sedimented via centrifugation at 1000 x g for 5 min after which the amount of enzyme immobilized on the particles was determined via a mass balance from assaying the activity of enzyme in the supernatant. For SM-FRET imaging, FRET-labeled lipA ($1.0x10^{-10}$ M) was immobilized on the brush-modified silica surfaces along with wild-type lipA ($5.0x10^{-5}$ M) to yield approximately monolayer coverage of the enzyme. After loading, the wafers were rinsed thoroughly with buffer before imaging to remove any enzyme that was non-covalently immobilized on the brush surface.

4.6.2 Characterization of Immobilized LipA Activity and Stability

The activity of lipA immobilized on particles was assayed with the substrate resorufin butyrate (10 µM) in 50 mM sodium phosphate (pH 7.5) in a Fluoromax-4 (Horiba) fluorimeter between 20-80 ºC with mixing in the cuvette holder. Activity was determined from the slope of the initial rate of the hydrolysis of resorufin butyrate by continuously monitoring emission at 593

nm with excitation at 570 nm and expressed on a mole product per second per mole enzyme basis. Moles of product was determined by measuring the fluorescence of purified resorufin standards under the same fluorometer conditions. Background hydrolysis in the absence of enzyme was subtracted for each temperature. To determine the temperature dependence of activity for lipA, the substrate and buffer were initially equilibrated to the desired temperature after which the enzyme (either immobilized or free) was added to the assay solution. Additionally, thermoinactivation of lipA was followed by periodically assaying the activity of free or immobilized lipA, which was incubated in 50 mM sodium phosphate (pH 7.5) at 50 ºC.

4.6.3 SM-FRET Imaging and Analysis

Briefly, SM-FRET trajectories were collected via alternating laser excitation with a 200 ms imaging acquisition time using a custom-built prism-based TIRF microscope with a 50 mW 532 nm DPSS laser (Cobolt, Samba) and a 50 mW 640 nm DPSS laser (Crystalaser). Emission from FRET-labeled lipA was separated using a dichroic mirror with a nominal separation wavelength of 610 nm (model T610LPXR, Chroma). Donor and acceptor emissions were further cleaned with a 585 nm bandpass filter with a bandwidth of 29 nm (Semrock) and a 685 nm bandpass filter with bandwidth of 40 nm (Semrock), respectively, and projected onto different regions of an Andor iXon3 888 EMCCD camera. Channel registration, object identification, and intensity quantification were performed with custom MATLAB software. Notably, trajectories were truncated at the moment of donor or acceptor photobleaching, and a two-state conformational model was used to assign each SM observation to either a folded or unfolded state (Figure E-3). Calculations of unfolding and re-folding rate constants are described elsewhere and account for static heterogeneity among molecules[46]. Root-mean-square deviations of folded and unfolded states was determined via analysis of timeseries of d values for trajectories that did not undergo a

structural transition. RMSDs were calculated on a per trajectory basis, and the distributions of RMSDs for each condition can be found in Figure E-4.

4.7 References

(1) Klibanov, A. M. Immobilized Enzymes and Cells as Practical Catalysts. *Science (80-.).* **1983**, *219* (4585), 722–727. https://doi.org/10.1126/science.219.4585.722.

(2) Klibanov, A. M. Enzyme Stabilization by Immobilization. *Anal. Biochem.* **1979**, *93*, 1–25. https://doi.org/10.1016/0076-6879(88)37055-2.

(3) Zacharis, E.; Moore, B. D.; Halling, P. J. Control of Enzyme Activity in Organic Media by Solid-State Acid−Base Buffers. *J. Am. Chem. Soc.* **1997**, *119* (50), 12396–12397. https://doi.org/10.1021/ja972635c.

(4) LeJeune, K. E.; Wild, J. R.; Russell, A. J. Nerve Agents Degraded by Enzymatic Foams. *Nature* **1998**, *395* (6697), 27–28. https://doi.org/10.1038/25634.

(5) Yang, Z.; Mesiano, A. J.; Venkatasubramanian, S.; Gross, S. H.; Harris, J. M.; Russell, A. J. Activity and Stability of Enzymes Incorporated into Acrylic Polymers. *J. Am. Chem. Soc.* **1995**, *117* (17), 4843–4850. https://doi.org/10.1021/ja00122a014.

(6) Mateo, C.; Grazu, V.; Palomo, J. M.; Lopez-Gallego, F.; Fernandez-Lafuente, R.; Guisan, J. M. Immobilization of Enzymes on Heterofunctional Epoxy Supports. *Nat. Protoc.* **2007**, *2* (5), 1022–1033. https://doi.org/10.1038/nprot.2007.133.

(7) Brzozowski, A. M.; Derewenda, U.; Derewenda, Z. S.; Dodson, G. G.; Lawson, D. M.; Turkenburg, J. P.; Bjorkling, F.; Huge-Jensen, B.; Patkar, S. A.; Thim, L. A Model for Interfacial Activation in Lipases from the Structure of a Fungal Lipase-Inhibitor Complex. *Nature* **1991**, *351* (6326), 491–494. https://doi.org/10.1038/351491a0.

(8) Fernández-Lorente, G.; Palomo, J. M.; Cabrera, Z.; Guisán, J. M.; Fernández-Lafuente, R. Specificity Enhancement towards Hydrophobic Substrates by Immobilization of Lipases by Interfacial Activation on Hydrophobic Supports. *Enzyme Microb. Technol.* **2007**, *41* (5), 565–569. https://doi.org/10.1016/j.enzmictec.2007.05.004.

(9) Bornscheuer, U. T.; Huisman, G. W.; Kazlauskas, R. J.; Lutz, S.; Moore, J. C.; Robins, K. Engineering the Third Wave of Biocatalysis. *Nature* **2012**, *485* (7397), 185–194. https://doi.org/10.1038/nature11117.

(10) Singh, P. SPR Biosensors: Historical Perspectives and Current Challenges. *Sensors Actuators, B Chem.* **2016**, *229*, 110–130. https://doi.org/10.1016/j.snb.2016.01.118.

(11) Vaisocherová, H.; Zhang, Z.; Yang, W.; Cao, Z.; Cheng, G.; Taylor, A. D.; Piliarik, M.; Homola, J.; Jiang, S. Functionalizable Surface Platform with Reduced Nonspecific Protein Adsorption from Full Blood Plasma-Material Selection and Protein Immobilization Optimization. *Biosens. Bioelectron.* **2009**, *24* (7), 1924–1930. https://doi.org/10.1016/j.bios.2008.09.035.

(12) Knecht, S.; Ricklin, D.; Eberle, A. N.; Ernst, B. Oligohis-Tags: Mechanisms of Binding to Ni2+-NTA Surfaces. *J. Mol. Recognit.* **2009**, *22* (4), 270–279. https://doi.org/10.1002/jmr.941.

(13) Haag, R.; Neffe, A. T.; Wischke, C.; Ballauff, M.; Lendlein, A.; Dzubiella, J.; Becherer, T.; Angioletti-Uberti, S.; Wei, Q. Protein Interactions with Polymer Coatings and Biomaterials. *Angew. Chemie Int. Ed.* **2014**, *53* (31), 8004–8031. https://doi.org/10.1002/anie.201400546.

(14) Tugulu, S.; Arnold, A.; Sielaff, I.; Johnsson, K.; Klok, H. A. Protein-Functionalized Polymer Brushes. *Biomacromolecules* **2005**, *6* (3), 1602–1607. https://doi.org/10.1021/bm050016n.
(15) Gautrot, J. E.; Huck, W. T. S.; Welch, M.; Ramstedt, M. Protein-Resistant NTA-Functionalized Polymer Brushes for Selective and Stable Immobilization of Histidine-Tagged Proteins. *ACS Appl. Mater. Interfaces* **2010**, *2* (1), 193–202. https://doi.org/10.1021/am9006484.
(16) Richins, R. D.; Kaneva, I.; Mulchandani, A.; Chen, W. Biodegradation of Organophosphorus Pesticides by Surface-Expressed Organophosphorus Hydrolase. *Nat. Biotechnol.* **1997**, *15*, 984–987.
(17) Mansee, A. H.; Chen, W.; Mulchandani, A. Detoxification of the Organophosphate Nerve Agent Coumaphos Using Organophosphorus Hydrolase Immobilized on Cellulose Materials. *J. Ind. Microbiol. Biotechnol.* **2005**, *32* (11–12), 554–560. https://doi.org/10.1007/s10295-005-0059-y.
(18) Mulchandani, A.; Kaneva, I.; Chen, W. Detoxification of Organophosphate Nerve Agents by Immobilized Escherichia Coli with Surface-Expressed Organophosphorus Hydrolase. *Biotechnol. Bioeng.* **1999**, *63* (2), 216–223. https://doi.org/10.1002/(SICI)1097-0290(19990420)63:2<216::AID-BIT10>3.0.CO;2-0.
(19) Schmid, A.; Dordick, J. S.; Hauer, B.; Kiener, A.; Wubbolt, M.; Witholt, B. Industrial Biocatalysis Today and Tomorrow. *Nature* **2001**, *409* (January), 258–268.
(20) Pollard, D. J.; Woodley, J. M. Biocatalysis for Pharmaceutical Intermediates: The Future Is Now. *Trends Biotechnol.* **2007**, *25* (2), 66–73. https://doi.org/10.1016/j.tibtech.2006.12.005.
(21) Bisen, P. Enzyme Immobilization. In *Laboratory Protocols in Applied Life Sciences*; 2014; pp 1213–1246. https://doi.org/10.1201/b16575-23.
(22) Mateo, C.; Palomo, J. M.; Fernandez-Lorente, G.; Guisan, J. M.; Fernandez-Lafuente, R. Improvement of Enzyme Activity, Stability and Selectivity via Immobilization Techniques. *Enzyme Microb. Technol.* **2007**, *40* (6), 1451–1463. https://doi.org/10.1016/j.enzmictec.2007.01.018.
(23) Iyer, P. V.; Ananthanarayan, L. Enzyme Stability and Stabilization-Aqueous and Non-Aqueous Environment. *Process Biochem.* **2008**, *43* (10), 1019–1032. https://doi.org/10.1016/j.procbio.2008.06.004.
(24) Zhao, H. Methods for Stabilizing and Activating Enzymes in Ionic Liquids - A Review. *J. Chem. Technol. Biotechnol.* **2010**, *85* (7), 891–907. https://doi.org/10.1002/jctb.2375.
(25) Cao, L. Immobilised Enzymes: Science or Art? *Curr. Opin. Chem. Biol.* **2005**, *9* (2), 217–226. https://doi.org/10.1016/j.cbpa.2005.02.014.
(26) Sheldon, R. A. Enzyme Immobilization: The Quest for Optimum Performance. *Adv. Synth. Catal.* **2007**, *349* (8–9), 1289–1307. https://doi.org/10.1002/adsc.200700082.
(27) Garcia-Galan, C.; Berenguer-Murcia, Á.; Fernandez-Lafuente, R.; Rodrigues, R. C. Potential of Different Enzyme Immobilization Strategies to Improve Enzyme Performance. *Adv. Synth. Catal.* **2011**, *353* (16), 2885–2904. https://doi.org/10.1002/adsc.201100534.
(28) Zou, X.; Wei, S.; Badieyan, S.; Schroeder, M.; Jasensky, J.; Brooks, C. L.; Marsh, E. N. G.; Chen, Z. Investigating the Effect of Two-Point Surface Attachment on Enzyme Stability and Activity. *J. Am. Chem. Soc.* **2018**, *140* (48), 16560–16569. https://doi.org/10.1021/jacs.8b08138.

(29) Wang, P.; Sergeeva, M. V.; Lim, L.; Dordick, J. S. Biocatalytic Plastics as Active and Stable Materials for Biotransformations. *Nat. Biotechnol.* **1997**, *15* (8), 789–793. https://doi.org/10.1038/nbt0897-789.
(30) Barbosa, O.; Torres, R.; Ortiz, C.; Berenguer-Murcia, Á.; Rodrigues, R. C.; Fernandez-Lafuente, R. Heterofunctional Supports in Enzyme Immobilization: From Traditional Immobilization Protocols to Opportunities in Tuning Enzyme Properties. *Biomacromolecules* **2013**, *14* (8), 2433–2462. https://doi.org/10.1021/bm400762h.
(31) Berberich, J. A.; Yang, L. W.; Madura, J.; Bahar, I.; Russell, A. J. A Stable Three-Enzyme Creatinine Biosensor. 1. Impact of Structure, Function and Environment on PEGylated and Immobilized Sarcosine Oxidase. *Acta Biomater.* **2005**, *1* (2), 173–181. https://doi.org/10.1016/j.actbio.2004.11.006.
(32) Romdhane, I. B. Ben; Romdhane, Z. Ben; Gargouri, A.; Belghith, H. Esterification Activity and Stability of Talaromyces Thermophilus Lipase Immobilized onto Chitosan. *J. Mol. Catal. B Enzym.* **2011**, *68* (3–4), 230–239. https://doi.org/10.1016/j.molcatb.2010.11.010.
(33) Bilal, M.; Asgher, M.; Cheng, H.; Yan, Y.; Iqbal, H. M. N. Multi-Point Enzyme Immobilization, Surface Chemistry, and Novel Platforms: A Paradigm Shift in Biocatalyst Design. *Crit. Rev. Biotechnol.* **2019**, *39* (2), 202–219. https://doi.org/10.1080/07388551.2018.1531822.
(34) LeJeune, K. E.; Mesiano, A. J.; Bower, S. B.; Grimsley, J. K.; Wild, J. R.; Russell, A. J. Dramatically Stabilized Phosphotriesterase-Polymers for Nerve Agent Degradation. *Biotechnol. Bioeng.* **1997**, *54* (2), 105–114. https://doi.org/10.1002/(SICI)1097-0290(19970420)54:2<105::AID-BIT2>3.0.CO;2-P.
(35) Tardioli, P. W.; Pedroche, J.; Giordano, R. L. C.; Fernández-Lafuente, R.; Guisán, J. M. Hydrolysis of Proteins by Immobilized-Stabilized Alcalase-Glyoxyl Agarose. *Biotechnol. Prog.* **2003**, *19* (2), 352–360. https://doi.org/10.1021/bp025588n.
(36) Mozhaev, V. V.; Melik-Nubarov, N. S.; Sergeeva, M. V.; Šikšnis, V.; Martinek, K. Strategy for Stabilizing Enzymes Part One: Increasing Stability of Enzymes via Their Multi-Point Interaction with a Support. *Biocatal. Biotransformation* **1990**, *3* (3), 179–187. https://doi.org/10.3109/10242429008992060.
(37) LeJeune, K. E.; Swers, J. S.; Hetro, A. D.; Donahey, G. P.; Russell, A. J. Increasing the Tolerance of Organophosphorus Hydrolase to Bleach. *Biotechnol. Bioeng.* **1999**, *64* (2), 250–254. https://doi.org/10.1002/(SICI)1097-0290(19990720)64:2<250::AID-BIT14>3.0.CO;2-9.
(38) Fernandez-Lafuente, R.; Guisan, J. M.; Ali, S.; Cowan, D. Immobilization of Functionally Unstable Catechol-2,3-Dioxygenase Greatly Improves Operational Stability. *Enzyme Microb. Technol.* **2000**, *26* (8), 568–573. https://doi.org/10.1016/S0141-0229(00)00144-7.
(39) Yilmaz, E.; Can, K.; Sezgin, M.; Yilmaz, M. Immobilization of Candida Rugosa Lipase on Glass Beads for Enantioselective Hydrolysis of Racemic Naproxen Methyl Ester. *Bioresour. Technol.* **2011**, *102* (2), 499–506. https://doi.org/10.1016/j.biortech.2010.08.083.
(40) Palomo, J. M.; Muoz, G.; Fernández-Lorente, G.; Mateo, C.; Fernández-Lafuente, R.; Guisán, J. M. Interfacial Adsorption of Lipases on Very Hydrophobic Support (Octadecyl-Sepabeads): Immobilization, Hyperactivation and Stabilization of the Open Form of Lipases. *J. Mol. Catal. B Enzym.* **2002**, *19* (20), 279–286. https://doi.org/10.1016/S1381-1177(02)00178-9.

(41) Henzler-Wildman, K.; Kern, D. Dynamic Personalities of Proteins. *Nature* **2007**, *450* (7172), 964–972. https://doi.org/10.1038/nature06522.
(42) Villali, J.; Kern, D. Choreographing an Enzyme's Dance. *Curr. Opin. Chem. Biol.* **2010**, *14* (5), 636–643. https://doi.org/10.1016/j.cbpa.2010.08.007.
(43) Kerns, S. J.; Agafonov, R. V; Cho, Y.; Pontiggia, F.; Otten, R.; Pachov, D. V; Kutter, S.; Phung, L. a; Murphy, P. N.; Thai, V.; et al. The Energy Landscape of Adenylate Kinase during Catalysis. **2015**, No. October 2014. https://doi.org/10.1038/nsmb.2941.
(44) Weltz, J. S.; Kienle, D. F.; Schwartz, D. K.; Kaar, J. L. Dramatic Increase in Catalytic Performance of Immobilized Lipases by Their Stabilization on Polymer Brush Supports. *ACS Catal.* **2019**, 4992–5001. https://doi.org/10.1021/acscatal.9b01176.
(45) Sosa, A. F. C.; Kienle, D. F.; Falatach, R. M.; Flanagan, J.; Kaar, J. L.; Schwartz, D. K. Stabilization of Immobilized Enzymes via the Chaperone- like Activity of Mixed Lipid Bilayers. *ACS Appl. Mater. Interfaces* **2018**, *10*, 19504–19513. https://doi.org/10.1021/acsami.8b05523.
(46) Kienle, D. F.; Falatach, R. M.; Kaar, J. L.; Schwartz, D. K. Correlating Structural and Functional Heterogeneity of Immobilized Enzymes. *ACS Nano* **2018**, *12*, 8091–8103. https://doi.org/10.1021/acsnano.8b02956.
(47) Wang, Y.; Lu, H. P. Bunching Effect in Single-Molecule T4 Lysozyme Nonequilibrium Conformational Dynamics under Enzymatic Reactions. *J. Phys. Chem. B* **2010**, *114* (19), 6669–6674. https://doi.org/10.1021/jp1004506.
(48) Kuzmenkina, E. V.; Heyes, C. D.; Nienhaus, G. U. Single-Molecule Förster Resonance Energy Transfer Study of Protein Dynamics under Denaturing Conditions. *Proc. …* **2005**, *102* (43), 15471–15476. https://doi.org/10.1073/pnas.0507728102.
(49) Aviram, H. Y.; Pirchi, M.; Mazal, H.; Barak, Y.; Riven, I.; Haran, G. Direct Observation of Ultrafast Large-Scale Dynamics of an Enzyme under Turnover Conditions. **2018**, 1–6. https://doi.org/10.1073/pnas.1720448115.
(50) Choi, J. M.; Han, S. S.; Kim, H. S. Industrial Applications of Enzyme Biocatalysis: Current Status and Future Aspects. *Biotechnology Advances*. Elsevier Inc. 2015, pp 1443–1454. https://doi.org/10.1016/j.biotechadv.2015.02.014.
(51) Ma, J.; Zhang, Z.; Wang, B.; Kong, X.; Wang, Y.; Cao, S.; Feng, Y. Overexpression and Characterization of a Lipase from Bacillus Subtilis. *Protein Expr. Purif.* **2006**, *45* (1), 22–29. https://doi.org/10.1016/j.pep.2005.06.004.
(52) Kawasaki, K.; Kondo, H.; Suzuki, M.; Ohgiya, S.; Tsuda, S. Alternate Conformations Observed in Catalytic Serine of Bacillus Subtilis Lipase Determined at 1.3 Å Resolution. *Acta Crystallogr. Sect. D Biol. Crystallogr.* **2002**, *58* (7), 1168–1174. https://doi.org/10.1107/S090744490200714X.
(53) Fersht, A. *Structure and Mechanism in Protein Science*; Julet, M. R., Ed.; W. H. Freeman and Company: New York, 1997; Vol. 13409.
(54) Romero, P. A.; Arnold, F. H. Exploring Protein Fitness Landscapes by Directed Evolution. *Nat. Rev. Mol. Cell Biol.* **2009**, *10* (12), 866–876. https://doi.org/10.1038/nrm2805.
(55) Soskine, M.; Tawfik, D. S. Mutational Effects and the Evolution of New Protein Functions. *Nat. Rev. Genet.* **2010**, *11* (8), 572–582. https://doi.org/10.1038/nrg2808.
(56) Hohlbein, J.; Craggs, T. D.; Cordes, T. Alternating-Laser Excitation: Single-Molecule FRET and Beyond. *Chem. Soc. Rev.* **2014**, *43* (4), 1156–1171. https://doi.org/10.1039/C3CS60233H.

(57) Pace, C. N.; Shirley, B. A. Forces Contributing Proteins of Proteins. *Faseb* **1996**, *10* (1), 75–83.
(58) Reznik, C.; Estillore, N.; Advincula, R. C.; Landes, C. F. Single Molecule Spectroscopy Reveals Heterogeneous Transport Mechanisms for Molecular Ions in a Polyelectrolyte Polymer Brush. *J. Phys. Chem. B* **2009**, *113* (44), 14611–14618. https://doi.org/10.1021/jp906487j.
(59) Sarshar, M.; Wong, W. T.; Anvari, B. Comparative Study of Methods to Calibrate the Stiffness of a Single-Beam Gradient-Force Optical Tweezers over Various Laser Trapping Powers. *J. Biomed. Opt.* **2014**, *19*. https://doi.org/10.1117/1.JBO.19.
(60) Zaccai, G. How Soft Is a Protein? A Protein Dynamics Force Constant Measured by Neutron Scattering. *Science (80-.).* **2000**, *288* (5471), 1604–1607.
(61) Schlierf, M.; Rief, M. Temperature Softening of a Protein in Single-Molecule Experiments. *J. Mol. Biol.* **2005**, *354* (2), 497–503. https://doi.org/10.1016/j.jmb.2005.09.070.
(62) Thorpe, M. F. Comment on Elastic Network Models and Proteins. *Phys. Biol.* **2007**, *4* (1), 60–63. https://doi.org/10.1088/1478-3975/4/1/N01.

Appendix B Bibliography

1. Fersht, A. *Structure and Mechanism in Protein Science*. **13409**, (W. H. Freeman and Company, 1997).

2. Bommarius, A. S. Biocatalysis: A Status Report. *Annu. Rev. Chem. Biomol. Eng.* **6**, 319–345 (2015).

3. Schmid, A. *et al.* Industrial Biocatalysis Today and Tomorrow. *Nature* **409**, 258–268 (2001).

4. DiCosimo, R., McAuliffe, J., Poulose, A. J. & Bohlmann, G. Industrial use of immobilized enzymes. *Chem. Soc. Rev.* **42**, 6437–74 (2013).

5. Dordick, J. S. An Introduction to Industrial Biocatalysis. in *Biocatalysts for Industry* (ed. Dordick, J. S.) (Springer, 1991). doi:https://doi.org/10.1007/978-1-4757-4597-9

6. Adams, M. W. W., Perler, F. B. & Kelly, R. M. Extremozymes: Expanding the limits of biocatalysis. *Nature Biotechnology* **13**, 662–668 (1995).

7. Sheldon, R. A., Schoevaart, R. & Van Langen, L. M. Cross-linked enzyme aggregates (CLEAs): A novel and versatile method for enzyme immobilization (a review). *Biocatal. Biotransformation* **23**, 141–147 (2005).

8. Bornscheuer, U. T. *et al.* Engineering the third wave of biocatalysis. *Nature* **485**, 185–194 (2012).

9. Gumulya, Y. *et al.* Engineering highly functional thermostable proteins using ancestral sequence reconstruction. *Nat. Catal.* **1**, 878–888 (2018).

10. Schmid, R. D. & Verger, R. Lipases: Interfacial Enzymes with Attractive Applications. *Angew. Chemie Int. Ed.* **37**, 1608–1633 (1998).

11. Iqbal, S. S. *et al.* A review of molecular recognition technologies for detection of biological threat agents. *Proc. SPE Int. Improv. Oil Recover. Conf. Asia Pacific* **15**, 549–578 (2003).

12. Smith, R. G., D'Souza, N. & Nicklin, S. A review of biosensors and biologically-inspired systems for explosives detection. *Analyst* **133**, 571–584 (2008).

13. Berberich, J. A., Yang, L. W., Bahar, I. & Russell, A. J. A stable three enzyme creatinine biosensor. 2. Analysis of the impact of silver ions on creatine amidinohydrolase. *Acta Biomater.* **1**, 183–191 (2005).

14. Bruen, D., Delaney, C., Florea, L. & Diamond, D. Glucose sensing for diabetes monitoring: Recent developments. *Sensors (Switzerland)* **17**, 1–21 (2017).

15. Shenton, W., Pum, D., Sleytr, U. B. & Mann, S. Synthesis of cadmium sulphide superlattices using self-assembled bacterial S-layers. *Nature* **389**, 585–587 (1997).

16. Zhong, C. *et al.* Strong underwater adhesives made by self-assembling multi-protein nanofibres. *Nat. Nanotechnol.* **9**, 858–866 (2014).

17. Huang, X. *et al.* Interfacial assembly of protein-polymer nano-conjugates into stimulus-responsive biomimetic protocells. *Nat. Commun.* **4**, 1–9 (2013).

18. Klibanov, A. M. Immobilized enzymes and cells as practical catalysts. *Science (80-.).* **219**, 722–727 (1983).

19. Prasad, S. & Roy, I. Converting Enzymes into Tools of Industrial Importance. *Recent Pat. Biotechnol.* **12**, 33–56 (2017).

20. Feng, D. *et al.* Stable metal-organic frameworks containing single-molecule traps for enzyme encapsulation. *Nat. Commun.* **6**, 1–8 (2015).

21. Scouten, W. H., Luong, J. H. T. & Stephen Brown, R. Enzyme or protein immobilization techniques for applications in biosensor design. *Trends Biotechnol.* **13**, 178–185 (1995).

22. Berberich, J. A., Yang, L. W., Madura, J., Bahar, I. & Russell, A. J. A stable three-enzyme creatinine biosensor. 1. Impact of structure, function and environment on PEGylated and immobilized sarcosine oxidase. *Acta Biomater.* **1**, 173–181 (2005).

23. Berberich, J. A., Chan, A., Boden, M. & Russell, A. J. A stable three-enzyme creatinine biosensor. 3. Immobilization of creatinine amidohydrolase and sensor development. *Acta Biomater.* **1**, 193–199 (2005).

24. Yan, H., Park, S. H., Finkelstein, G., Reif, J. H. & LaBean, T. H. DNA-templated self-assembly of protein arrays and highly conductive nanowires. *Science (80-.).* **301**, 1882–1884 (2003).

25. Zhang, S. Fabrication of novel biomaterials through molecular self-assembly. *Nat. Biotechnol.* **21**, 1171–1178 (2003).

26. Knowles, T. P. J., Oppenheim, T. W., Buell, A. K., Chirgadze, D. Y. & Welland, M. E. Nanostructured films from hierarchical self-assembly of amyloidogenic proteins. *Nat. Nanotechnol.* **5**, 204–207 (2010).

27. BEE, J. S., RANDOLPH, T., CARPENTER, J. F., BISHOP, S. M. & DIMITROVA, M. N. Effects of Surfaces and Leachables on the Stability of Biopharmaceuticals. *J. Pharm. Sci.* **100**, 4158–4170 (2011).

28. Burke, C. J. *et al.* The adsorption of proteins to pharmaceutical container surfaces. *Int. J. Pharm.* **86**, 89–93 (1992).

29. Jungbauer, A., Machold, C. & Hahn, R. Hydrophobic interaction chromatography of proteins: III. Unfolding of proteins upon adsorption. *J. Chromatogr. A* **1079**, 221–228 (2005).

30. Norde, W. & Lyklema, J. Thermodynamics of Protein Adsorption. *J. Colloid Interface Sci.* **71**, 350–366 (1979).

31. Ramsden, J. J. Puzzles and paradoxes in protein adsorption. *Chem. Soc. Rev.* **24**, 73 (1995).

32. Gray, J. J. The interaction of proteins with solid surfaces. *Curr. Opin. Struct. Biol.* **14**, 110–5 (2004).

33. Whitesides, G. M. & Prime, K. L. Self-assembled organic monolayers: model systems for studying adsorption of proteins at surfaces. *Science (80-.).* **252**, 1164–1167 (1991).

34. Calonder, C., Tie, Y. & Tassel, P. R. Van. Protein adsorption: Kinetics and history dependence of protein adsorption kinetics. *Proc. Natl. Acad. Sci.* **98**, 10664–10669 (2001).

35. Lee, R. G. & Kim, S. W. Adsorption of proteins onto hydrophobic polymer surfaces: Adsorption isotherms and kinetics. *J. Biomed. Mater. Res.* **8**, 251–259 (1974).

36. Yuan, Y., Velev, O. D. & Lenhoff, A. M. Mobility of adsorbed proteins studied by fluorescence recovery after photobleaching. *Langmuir* **19**, 3705–3711 (2003).

37. Ries, J., Petrov, E. P. & Schwille, P. Total internal reflection fluorescence correlation spectroscopy: Effects of lateral diffusion and surface-generated fluorescence. *Biophys. J.* **95**, 390–399 (2008).

38. Skaug, M. J., Mabry, J. & Schwartz, D. K. Intermittent Molecular Hopping at the Solid-Liquid Interface. *Phys. Rev. Lett.* **110**, 256101 (2013).

39. Graham, D. E. & Phillips, M. C. Proteins at Liquid Interfaces: Kinetics of Adsorption and Surface Denaturation. *J. Colloid Interface Sci.* **70**, 403–414 (1978).

40. Shang, W., Nuffer, J. H., Dordick, J. S. & Siegel, R. W. Unfolding of ribonuclease a on silica nanoparticle surfaces. *Nano Lett.* **7**, 1991–1995 (2007).

41. Nakanishi, K., Sakiyama, T. & Imamura, K. On the adsorption of proteins on solid surfaces, a common but very complicated phenomenon. *J. Biosci. Bioeng.* **91**, 233–44 (2001).

42. Essa, H., Magner, E., Cooney, J. & Hodnett, B. K. Influence of pH and ionic strength on the adsorption, leaching and activity of myoglobin immobilized onto ordered mesoporous silicates. *J. Mol. Catal. B Enzym.* **49**, 61–68 (2007).

43. Ansorge-Schumacher, M. B. & Thum, O. Immobilised lipases in the cosmetics industry. *Chem. Soc. Rev.* **42**, 6475–6490 (2013).

44. Bo Chen, Jun Hu, Elizabeth M. Miller, Wenchun Xie, Minmin Cai, R. A. G. *et al.* Candida antarctica Lipase B Chemically Immobilized on Epoxy-Activated Micro- and Nanobeads: Catalysts for Polyester Synthesis. *Biomacromolecules* 463–471 (2008). doi:10.1021/bm700949x

45. Mabry, J. N., Skaug, M. J. & Schwartz, D. K. Single-Molecule Insights into Retention at a Reversed-Phase Chromatographic Interface. (2014).

46. Wirth, M. J., Swinton, D. J. & Ludes, M. D. Adsorption and Diffusion of Single

Molecules at Chromatographic Interfaces. *J. Phys. Chem. B* **107**, 6258–6268 (2003).

47. Kisley, L. *et al.* Unified superresolution experiments and stochastic theory provide mechanistic insight into protein ion-exchange adsorptive separations. *Proc. Natl. Acad. Sci. U. S. A.* **111**, 2075–80 (2014).

48. Hlady, V. & Buijs, J. Protein adsorption on solid surfaces. *Curr. Opin. Biotechnol.* **7**, 72–7 (1996).

49. Rabe, M., Verdes, D. & Seeger, S. Understanding protein adsorption phenomena at solid surfaces. *Adv. Colloid Interface Sci.* **162**, 87–106 (2011).

50. Singla, B., Krisdhasima, V. & McGuire, J. Adsorption kinetics of wild type and two synthetic stability mutants of T4 phage lysozyme at silanized silica surfaces. *J. Colloid Interface Sci.* **182**, 292–296 (1996).

51. Prime, K. L. & Whitesides, G. M. Adsorption of Proteins onto Surfaces Containing End-Attached Oligo(ethylene oxide): A Model System Using Self-Assembled Monolayers. *J. Am. Chem. Soc.* **115**, 10714–10721 (1993).

52. Mrksich, M. & Whitesides, G. M. Using Self-Assembled Monolayers to Understand the Interactions of Man-Made Surfaces With Proteins and Cells. *Annu. Rev. Biophys. Biomol. Struct.* **25**, 55–78 (1996).

53. Ostuni, E., Chapman, R. G., Holmlin, R. E., Takayama, S. & Whitesides, G. M. A survey of structure-property relationships of surfaces that resist the adsorption of protein. *Langmuir* **17**, 5605–5620 (2001).

54. Dismer, F., Petzold, M. & Hubbuch, J. Effects of ionic strength and mobile phase pH on the binding orientation of lysozyme on different ion-exchange adsorbents. *J. Chromatogr. A* **1194**, 11–21 (2008).

55. Wu, X. & Narsimhan, G. Effect of surface concentration on secondary and tertiary conformational changes of lysozyme adsorbed on silica nanoparticles. *Biochim. Biophys. Acta - Proteins Proteomics* **1784**, 1694–1701 (2008).

56. Barbosa, O., Torres, R., Ortiz, C. & Fernandez-Lafuente, R. Versatility of glutaraldehyde to immobilize lipases: Effect of the immobilization protocol on the properties of lipase B from Candida antarctica. *Process Biochem.* **47**, 1220–1227 (2012).

57. Jeon, S. I. & Andrade, J. D. Protein-Surface Interactions in the Presence of Polyethylene Oxide: II. Effect of Protein Size. *J. Colloid Interface Sci.* **142**, 159–166 (1991).

58. Silberberg, A. Adsorption of Collagen , Serum Albumin , and Fibronectin to Glass and to Each Other. **126**, (1988).

59. Cao, L. Immobilised enzymes: Science or art? *Curr. Opin. Chem. Biol.* **9**, 217–226 (2005).

60. Kastantin, M., Langdon, B. B. & Schwartz, D. K. A bottom-up approach to understanding

protein layer formation at solid-liquid interfaces. *Adv. Colloid Interface Sci.* **207**, 240–252 (2014).

61. Skaug, M. J., Mabry, J. N. & Schwartz, D. K. Single-Molecule Tracking of Polymer Surface Di ff usion. *J. Am. Chem. Soc.* (2013).

62. Langdon, B. B., Kastantin, M. & Schwartz, D. K. Surface Chemistry Influences Interfacial Fibrinogen Self-Association. *Biomacromolecules* 150910134203000 (2015). doi:10.1021/acs.biomac.5b00869

63. McLoughlin, S. Y., Kastantin, M., Schwartz, D. K. & Kaar, J. L. Single-molecule resolution of protein structure and interfacial dynamics on biomaterial surfaces. *Proc. Natl. Acad. Sci.* **110**, 19396–19401 (2013).

64. Kastl, K. *et al.* Partially reversible adsorption of annexin A1 on POPC/POPS bilayers investigated by QCM measurements, SFM, and DMC simulations. *ChemBioChem* **7**, 106–115 (2006).

65. Krisdhasima, V., Vinaraphong, P. & McGuire, J. Adsorption Kinetics and Elutability of α-Lactalbumin, β-Casein, β-Lactoglobulin, and Bovine Serum Albumin at Hydrophobic and Hydrophilic Interfaces. *Journal of Colloid and Interface Science* **161**, 325–334 (1993).

66. Castillo, E. J., Koenig, J. L., Anderson, J. M. & Lo, J. Protein adsorption on hydrogels. II. Reversible and irreversible interactions between lysozyme and soft contact lens surfaces. *Biomaterials* **6**, 338–345 (1985).

67. Karlsson, M., Ekeroth, J., Elwing, H. & Carlsson, U. Reduction of irreversible protein adsorption on solid surfaces by protein engineering for increased stability. *J. Biol. Chem.* **280**, 25558–64 (2005).

68. Giacomelli, C. E. & Norde, W. The Adsorption–Desorption Cycle. Reversibility of the BSA–Silica System. *J. Colloid Interface Sci.* **233**, 234–240 (2001).

69. Daly, S. M., Przybycien, T. M. & Tilton, R. D. Adsorption of poly(ethylene glycol)-modified lysozyme to silica. *Langmuir* **21**, 1328–1337 (2005).

70. Richert, L., Variola, F., Rosei, F., Wuest, J. D. & Nanci, A. Adsorption of proteins on nanoporous Ti surfaces. *Surf. Sci.* **604**, 1445–1451 (2010).

71. Wang, J., Buck, S. M. & Chen, Z. Sum frequency generation vibrational spectroscopy studies on protein adsorption. *J. Phys. Chem. B* **106**, 11666–11672 (2002).

72. Lau, K. H. A., Bang, J., Hawker, C. J., Dong, H. K. & Knoll, W. Modulation of protein-surface interactions on nanopatterned polymer films. *Biomacromolecules* **10**, 1061–1066 (2009).

73. Daly, S. M., Przybycien, T. M. & Tilton, R. D. Coverage-dependent orientation of lysozyme adsorbed on silica. *Langmuir* **19**, 3848–3857 (2003).

74. Chen, S., Li, L., Zhao, C. & Zheng, J. Surface hydration: Principles and applications

toward low-fouling/nonfouling biomaterials. *Polymer (Guildf).* **51**, 5283–5293 (2010).

75. Kane, R. S., Deschatelets, P. & Whitesides, G. M. Kosmotropes form the basis of protein-resistant surfaces. *Langmuir* **19**, 2388–2391 (2003).

76. Zamfir, M. *et al.* Controlled growth of protein resistant PHEMA brushes via S-RAFT polymerization. *J. Mater. Chem. B* **1**, 6027–6034 (2013).

77. Tidwell, C. D. *et al.* Glow discharge plasma deposition of tetraethylene glycol dimethyl ether for fouling-resistant biomaterial surfaces. *J. Biomed. Mater. Res.* **26**, 415–439 (2005).

78. Latour, R. Biomaterials: protein-surface interactions. *... Biomater. Biomed. Eng.* 1–15 (2005). doi:10.1081/E-EBBE-120041856

79. Wang, Y. X., Robertson, J. L., Spillman, W. B. & Claus, R. O. Effects of the chemical structure and the surface properties of polymeric biomaterials on their biocompatibility. *Pharm. Res.* **21**, 1362–1373 (2004).

80. Gautrot, J. E., Huck, W. T. S., Welch, M. & Ramstedt, M. Protein-resistant NTA-functionalized polymer brushes for selective and stable immobilization of histidine-tagged proteins. *ACS Appl. Mater. Interfaces* **2**, 193–202 (2010).

81. Nieba, L. *et al.* BIACORE Analysis of Histidine-Tagged Proteins Using a Chelating NTA Sensor Chip. *Anal. Biochem.* **252**, 217–228 (1997).

82. Wertz, C. F. & Santore, M. M. Fibrinogen adsorption on hydrophilic and hydrophobic surfaces: Geometrical and energetic aspects of interfacial relaxations. *Langmuir* **18**, 706–715 (2002).

83. Vroman, L. Effect of Adsorbed Proteins on the Wettability of Hydrophilic and Hydrophobic Solids. *Nature* **196**, 1097–1098 (1962).

84. Wojciechowski, P., Ten Hove, P. & Brash, J. . Phenomenology and mechanism of the transient adsorption of fibrinogen from plasma (Vroman effect). *J. Colloid Interface Sci.* **111**, 455–465 (1986).

85. Casals, E., Pfaller, T., Duschl, A., Oostingh, G. J. & Puntes, V. Time evolution of nanoparticle protein corona. **4**, 3623–3632 (2010).

86. Deyme, M., Baszkin, A., Proust, J. E., Perez, E. & Boissonnade, M. M. Collagen at interfaces I. In situ collagen adsorption at solution/air and solution/polymer interfaces. *J. Biomed. Mater. Res.* **20**, 951–962 (1986).

87. Karlsson, M., Ekeroth, J., Elwing, H. & Carlsson, U. Reduction of irreversible protein adsorption on solid surfaces by protein engineering for increased stability. *J. Biol. Chem.* **280**, 25558–25564 (2005).

88. Benedek, K., Dong, S. & Karger, B. L. Kinetics of unfolding of proteins on hydrophobic surfaces in reversed-phase liquid chromatography. *J. Chromatogr. A* **317**, 227–243

(1984).

89. Kulik, E. A., Kalinin, I. D. & Sevastianov, V. I. The heterogeneity of protein/surface interactions and structural alterations of adsorbed albumin and immunoglobulin G. *Artif. Organs* **15**, 386–391 (1991).

90. McUmber, A. C., Randolph, T. W. & Schwartz, D. K. Electrostatic Interactions Influence Protein Adsorption (but Not Desorption) at the Silica-Aqueous Interface. *J. Phys. Chem. Lett.* **6**, 2583–2587 (2015).

91. Walder, R. & Schwartz, D. K. Single molecule observations of multiple protein populations at the oil-water interface. *Langmuir* **26**, 13364–13367 (2010).

92. Kastantin, M., Langdon, B. B., Chang, E. L. & Schwartz, D. K. Single-molecule resolution of interfacial fibrinogen behavior: effects of oligomer populations and surface chemistry. *J. Am. Chem. Soc.* **133**, 4975–83 (2011).

93. Kisley, L. *et al.* High ionic strength narrows the population of sites participating in protein ion-exchange adsorption: A single-molecule study. *J. Chromatogr. A* **1343**, 135–142 (2014).

94. Langdon, B. B., Kastantin, M. & Schwartz, D. K. Apparent activation energies associated with protein dynamics on hydrophobic and hydrophilic surfaces. *Biophys. J.* **102**, 2625–2633 (2012).

95. Mabry, J. N., Kastantin, M. & Schwartz, D. K. Capturing Conformation-Dependent Molecule-Surface Interactions When Surface Chemistry Is Heterogeneous. *ACS Nano* **9**, 7237–7247 (2015).

96. Langdon, B. B. *et al.* Single-Molecule Resolution of Protein Dynamics on Polymeric Membrane Surfaces: The Roles of Spatial and Population Heterogeneity. *ACS Appl. Mater. Interfaces* 150203144035006 (2015). doi:10.1021/am507730k

97. Langdon, B. B., Kastantin, M., Walder, R. & Schwartz, D. K. Interfacial protein-protein associations. *Biomacromolecules* **15**, 66–74 (2014).

98. Bhushan, B., Kwak, K. J., Gupta, S. & Lee, S. C. Nanoscale adhesion, friction and wear studies of biomolecules on silicon based surfaces. *J. R. Soc. Interface* **6**, 719–733 (2008).

99. Bromley, K. M. *et al.* Interfacial self-assembly of a bacterial hydrophobin. *Proc. Natl. Acad. Sci.* **112**, 5419–5424 (2015).

100. Kisley, L. & Landes, C. F. Molecular Approaches to Chromatography Using Single Molecule Spectroscopy. (2015).

101. Yang, Z., Galloway, J. A. & Yu, H. Protein interactions with poly(ethylene glycol) self-assembled monolayers on glass substrates: Diffusion and adsorption. *Langmuir* **15**, 8405–8411 (1999).

102. Tilton, R. D., Robertson, C. R. & Gast, A. P. Lateral diffusion of bovine serum albumin

adsorbed at the solid-liquid interface. *J. Colloid Interface Sci.* **137**, 192–203 (1990).

103. Yu, C., Guan, J., Chen, K., Bae, S. C. & Granick, S. Single-molecule observation of long jumps in polymer adsorption. *ACS Nano* **7**, 9735–9742 (2013).

104. Bychuk, O. V. & O'Shaughnessy, B. Anomalous Diffusion at Liquid Surfaces. *Phys. Rev. Lett.* **74**, 1795–1798 (1995).

105. Monserud, J. H. & Schwartz, D. K. Interfacial Molecular Searching Using Forager Dynamics. *Phys. Rev. Lett.* **116**, 098303 (2016).

106. Skaug, M. J. *et al.* Single-molecule diffusion in a periodic potential at a solid-liquid interface. *Soft Matter* **10**, 753–9 (2014).

107. Wang, D., Chin, H.-Y., He, C., Stoykovich, M. P. & Schwartz, D. K. Polymer Surface Transport Is a Combination of in-Plane Diffusion and Desorption-Mediated Flights. *ACS Macro Lett.* **5**, 509–514 (2016).

108. Wang, D., He, C., Stoykovich, M. P. & Schwartz, D. K. Nanoscale Topography Influences Polymer Surface Diffusion. *ACS Nano* (2015).

109. Langmuir, I. & Schaefer, V. J. Activities of Urease and Pepsin Monolayers. *J. Am. Chem. Soc.* **60**, 1351–1360 (1938).

110. Lumry, R. & Eyring, H. Conformation changes of proteins. *J. Phys. Chem* **58**, 110–120 (1954).

111. Norde, W. & Zoungrana, T. Surface-induced changes in the structure and activity of enzymes physically immobilized at solid/liquid interfaces. *Biotechnol. Appl. Biochem.* **28**, 133–143 (1998).

112. Das, P., Das, M., Chinnadayyala, S. R., Singha, I. M. & Goswami, P. Recent advances on developing 3rd generation enzyme electrode for biosensor applications. *Biosens. Bioelectron.* **79**, 386–397 (2016).

113. Garman, E. F. Developments in X-ray crystallographic structure determination of biological macromolecules. *Science (80-.).* **343**, 1102–1108 (2014).

114. Fischer, N. *et al.* Structure of the E. coli ribosome-EF-Tu complex at <3 Å resolution by Cs-corrected cryo-EM. *Nature* **520**, 567–570 (2015).

115. Cavalli, A., Salvatella, X., Dobson, C. M. & Vendruscolo, M. Protein structure determination from NMR chemical shifts. *Proc. Natl. Acad. Sci.* **104**, 9615–9620 (2007).

116. Huang, R., Carney, R. P., Ikuma, K., Stellacci, F. & Lau, B. L. T. Effects of surface compositional and structural heterogeneity on nanoparticle-protein interactions: Different protein configurations. *ACS Nano* **8**, 5402–5412 (2014).

117. Vertegel, A. a, Siegel, R. W. & Dordick, J. S. Silica nanoparticle size influences the structure and enzymatic activity of adsorbed lysozyme. *Langmuir* **20**, 6800–6807 (2004).

118. Buijs, J., Norde, W. & Lichtenbelt, J. W. T. Changes in the Secondary Structure of Adsorbed IgG and F (ab ′) 2 Studied by FTIR Spectroscopy. *Langmuir* **12**, 1605–1613 (1996).

119. Lensun, L., Smith, T. A. & Gee, M. L. Partial denaturation of silica-adsorbed bovine serum albumin determined by time-resolved evanescent wave-induced fluorescence spectroscopy. *Langmuir* **18**, 9924–9931 (2002).

120. Sota, H., Hasegawa, Y. & Iwakura, M. Detection of Conformational Changes in an Immobilized Protein Using Surface Plasmon Resonance. *Anal. Chem.* **70**, 2019–2024 (1998).

121. Wertz, C. F. & Santore, M. M. Effect of surface hydrophobicity on adsorption and relaxation kinetics of albumin and fibrinogen: Single-species and competitive behavior. *Langmuir* **17**, 3006–3016 (2001).

122. Sadana, A. Protein adsorption and inactivation on surfaces. Influence of heterogeneities. *Chem. Rev.* **92**, 1799–1818 (1992).

123. Mateo, C. *et al.* Immobilization of enzymes on heterofunctional epoxy supports. *Nat. Protoc.* **2**, 1022–1033 (2007).

124. Campbell, A. S. *et al.* Polymer-based protein engineering grown ferrocene-containing redox polymers improve current generation in an enzymatic biofuel cell. *Biosens. Bioelectron.* **86**, 446–453 (2016).

125. Ortiz, C. *et al.* Novozym 435: The 'perfect' lipase immobilized biocatalyst? *Catal. Sci. Technol.* **9**, 2380–2420 (2019).

126. El Bialy, I., Jiskoot, W. & Reza Nejadnik, M. Formulation, Delivery and Stability of Bone Morphogenetic Proteins for Effective Bone Regeneration. *Pharm. Res.* **34**, 1152–1170 (2017).

127. Klibanov, A. M. Stabilization of Enzymes against Thermal Inactivation. *Adv. Appl. Microbiol.* **29**, 1–28 (1983).

128. Zamost, B. L., Nielsen, H. K. & Starnes, R. L. Thermostable enzymes for industrial applications. *Journal of Industrial Microbiology* **8**, 71–81 (1991).

129. Visser, R., Arrabal, P. M., Becerra, J., Rinas, U. & Cifuentes, M. The effect of an rhBMP-2 absorbable collagen sponge-targeted system on bone formation in vivo. *Biomaterials* **30**, 2032–2037 (2009).

130. Jesionowski, T., Zdarta, J. & Krajewska, B. Enzyme immobilization by adsorption: A review. *Adsorption* **20**, 801–821 (2014).

131. Barbosa, O. *et al.* Strategies for the one-step immobilization-purification of enzymes as industrial biocatalysts. *Biotechnol. Adv.* **33**, 435–456 (2015).

132. Palomo, J. M. *et al.* Purification, immobilization, and stabilization of a lipase from

Bacillus thermocatenulatus by interfacial adsorption on hydrophobic supports. *Biotechnol. Prog.* **20**, 630–635 (2004).

133. Verger, R. Interfacial activation of lipases facts and artifacts. *Trends Biotechnol.* **15**, 32–38 (1997).

134. Rodrigues, R. C. & Fernandez-Lafuente, R. Lipase from Rhizomucor miehei as a biocatalyst in fats and oils modification. *J. Mol. Catal. B Enzym.* **66**, 15–32 (2010).

135. Brzozowski, A. M. *et al.* A model for interfacial activation in lipases from the structure of a fungal lipase-inhibitor complex. *Lett. to Nat.* **351**, 491–494 (1991).

136. Grochulski, P. *et al.* Insights into interfacial activation from an open structure of Candida rugosa lipase. *J. Biol. Chem.* **268**, 12843–12847 (1993).

137. Grochulski, P., Li, Y., Schrag, J. D. & Cygler, M. Two conformational states of Candida rugosa lipase. *Protein Sci.* **3**, 82–91 (1994).

138. Zhao, X., Qi, F., Yuan, C., Du, W. & Liu, D. Lipase-catalyzed process for biodiesel production: Enzyme immobilization, process simulation and optimization. *Renew. Sustain. Energy Rev.* **44**, 182–197 (2015).

139. Arruebo, M. Drug delivery from structured porous inorganic materials. *Wiley Interdiscip. Rev. Nanomedicine Nanobiotechnology* **4**, 16–30 (2012).

140. Slowing, I. I., Trewyn, B. G. & Lin, V. S. Y. Mesoporous silica nanoparticles for intracellular delivery of membrane-impermeable proteins. *J. Am. Chem. Soc.* **129**, 8845–8849 (2007).

141. Ravindra, R., Zhao, S., Gies, H. & Winter, R. Protein encapsulation in mesoporous silicate: The effects of confinement on protein stability, hydration, and volumetric properties. *J. Am. Chem. Soc.* **126**, 12224–12225 (2004).

142. Itoh, T. *et al.* Enhancement in thermal stability and resistance to denaturants of lipase encapsulated in mesoporous silica with alkyltrimethylammonium (CTAB). *Colloids Surfaces B Biointerfaces* **75**, 478–482 (2010).

143. Zhou, H. X. & Dill, K. A. Stabilization of proteins in confined spaces. *Biochemistry* **40**, 11289–11293 (2001).

144. Zhou, H.-X., Rivas, G. & Minton, A. P. Macromolecular crowding and confinemment: biochemical, biophysical, and potential physiological consequences. *Annu Rev Biophys* **37**, 375–397 (2010).

145. Eggers, D. K. & Valentine, J. S. Molecular confinement influences protein structure and enhances thermal protein stability. *Protein Sci.* **10**, 250–261 (2001).

146. Sheldon, R. A. Enzyme Immobilization: The Quest for Optimum Performance. *Adv. Synth. Catal.* **349**, 1289–1307 (2007).

147. Mateo, C., Abian, O., Fernandez-Lafuente, R. & Guisan, J. M. Reversible enzyme

immobilization via a very strong and nondistorting ionic adsorption on support-polyethylenimine composites. *Biotechnol. Bioeng.* **68**, 98–105 (2000).

148. Avnir, D., Braun, S., Lev, O. & Ottolenghi, M. Enzymes and Other Proteins Entrapped in Sol-Gel Materials. *Chem. Mater.* **6**, 1605–1614 (1994).

149. Dave, B. C., Dunn, B., Valentine, J. S. & Zink, J. I. Sol-Gel Encapsulation Methods for Biosensors. *Anal. Chem.* **66**, 1120A-1127A (1994).

150. Reetz, M. T., Zonta, A. & Simpelkamp, J. Efficient immobilization of lipases by entrapment in hydrophobic sol-gel materials. *Biotechnol. Bioeng.* **49**, 527–534 (1996).

151. Zhao, Z. *et al.* Nanocaged enzymes with enhanced catalytic activity and increased stability against protease digestion. *Nat. Commun.* **7**, 10619 (2016).

152. Drevon, G. F. *et al.* High-activity enzyme-polyurethane coatings. *Biotechnol. Bioeng.* **79**, 785–794 (2002).

153. Liu, H. H. *et al.* Direct electrochemistry and electrocatalysis of heme-proteins entrapped in agarose hydrogel films. *Biosens. Bioelectron.* **20**, 294–304 (2004).

154. Hudson, S., Cooney, J. & Magner, E. Proteins in Mesoporous Silicates. *Angew. Chemie Int. Ed.* **47**, 8582–8594 (2008).

155. Hartono, S. B. *et al.* Functionalized mesoporous silica with very large pores for cellulase immobilization. *J. Phys. Chem. C* **114**, 8353–8362 (2010).

156. Jin, W. & Brennan, J. D. Properties and applications of proteins encapsulated within sol-gel derived materials. *Anal. Chim. Acta* **461**, 1–36 (2002).

157. Huang, J. *et al.* Immobilization of penicillin G acylase on poly [(glycidyl methacrylate)-co-(glycerol monomethacrylate)]-grafted magnetic microspheres. *Macromol. Biosci.* **8**, 508–515 (2008).

158. Koepsel, R. R. & Russell, A. J. Directed capture of enzymes and bacteria on bioplastic films. *Biomacromolecules* **4**, 850–855 (2003).

159. Rodrigues, R. C. & Fernandez-Lafuente, R. Lipase from Rhizomucor miehei as an industrial biocatalyst in chemical process. *Journal of Molecular Catalysis B: Enzymatic* **64**, 1–22 (2010).

160. Bornscheuer, U. T. Immobilizing enzymes: How to create more suitable biocatalysts. *Angew. Chemie - Int. Ed.* **42**, 3336–3337 (2003).

161. Garcia-Galan, C., Berenguer-Murcia, Á., Fernandez-Lafuente, R. & Rodrigues, R. C. Potential of different enzyme immobilization strategies to improve enzyme performance. *Adv. Synth. Catal.* **353**, 2885–2904 (2011).

162. Sheldon, R. A. Cross-linked enzyme aggregates (CLEA®s): stable and recyclable biocatalysts. *Biochem. Soc. Trans.* **35**, 1583–1587 (2007).

163. Mafra, A. C. O. *et al.* Diffusion effects of bovine serum albumin on cross-linked aggregates of catalase. *J. Mol. Catal. B Enzym.* **133**, 107–116 (2016).

164. Tardioli, P. W., Pedroche, J., Giordano, R. L. C., Fernández-Lafuente, R. & Guisán, J. M. Hydrolysis of proteins by immobilized-stabilized Alcalase-glyoxyl agarose. *Biotechnol. Prog.* **19**, 352–360 (2003).

165. Yilmaz, E., Can, K., Sezgin, M. & Yilmaz, M. Immobilization of Candida rugosa lipase on glass beads for enantioselective hydrolysis of racemic Naproxen methyl ester. *Bioresour. Technol.* **102**, 499–506 (2011).

166. Bayramoğlu, G., Kaçar, Y., Denizli, A. & Yakup Arica, M. Covalent immobilization of lipase onto hydrophobic group incorporated poly(2-hydroxyethyl methacrylate) based hydrophilic membrane matrix. *J. Food Eng.* **52**, 367–374 (2002).

167. Guncheva, M. & Zhiryakova, D. Catalytic properties and potential applications of Bacillus lipases. *J. Mol. Catal. B Enzym.* **68**, 1–21 (2011).

168. Palomo, J. M. *et al.* Modulation of the enantioselectivity of lipases via controlled immobilization and medium engineering: Hydrolytic resolution of mandelic acid esters. *Enzyme Microb. Technol.* **31**, 775–783 (2002).

169. Mateo, C. *et al.* Epoxy Sepabeads: A novel epoxy support for stabilization of industrial enzymes via very intense multipoint covalent attachment. *Biotechnol. Prog.* **18**, 629–634 (2002).

170. Zhang, C., Dong, X., Guo, Z. & Sun, Y. Remarkably enhanced activity and substrate affinity of lipase covalently bonded on zwitterionic polymer-grafted silica nanoparticles. *J. Colloid Interface Sci.* **519**, 145–153 (2018).

171. Zaak, H. *et al.* Effect of immobilization rate and enzyme crowding on enzyme stability under different conditions. The case of lipase from Thermomyces lanuginosus immobilized on octyl agarose beads. *Process Biochem.* **56**, 117–123 (2017).

172. Rodrigues, D. S., Mendes, A. A., Adriano, W. S., Gonçalves, L. R. B. & Giordano, R. L. C. Multipoint covalent immobilization of microbial lipase on chitosan and agarose activated by different methods. *J. Mol. Catal. B Enzym.* **51**, 100–109 (2008).

173. Jiang, H. & Xu, F. J. Biomolecule-functionalized polymer brushes. *Chem. Soc. Rev.* **42**, 3394–3426 (2013).

174. Fernández-Suárez, M. *et al.* Redirecting lipoic acid ligase for cell surface protein labeling with small-molecule probes. *Nat. Biotechnol.* **25**, 1483–7 (2007).

175. Puthenveetil, S., Liu, D. S., White, K. a, Thompson, S. & Ting, A. Y. Yeast display evolution of a kinetically efficient 13-amino acid substrate for lipoic acid ligase. *J. Am. Chem. Soc.* **131**, 16430–8 (2009).

176. Warden-Rothman, R., Caturegli, I., Popik, V. & Tsourkas, A. Sortase-tag expressed protein ligation: Combining protein purification and site-specific bioconjugation into a

single step. *Anal. Chem.* **85**, 11090–11097 (2013).

177. Hohsaka, T. & Sisido, M. Incorporation of non-natural amino acids into proteins. *Curr. Opin. Biosci. Biotechnol.* **6**, 809–815 (2002).

178. Wang, K. *et al.* Optimized orthogonal translation of unnatural amino acids enables spontaneous protein double-labeling and FRET. *Nat. Chem.* **6**, 393–403 (2014).

179. Lang, K. & Chin, J. W. Cellular incorporation of unnatural amino acids and bioorthogonal labeling of proteins. *Chem. Rev.* **114**, 4764–806 (2014).

180. Mateo, C., Palomo, J. M., Fernandez-Lorente, G., Guisan, J. M. & Fernandez-Lafuente, R. Improvement of enzyme activity, stability and selectivity via immobilization techniques. *Enzyme Microb. Technol.* **40**, 1451–1463 (2007).

181. Janssen, K. P. F. *et al.* Single molecule methods for the study of catalysis: from enzymes to heterogeneous catalysts. *Chem. Soc. Rev.* **43**, 990–1006 (2014).

182. Rao, S. V., Anderson, K. W. & Bachas, L. G. Oriented immobilization of proteins. *Mikrochim. Acta* **128**, 127–143 (1998).

183. Lavis, L. D. & Raines, R. T. Bright Ideas for Chemical Biology. *ACS Chem. Biol.* **3**, (2007).

184. Zheng, Q. *et al.* Ultra-stable organic fluorophores for single-molecule research. *Chemical Society Reviews* **43**, 1044–1056 (2014).

185. Hu, Y. S., Zimmerley, M., Li, Y., Watters, R. & Cang, H. Single-molecule super-resolution light-sheet microscopy. *ChemPhysChem* **15**, 577–586 (2014).

186. Leung, B. O. & Chou, K. C. Review of super - Resolution fluorescence microscopy for biology. *Appl. Spectrosc.* **65**, 967–980 (2011).

187. Axelrod, D. Total internal reflection fluorescence microscopy in cell biology. *Methods Enzymol.* **361**, 1–33 (2003).

188. Roy, R., Hohng, S. & Ha, T. A practical guide to single-molecule FRET. **5**, 507–516 (2008).

189. Piston, D. W. & Kremers, G.-J. Fluorescent protein FRET: the good, the bad and the ugly. *Trends Biochem. Sci.* **32**, 407–414 (2007).

190. Wallace, B. & Atzberger, P. J. Förster resonance energy transfer: Role of diffusion of fluorophore orientation and separation in observed shifts of FRET efficiency. *PLoS One* **12**, 1–17 (2017).

191. Lerner, E. *et al.* Toward dynamic structural biology: Two decades of single-molecule Förster resonance energy transfer. *Science (80-.).* **359**, eaan1133 (2018).

192. Rhoades, E., Cohen, M., Schuler, B. & Haran, G. Two-state folding observed in individual protein molecules. *J. Am. Chem. Soc.* **126**, 14686–14687 (2004).

193. Kipper, K. *et al.* Structure-guided approach to site-specific fluorophore labeling of the lac repressor LacI. *PLoS One* **13**, 1–17 (2018).

194. Miyake-Stoner, S. J. *et al.* Probing protein folding using site-specifically encoded unnatural amino acids as FRET donors with tryptophan. *Biochemistry* **48**, 5953–5962 (2009).

195. Jackson, J. C., Duffy, S. P., Hess, K. R. & Mehl, R. A. Improving nature's enzyme active site with genetically encoded unnatural amino acids. *J. Am. Chem. Soc.* **128**, 11124–11127 (2006).

196. Mehl, R. A. *et al.* Generation of a bacterium with a 21 amino acid genetic code. *J. Am. Chem. Soc.* **125**, 935–939 (2003).

197. Heinemann, I. U. *et al.* Enhanced phosphoserine insertion during Escherichia coli protein synthesis via partial UAG codon reassignment and release factor 1 deletion. *FEBS Lett.* **586**, 3716–3722 (2012).

198. Ávila, S. N. S., Gutarra, M. L. E., Fernandez-Lafuente, R., Cavalcanti, E. D. C. & Freire, D. M. G. Multipurpose fixed-bed bioreactor to simplify lipase production by solid-state fermentation and application in biocatalysis. *Biochem. Eng. J.* **144**, 1–7 (2019).

199. De Godoy Daiha, K., Angeli, R., De Oliveira, S. D. & Almeida, R. V. Are lipases still important biocatalysts? A study of scientific publications and patents for technological forecasting. *PLoS One* **10**, 1–20 (2015).

200. Klibanov, A. M. Improving enzymes by using them in organic solvents. *Nature* **409**, 241–246 (2001).

201. Gotor-Fernández, V., Brieva, R. & Gotor, V. Lipases: Useful biocatalysts for the preparation of pharmaceuticals. *J. Mol. Catal. B Enzym.* **40**, 111–120 (2006).

202. Mustranta, A. Use of lipases in the resolution of racemic ibuprofen. *Appl. Microbiol. Biotechnol.* **38**, 61–66 (1992).

203. Jacobsen, E. E., Hoff, B. H., Moen, A. R. & Anthonsen, T. Enantioselective enzymatic preparation of chiral glutaric monocarboxylic acids and amides. *J. Mol. Catal. B Enzym.* **21**, 55–58 (2003).

204. Dong, H. P., Wang, Y. J. & Zheng, Y. G. Enantioselective hydrolysis of diethyl 3-hydroxyglutarate to ethyl (S)-3-hydroxyglutarate by immobilized Candida antarctica lipase B. *J. Mol. Catal. B Enzym.* **66**, 90–94 (2010).

205. Shimada, Y. *et al.* Conversion of vegetable oil to biodiesel using immobilized Candida antarctica lipase. *J. Am. Oil Chem. Soc.* **76**, 789–793 (1999).

206. Fernández-Lorente, G. *et al.* Modulation of lipase properties in macro-aqueous systems by controlled enzyme immobilization: Enantioselective hydrolysis of a chiral ester by immobilized Pseudomonas lipase. *Enzyme Microb. Technol.* **28**, 389–396 (2001).

207. Palomo, J. M., Segura, R. L., Fernandez-Lorente, G., Guisán, J. M. & Fernandez-Lafuente, R. Enzymatic resolution of (±)-glycidyl butyrate in aqueous media. Strong modulation of the properties of the lipase from Rhizopus oryzae via immobilization techniques. *Tetrahedron Asymmetry* **15**, 1157–1161 (2004).

208. Vorlova, S. *et al.* Enantioselective Hydrolysis of d , l -Menthyl Benzoate. *Adv. Synth. Catal.* **344**, 1152–1155 (2002).

209. Hasan, F., Shah, A. A. & Hameed, A. Industrial applications of microbial lipases. *Enzyme Microb. Technol.* **39**, 235–251 (2006).

210. Taverna, D. M. & Goldstein, R. A. Why are proteins marginally stable? *Proteins Struct. Funct. Genet.* **46**, 105–109 (2002).

211. Haki, G. D. & Rakshit, S. K. Developments in industrially important thermostable enzymes: A review. *Bioresour. Technol.* **89**, 17–34 (2003).

212. Rodrigues, R. C., Ortiz, C., Berenguer-Murcia, Á., Torres, R. & Fernández-Lafuente, R. Modifying enzyme activity and selectivity by immobilization. *Chem. Soc. Rev.* **42**, 6290–6307 (2013).

213. Fernández-Lorente, G., Palomo, J. M., Cabrera, Z., Guisán, J. M. & Fernández-Lafuente, R. Specificity enhancement towards hydrophobic substrates by immobilization of lipases by interfacial activation on hydrophobic supports. *Enzyme Microb. Technol.* **41**, 565–569 (2007).

214. Almeida, R. V. *et al.* Preparation of core–shell polymer supports to immobilize lipase B from Candida antarctica. *J. Mol. Catal. B Enzym.* **100**, 59–67 (2013).

215. Palomo, J. M. *et al.* Use of immobilized lipases for lipase purification via specific lipase-lipase interactions. *J. Chromatogr. A* **1038**, 267–273 (2004).

216. Cabrera, Z., Fernandez-Lorente, G., Fernandez-Lafuente, R., Palomo, J. M. & Guisan, J. M. Novozym 435 displays very different selectivity compared to lipase from Candida antarctica B adsorbed on other hydrophobic supports. *J. Mol. Catal. B Enzym.* **57**, 171–176 (2009).

217. Arroyo, M., Sánchez-Montero, J. M. & Sinisterra, J. V. Thermal stabilization of immobilized lipase B from Candida antarctica on different supports: Effect of water activity on enzymatic activity in organic media. *Enzyme Microb. Technol.* **24**, 3–12 (1999).

218. Palomo, J. M. *et al.* Interfacial adsorption of lipases on very hydrophobic support (octadecyl-Sepabeads): Immobilization, hyperactivation and stabilization of the open form of lipases. *J. Mol. Catal. B Enzym.* **19**, 279–286 (2002).

219. Derewenda, Z. S., Derewenda, U. & Dodson, G. G. The crystal and molecular structure of the Rhizomucor miehei triacylglyceride lipase at 1.9 Å resolution. *J. Mol. Biol.* **227**, 818–839 (1992).

220. Pleiss, J., Fischer, M. & Schmid, R. D. Anatomy of lipase binding sites: The scissile fatty acid binding site. *Chem. Phys. Lipids* **93**, 67–80 (1998).

221. Manoel, E. A., dos Santos, J. C. S., Freire, D. M. G., Rueda, N. & Fernandez-Lafuente, R. Immobilization of lipases on hydrophobic supports involves the open form of the enzyme. *Enzyme Microb. Technol.* **71**, 53–57 (2015).

222. Wilson, C. J., Clegg, R. E., Leavesley, D. I. & Pearcy, M. J. Mediation of Biomaterial–Cell Interactions by Adsorbed Proteins: A Review. *Tissue Eng.* **11**, 1–18 (2005).

223. Qi, H., Du, Y., Hu, G. & Zhang, L. Poly(carboxybetaine methacrylate)-functionalized magnetic composite particles: A biofriendly support for lipase immobilization. *Int. J. Biol. Macromol.* **107**, 2660–2666 (2018).

224. Stuart, M. A. C. *et al.* Emerging applications of stimuli-responsive polymer materials. *Nat. Mater.* **9**, 101–113 (2010).

225. Haag, R. *et al.* Protein Interactions with Polymer Coatings and Biomaterials. *Angew. Chemie Int. Ed.* **53**, 8004–8031 (2014).

226. Gunkel, G. & Huck, W. T. S. Cooperative adsorption of lipoprotein phospholipids, triglycerides, and cholesteryl esters are a key factor in nonspecific adsorption from blood plasma to antifouling polymer surfaces. *J. Am. Chem. Soc.* **135**, 7047–7052 (2013).

227. Jiang, S. & Cao, Z. Ultralow-fouling, functionalizable, and hydrolyzable zwitterionic materials and their derivatives for biological applications. *Adv. Mater.* **22**, 920–932 (2010).

228. Zdarta, J. *et al.* Lipase B from Candida antarctica Immobilized on a Silica-Lignin Matrix as a Stable and Reusable Biocatalytic System. *Catalysts* **7**, 1–21 (2016).

229. Niu, W., Li, Z., Zhang, D., Yu, M. & Tan, T. Improved thermostability and the optimum temperature of Rhizopus arrhizus lipase by directed evolution. *J. Mol. Catal. B Enzym.* **43**, 33–39 (2006).

230. Ahmad, S., Kamal, M. Z., Sankaranarayanan, R. & Rao, N. M. Thermostable Bacillus subtilis Lipases: In Vitro Evolution and Structural Insight. *J. Mol. Biol.* **381**, 324–340 (2008).

231. Gumulya, Y. *et al.* Engineering highly functional thermostable proteins using ancestral sequence reconstruction. *Nat. Catal.* **1**, 878–888 (2018).

232. Chado, G. R., Holland, E. N., Tice, A. K., Stoykovich, M. P. & Kaar, J. L. Exploiting the Benefits of Homogeneous and Heterogeneous Biocatalysis: Tuning the Molecular Interaction of Enzymes with Solvents via Polymer Modification. *ACS Catal.* **8**, 11579–11588 (2018).

233. Sosa, A. F. C. *et al.* Stabilization of Immobilized Enzymes via the Chaperone- like Activity of Mixed Lipid Bilayers. *ACS Appl. Mater. Interfaces* **10**, 19504–19513 (2018).

234. Hohlbein, J., Craggs, T. D. & Cordes, T. Alternating-laser excitation: single-molecule FRET and beyond. *Chem. Soc. Rev.* **43**, 1156–1171 (2014).

235. Weltz, J. S., Schwartz, D. K. & Kaar, J. L. Surface-Mediated Protein Unfolding as a Search Process for Denaturing Sites. *ACS Nano* **10**, 730–738 (2015).

236. Kienle, D. F., Falatach, R. M., Kaar, J. L. & Schwartz, D. K. Correlating Structural and Functional Heterogeneity of Immobilized Enzymes. *ACS Nano* **12**, 8091–8103 (2018).

237. Lewis, R. M., Torczon, V. & Trosset, M. W. Direct Search Methods : Then and Now. *J. Comput. Appl. Math.* **124**, 191–207 (2000).

238. Gianni, S. *et al.* Unifying features in protein-folding mechanisms. *Proc. Natl. Acad. Sci.* **100**, 13286–13291 (2003).

239. Faulón Marruecos, D., Kienle, D. F., Kaar, J. L. & Schwartz, D. K. Grafting Density Impacts Local Nanoscale Hydrophobicity in Poly(ethylene glycol) Brushes. *ACS Macro Lett.* **7**, 498–503 (2018).

240. Unsworth, L. D., Sheardown, H. & Brash, J. L. Protein-resistant poly(ethylene oxide)-grafted surfaces: chain density-dependent multiple mechanisms of action. *Langmuir* **24**, 1924–9 (2008).

241. Faulón Marruecos, D., Kastantin, M., Schwartz, D. K. & Kaar, J. L. Dense Poly(ethylene glycol) Brushes Reduce Adsorption and Stabilize the Unfolded Conformation of Fibronectin. *Biomacromolecules* **17**, 1017–1025 (2016).

242. Benjamin, S. & Pandey, A. Candida rugosa lipases: Molecular biology and versatility in biotechnology. *Yeast* **14**, 1069–1087 (1998).

243. Kirk, O. & Christensen, M. W. Lipases from Candida antarctica: Unique biocatalysts from a unique origin. *Org. Process Res. Dev.* **6**, 446–451 (2002).

244. Villeneuve, P., Muderhwa, J. M., Graille, J. & Haas, M. J. Customizing lipases for biocatalysis: A survey of chemical, physical and molecular biological approaches. *J. Mol. Catal. - B Enzym.* **9**, 113–148 (2000).

245. Willard, L. *et al.* VADAR: A web server for quantitative evaluation of protein structure quality. *Nucleic Acids Res.* **31**, 3316–3319 (2003).

246. Fuentes, M. *et al.* General Trend of Lipase to Self-Assemble Giving Bimolecular Aggregates Greatly Modifies the Enzyme Functionality. *Biomacromolecules* **4**, 1–6 (2003).

247. Uppenberg, J., Hansen, M. T., Patkar, S. & Jones, T. A. The sequence, crystal structure determination and refinement of two crystal forms of lipase B from Candida antarctica. *Structure* **15**, 293–308 (1994).

248. Guo, S. *et al.* Surface charge control for zwitterionic polymer brushes: Tailoring surface properties to antifouling applications. *J. Colloid Interface Sci.* **452**, 43–53 (2015).

249. Peeler, J. C. & Mehl, R. A. Site-Specific Incorporation of Unnatural Amino Acids as Probes for Protein Conformational Changes. in *Unnatural Amino Acids: Methods and Protocols* (eds. Pollegioni, L. & Servi, S.) **794**, 125–134 (Humana Press, 2012).

250. Kawasaki, K., Kondo, H., Suzuki, M., Ohgiya, S. & Tsuda, S. Alternate conformations observed in catalytic serine of Bacillus subtilis lipase determined at 1.3 Å resolution. *Acta Crystallogr. Sect. D Biol. Crystallogr.* **58**, 1168–1174 (2002).

251. Klibanov, A. M. Enzyme Stabilization by Immobilization. *Anal. Biochem.* **93**, 1–25 (1979).

252. Zacharis, E., Moore, B. D. & Halling, P. J. Control of Enzyme Activity in Organic Media by Solid-State Acid−Base Buffers. *J. Am. Chem. Soc.* **119**, 12396–12397 (1997).

253. LeJeune, K. E., Wild, J. R. & Russell, A. J. Nerve agents degraded by enzymatic foams. *Nature* **395**, 27–28 (1998).

254. Yang, Z. *et al.* Activity and Stability of Enzymes Incorporated into Acrylic Polymers. *J. Am. Chem. Soc.* **117**, 4843–4850 (1995).

255. Brzozowski, A. M. *et al.* A model for interfacial activation in lipases from the structure of a fungal lipase-inhibitor complex. *Nature* **351**, 491–494 (1991).

256. Singh, P. SPR Biosensors: Historical Perspectives and Current Challenges. *Sensors Actuators, B Chem.* **229**, 110–130 (2016).

257. Vaisocherová, H. *et al.* Functionalizable surface platform with reduced nonspecific protein adsorption from full blood plasma-Material selection and protein immobilization optimization. *Biosens. Bioelectron.* **24**, 1924–1930 (2009).

258. Knecht, S., Ricklin, D., Eberle, A. N. & Ernst, B. Oligohis-tags: mechanisms of binding to Ni2+-NTA surfaces. *J. Mol. Recognit.* **22**, 270–9 (2009).

259. Tugulu, S., Arnold, A., Sielaff, I., Johnsson, K. & Klok, H. A. Protein-functionalized polymer brushes. *Biomacromolecules* **6**, 1602–1607 (2005).

260. Richins, R. D., Kaneva, I., Mulchandani, A. & Chen, W. Biodegradation of organophosphorus pesticides by surface-expressed organophosphorus hydrolase. *Nat. Biotechnol.* **15**, 984–987 (1997).

261. Mansee, A. H., Chen, W. & Mulchandani, A. Detoxification of the organophosphate nerve agent coumaphos using organophosphorus hydrolase immobilized on cellulose materials. *J. Ind. Microbiol. Biotechnol.* **32**, 554–560 (2005).

262. Mulchandani, A., Kaneva, I. & Chen, W. Detoxification of organophosphate nerve agents by immobilized Escherichia coli with surface-expressed organophosphorus hydrolase. *Biotechnol. Bioeng.* **63**, 216–223 (1999).

263. Pollard, D. J. & Woodley, J. M. Biocatalysis for pharmaceutical intermediates: the future is now. *Trends Biotechnol.* **25**, 66–73 (2007).

264. Bisen, P. Enzyme Immobilization. in *Laboratory Protocols in Applied Life Sciences* 1213–1246 (2014). doi:10.1201/b16575-23

265. Iyer, P. V. & Ananthanarayan, L. Enzyme stability and stabilization-Aqueous and non-aqueous environment. *Process Biochem.* **43**, 1019–1032 (2008).

266. Zhao, H. Methods for stabilizing and activating enzymes in ionic liquids - A review. *J. Chem. Technol. Biotechnol.* **85**, 891–907 (2010).

267. Zou, X. *et al.* Investigating the Effect of Two-Point Surface Attachment on Enzyme Stability and Activity. *J. Am. Chem. Soc.* **140**, 16560–16569 (2018).

268. Wang, P., Sergeeva, M. V., Lim, L. & Dordick, J. S. Biocatalytic plastics as active and stable materials for biotransformations. *Nat. Biotechnol.* **15**, 789–793 (1997).

269. Barbosa, O. *et al.* Heterofunctional supports in enzyme immobilization: From traditional immobilization protocols to opportunities in tuning enzyme properties. *Biomacromolecules* **14**, 2433–2462 (2013).

270. Romdhane, I. B. Ben, Romdhane, Z. Ben, Gargouri, A. & Belghith, H. Esterification activity and stability of Talaromyces thermophilus lipase immobilized onto chitosan. *J. Mol. Catal. B Enzym.* **68**, 230–239 (2011).

271. Bilal, M., Asgher, M., Cheng, H., Yan, Y. & Iqbal, H. M. N. Multi-point enzyme immobilization, surface chemistry, and novel platforms: a paradigm shift in biocatalyst design. *Crit. Rev. Biotechnol.* **39**, 202–219 (2019).

272. LeJeune, K. E. *et al.* Dramatically stabilized phosphotriesterase-polymers for nerve agent degradation. *Biotechnol. Bioeng.* **54**, 105–114 (1997).

273. Mozhaev, V. V., Melik-Nubarov, N. S., Sergeeva, M. V., Šikšnis, V. & Martinek, K. Strategy for stabilizing enzymes part one: Increasing stability of enzymes via their multi-point interaction with a support. *Biocatal. Biotransformation* **3**, 179–187 (1990).

274. LeJeune, K. E., Swers, J. S., Hetro, A. D., Donahey, G. P. & Russell, A. J. Increasing the tolerance of organophosphorus hydrolase to bleach. *Biotechnol. Bioeng.* **64**, 250–254 (1999).

275. Fernandez-Lafuente, R., Guisan, J. M., Ali, S. & Cowan, D. Immobilization of functionally unstable catechol-2,3-dioxygenase greatly improves operational stability. *Enzyme Microb. Technol.* **26**, 568–573 (2000).

276. Henzler-Wildman, K. & Kern, D. Dynamic personalities of proteins. *Nature* **450**, 964–972 (2007).

277. Villali, J. & Kern, D. Choreographing an enzyme's dance. *Curr. Opin. Chem. Biol.* **14**, 636–643 (2010).

278. Kerns, S. J. *et al.* The energy landscape of adenylate kinase during catalysis. (2015). doi:10.1038/nsmb.2941

279. Weltz, J. S., Kienle, D. F., Schwartz, D. K. & Kaar, J. L. Dramatic Increase in Catalytic Performance of Immobilized Lipases by Their Stabilization on Polymer Brush Supports. *ACS Catal.* 4992–5001 (2019). doi:10.1021/acscatal.9b01176

280. Wang, Y. & Lu, H. P. Bunching effect in single-molecule T4 lysozyme nonequilibrium conformational dynamics under enzymatic reactions. *J. Phys. Chem. B* **114**, 6669–74 (2010).

281. Kuzmenkina, E. V., Heyes, C. D. & Nienhaus, G. U. Single-molecule Förster resonance energy transfer study of protein dynamics under denaturing conditions. *Proc. …* **102**, 15471–6 (2005).

282. Aviram, H. Y. *et al.* Direct observation of ultrafast large-scale dynamics of an enzyme under turnover conditions. 1–6 (2018). doi:10.1073/pnas.1720448115

283. Choi, J. M., Han, S. S. & Kim, H. S. Industrial applications of enzyme biocatalysis: Current status and future aspects. *Biotechnology Advances* **33**, 1443–1454 (2015).

284. Ma, J. *et al.* Overexpression and characterization of a lipase from Bacillus subtilis. *Protein Expr. Purif.* **45**, 22–29 (2006).

285. Romero, P. A. & Arnold, F. H. Exploring protein fitness landscapes by directed evolution. *Nat. Rev. Mol. Cell Biol.* **10**, 866–876 (2009).

286. Soskine, M. & Tawfik, D. S. Mutational effects and the evolution of new protein functions. *Nat. Rev. Genet.* **11**, 572–582 (2010).

287. Pace, C. N. & Shirley, B. A. Forces contributing proteins of proteins. *Faseb* **10**, 75–83 (1996).

288. Reznik, C., Estillore, N., Advincula, R. C. & Landes, C. F. Single molecule spectroscopy reveals heterogeneous transport mechanisms for molecular ions in a polyelectrolyte polymer brush. *J. Phys. Chem. B* **113**, 14611–14618 (2009).

289. Sarshar, M., Wong, W. T. & Anvari, B. Comparative study of methods to calibrate the stiffness of a single-beam gradient-force optical tweezers over various laser trapping powers. *J. Biomed. Opt.* **19**, (2014).

290. Zaccai, G. How Soft Is a Protein? A Protein Dynamics Force Constant Measured by Neutron Scattering. *Science (80-.).* **288**, 1604–1607 (2000).

291. Schlierf, M. & Rief, M. Temperature softening of a protein in single-molecule experiments. *J. Mol. Biol.* **354**, 497–503 (2005).

292. Thorpe, M. F. Comment on elastic network models and proteins. *Phys. Biol.* **4**, 60–63 (2007).

Appendix C : Supporting Information for Chapter 2

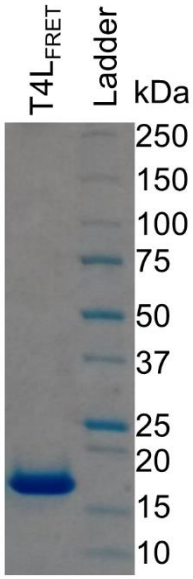

Figure C-1: Coomassie-stained SDS-PAGE of T4L$_{FRET}$ after purification. The gel contains a single band of approximately 18 kDa that corresponds to the expected molecular weight of T4L$_{FRET}$.

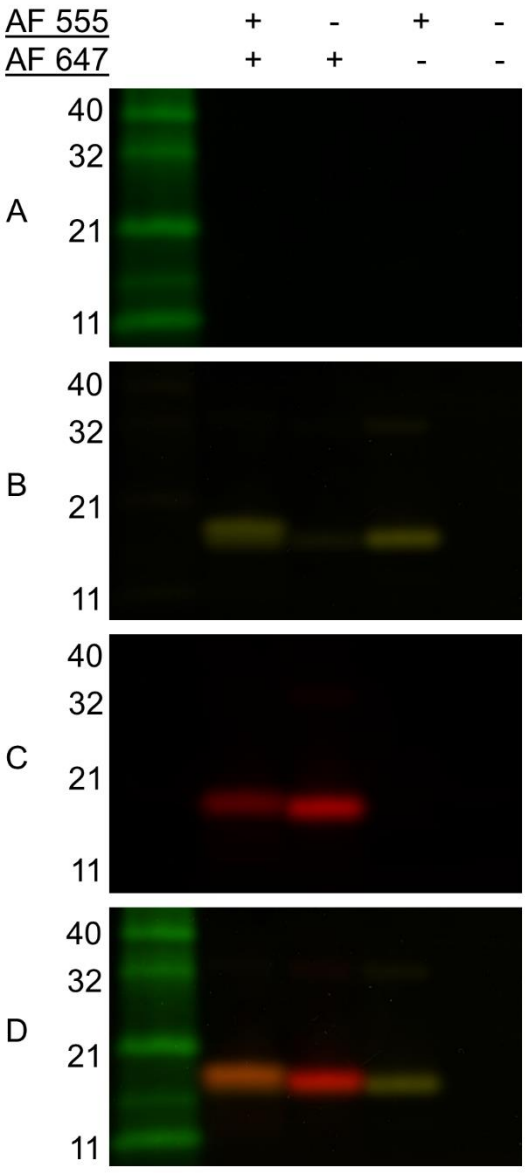

Figure C-2: In-gel fluorescence imaging of labeled $T4L_{FRET}$ with direct excitation of (A) Alexa 488 (for the protein ladder), (B) Alexa 555, (C) Alexa 647, and (D) the composite (i.e., overlay) image confirmed covalent attachment of donor and acceptor dye molecules.

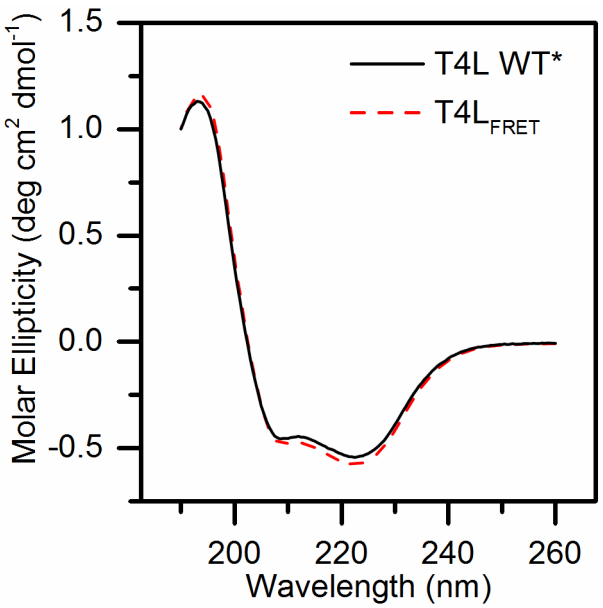

Figure C-3: Circular dichroism spectra (Chirascan Plus, Applied Photophysics) for unlabeled T4L WT* and T4L$_{FRET}$ was measured in 50 mM sodium phosphate, pH 6.80 at 1 mg/mL protein concentration. The spectra represent the average of five successive scans from 190-260 nm in 0.5 nm increments with an integration time of 0.5 s per increment.

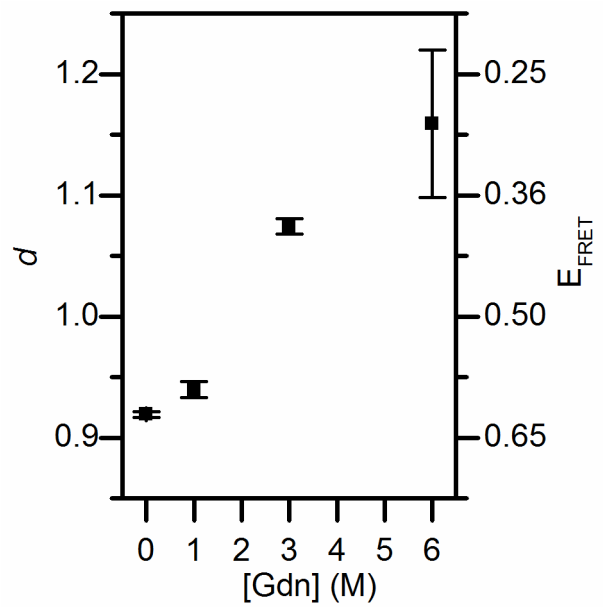

Figure C-4: Ensemble denaturation of labeled $T4L_{FRET}$ in solution , showing a monotonic increase in d-value and corresponding decrease in FRET efficiency with increasing denaturant. Solutions containing 5 μg/mL of labeled $T4L_{FRET}$ were incubated at room temperature in 50 mM sodium phosphate buffer, pH 6.80, containing 0-6 M guanidine hydrochloride (Gdn) for 1 h. FRET was measured by exciting the protein solution at 555 nm and measuring fluorescence emission of the donor and acceptor at 580 and 665 nm, respectively, using a Fluoromax-4 (Horiba) fluorimeter. Error bars represent the standard deviation of d-values obtained from three independent replicates.

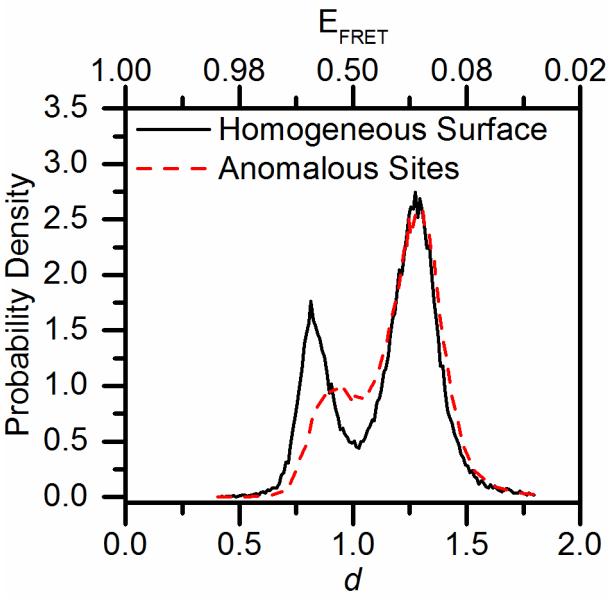

Figure C-5: Distribution of d–values for $T4L_{FRET}$ for approximately 10^6 observations on FS, which was used to identify molecular signatures of folded and unfolded states. Each observation was segmented based on the location as either on the homogeneous surface or regions with anomalously high numbers of adsorption events. Histograms of d-values for the homogeneous surface showed two well-separated populations centered at d=0.85 and d=1.27, corresponding to folded and unfolded states, respectively. Compared to on the homogenous surface, a greater fraction of protein molecules adsorbed to anomalous sites were unfolded, suggesting that the anomalous sites were denaturing.

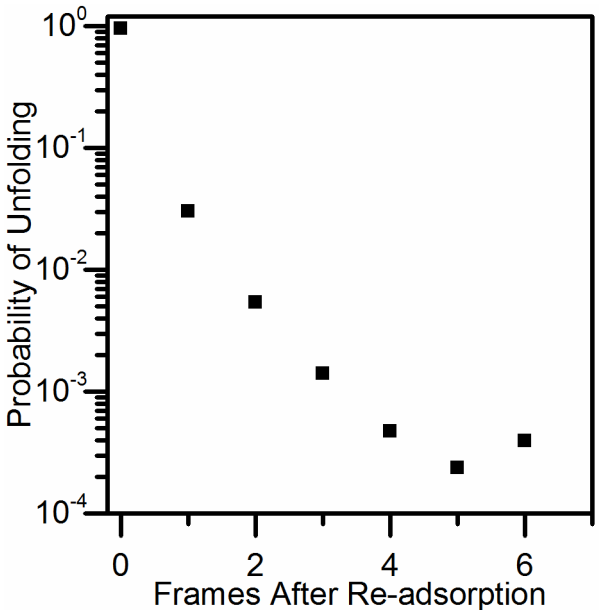

Figure C-6: The distribution of the number of frames in which a folded protein molecule appears immobile before unfolding. Motion was considered significant if the protein exhibited an apparent displacement >50 nm between frames.

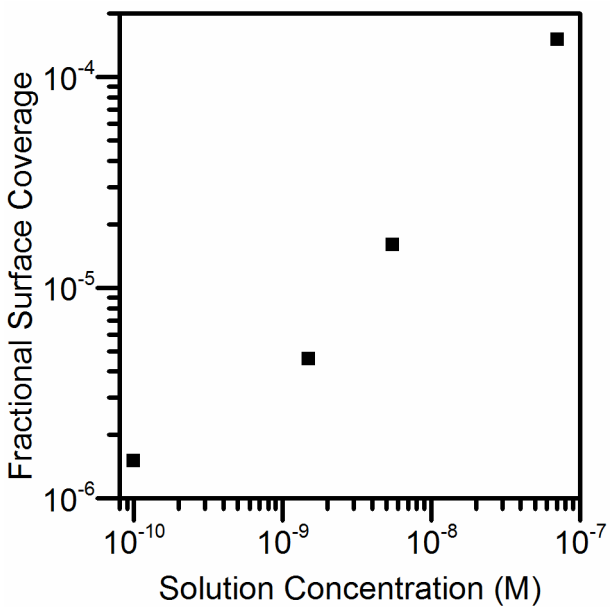

Figure C-7: Fractional surface coverage of unlabeled T4L WT* as a function of the concentration of T4L WT* in the bulk solution exposed to FS. Surface coverages were estimated from the ratio of labeled-to-unlabeled protein used for each condition, the number of labeled molecules adsorbed, and the estimated footprint of T4L WT* from the crystal structure (PDB 1L63).

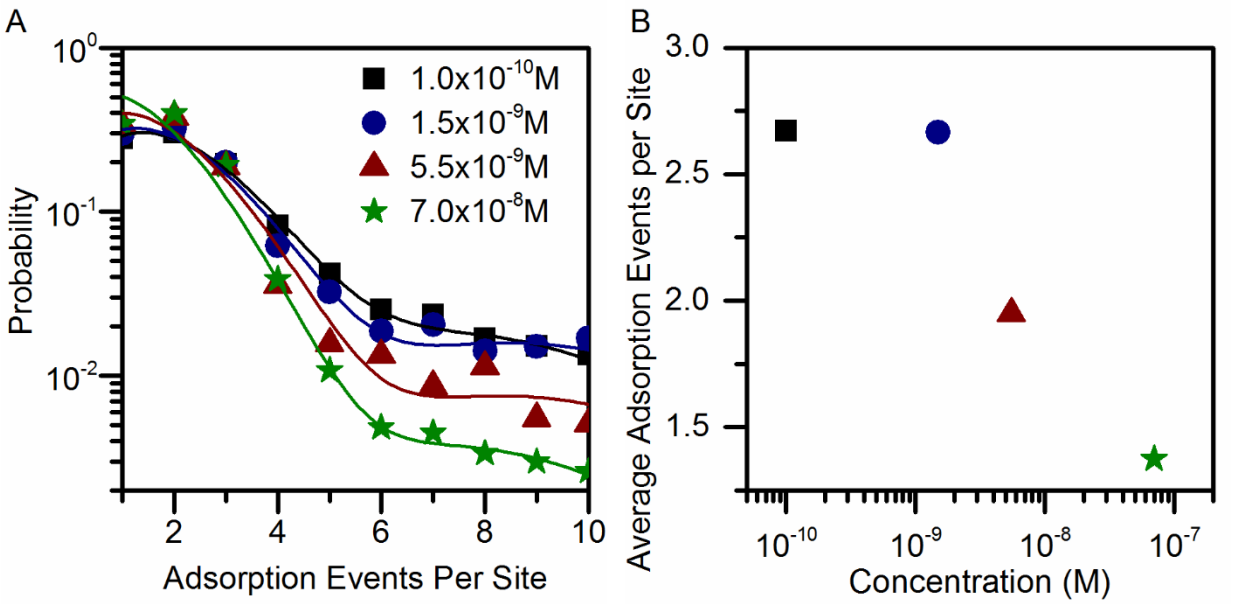

Figure C-8: (A) Sites that demonstrated anomalously high numbers of adsorption events were identified and the number of adsorption events to each continuous site was quantified. The adsorption site histogram was fit to a three-component Poisson mixture model. (B) The average number of adsorption events per site calculated from the fitted Poisson mixture model.

Appendix D : Supporting Information for Chapter 3

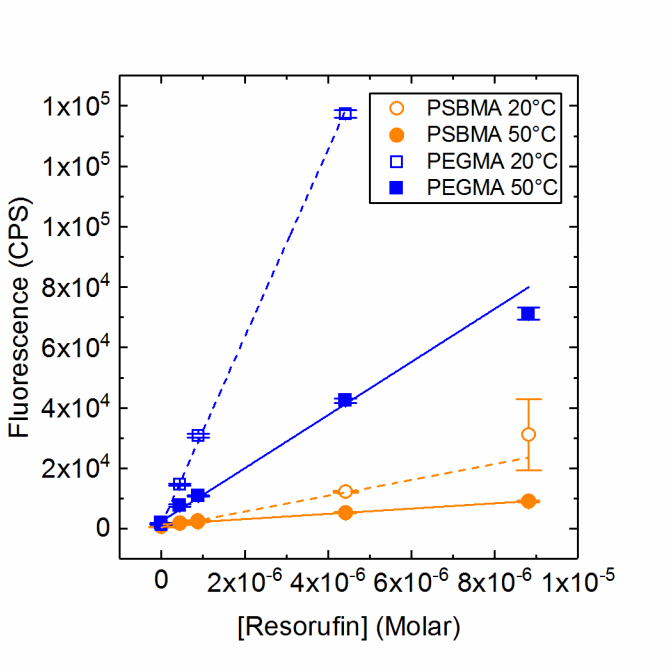

Figure D-1: Adsorption isotherms of resorufin on PSBMA and PEGMA brushes. Adsorbed quantity of the fluorescent product resorufin as measured by total internal reflection fluorescence and displayed as a fluorescence intensity in counts per second. The quantity of adsorbed resorufin in greater on the PEGMA surface compared to PSBMA and decrease on both surfaces with increasing temperature.

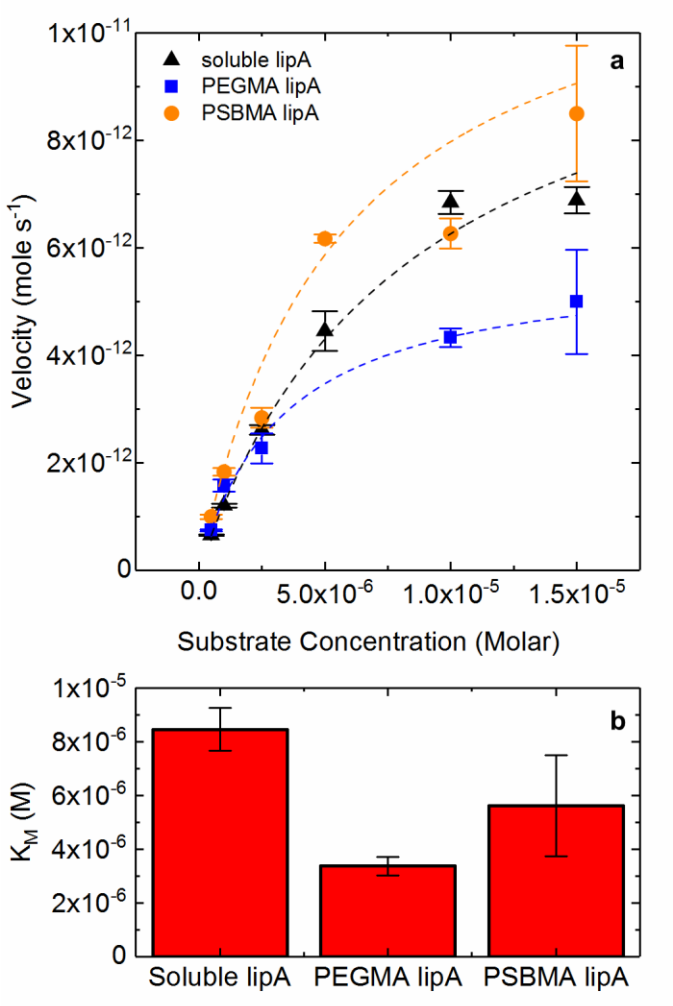

Figure D-2: Michaelis-Menten kinetics of soluble and immobilized lipA. (a) Activity of soluble lipA (black triangles), PEGMA immobilized lipA (blue squares) and PSBMA immobilized lipA (orange circles) as a function of substrate concentration. Each measurement was performed in triplicate and error bars represent the standard deviation of the experimental replicates. Two-parameter, non-linear Michaelis-Menten fits of V_{max} and K_M are shown as dotted lines of the corresponding color for each condition. (b) Values for the fitted parameter K_M for each lipase, with error bars representing the standard error of the fit.

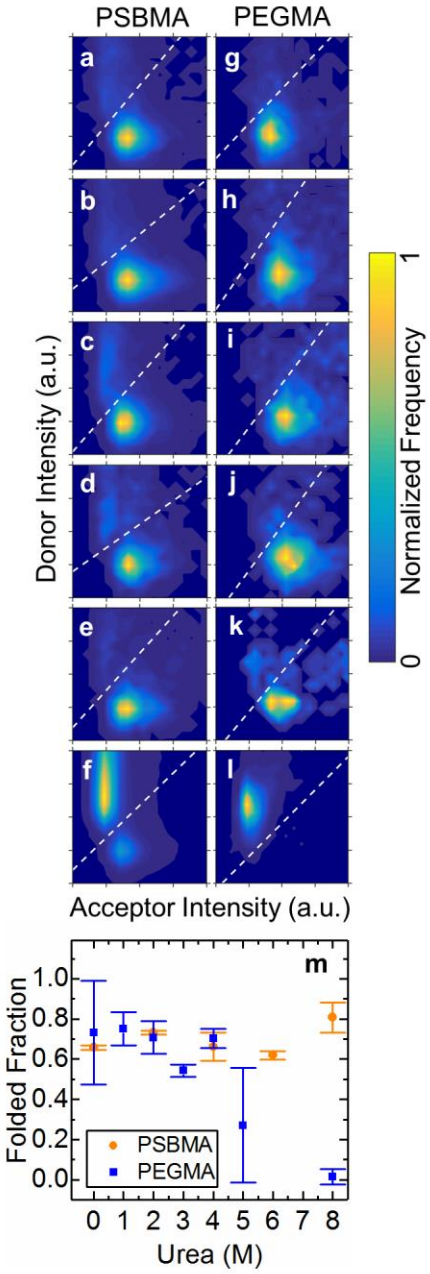

Figure D-3: SM chemical denaturation of immobilized lipA. (a-f) SM-FRET maps of the chemical denaturation of lipA immobilized on PSBMA in 50 mM sodium phosphate at 20°C with (a) 0 M (2,930 trajectories), (b) 2 M (8,935 trajectories), (c) 4 M (3,447 trajectories), (d) 6 M (979 trajectories), (e) 8 M urea (1,560 trajectories) and (f) 8 M urea at 45°C (9,157 trajectories). (g-l) SM-FRET maps of the chemical denaturation of lipA immobilized on PEGMA in 50 mM sodium phosphate at 20°C with (g) 0 M (1,280 trajectories), (h) 1 M (1,751 trajectories), (i) 2 M (1,276 trajectories), (j) 3 M (714 trajectories), (k) 5 M (566 trajectories), and (l) 8 M urea (1,855 trajectories). (m) Folded fraction of lipA immobilized on PEGMA

(blue squares) and PSBMA (orange circles) as determined from quantitative analysis of the SM-FRET maps in panels a-l. Error bars represent the standard error of folded fraction, which was estimated using jackknife resampling with replacement of trajectories for each condition. All samples were incubated under the given conditions for 1 h before imaging to ensure measurements were performed at equilibrium. Notably, a significant peak for the unfolded state of lipA on PSBMA is only obtained in 8 M urea and 45°C. The retention of a significant folded population above 5 M urea on PSBMA supports demonstrated that lipA was more stable on this support than on PEGMA at elevated concentrations of urea. Additionally, lipA was more stable on both the PEGMA and PSBMA supports than in solution, as demonstrated by the solution chemical denaturation of lipA shown in **Supporting Figure S6**.

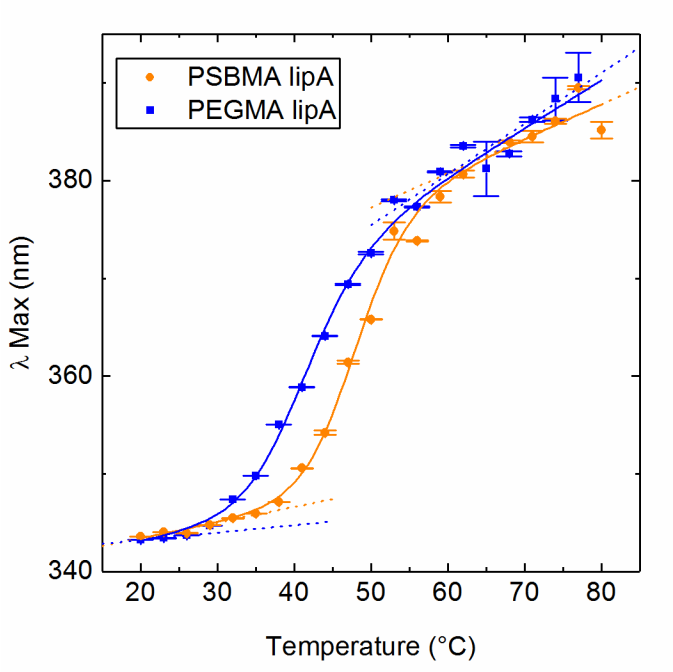

Figure D-4: Ensemble thermal denaturation of immobilized wild-type lipA. Native tryptophan fluorescence of lipA immobilized on PSBMA and PEGMA supports was measured as a 5 mg/mL suspension in 50 mM sodium phosphate at pH 7.5. Samples were continuously stirred to prevent sedimentation in a temperature-controlled quartz cuvette with excitation at 295 nm. Samples were equilibrated for 30 min before acquiring spectra. Tryptophan emission spectra were fitted to a third-order polynomial to determine the emission maxima and error bars are expressed as the standard error of the maximum of fit by jackknife sampling of the emission spectra. Fits of denaturation curves was based on a two-state unfolding model and the linear folded and unfolded baselines are displayed as dashed lines. The melting temperature for lipA was 47.7°C ± 0.8°C and 40.7°C ± 0.4°C for PSBMA and PEGMA supports, respectively.

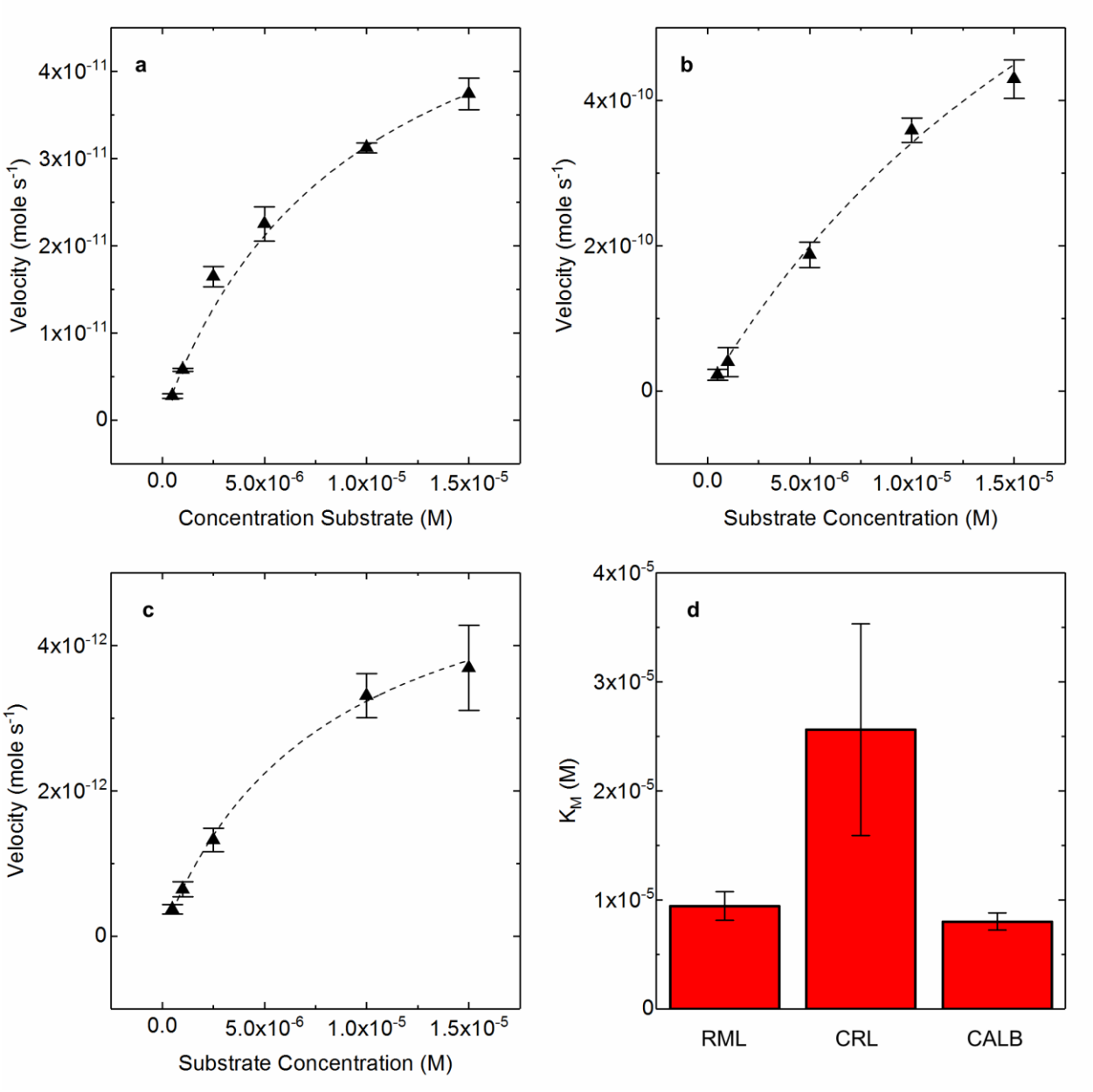

Figure D-5: Michaelis-Menten kinetics for (a) RML, (b) CRL, and (c) CALB. Measurements were performed in triplicate and error bars represent the standard deviation of the experimental replicates. Two-parameter, non-linear Michaelis-Menten fits of V_{max} and K_M are shown as dotted lines. (d) Values for the fitted parameter K_M for each lipase, with error bars representing the standard error of the fit.

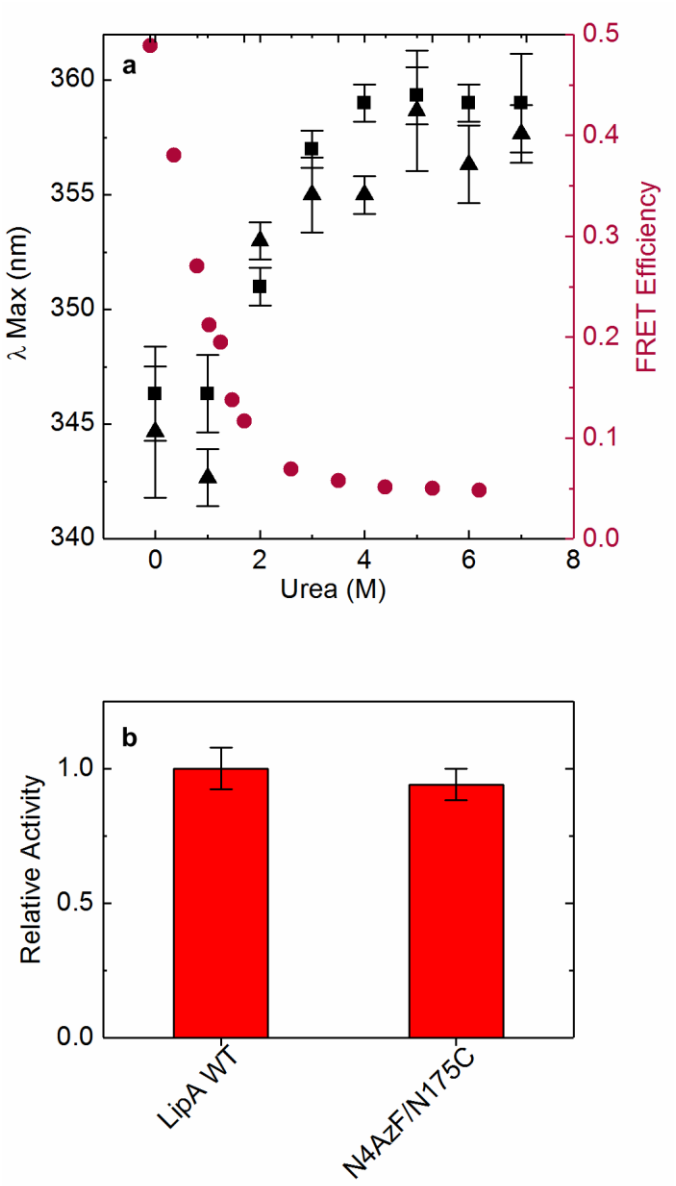

Figure D-6: Characterization of labeled lipA. (a) Chemical denaturation of wild-type lipA (black squares) and labeled lipA (black triangles) monitored by the peak emission of the native tryptophan fluorescence excited with 295 nm light and displayed on the left y-axis in black. Error bars represent the standard deviation of three replicates. Emission of exogeneous fluorophore labels excited with 532 nm light and displayed as a FRET efficiency on the right y-axis in red for labeled lipA (circles). (b) Relative activity of the wild type and mutant lipA using the fluorogenic substrate resorufin butyrate, normalized to the activity of the wild-type enzyme.

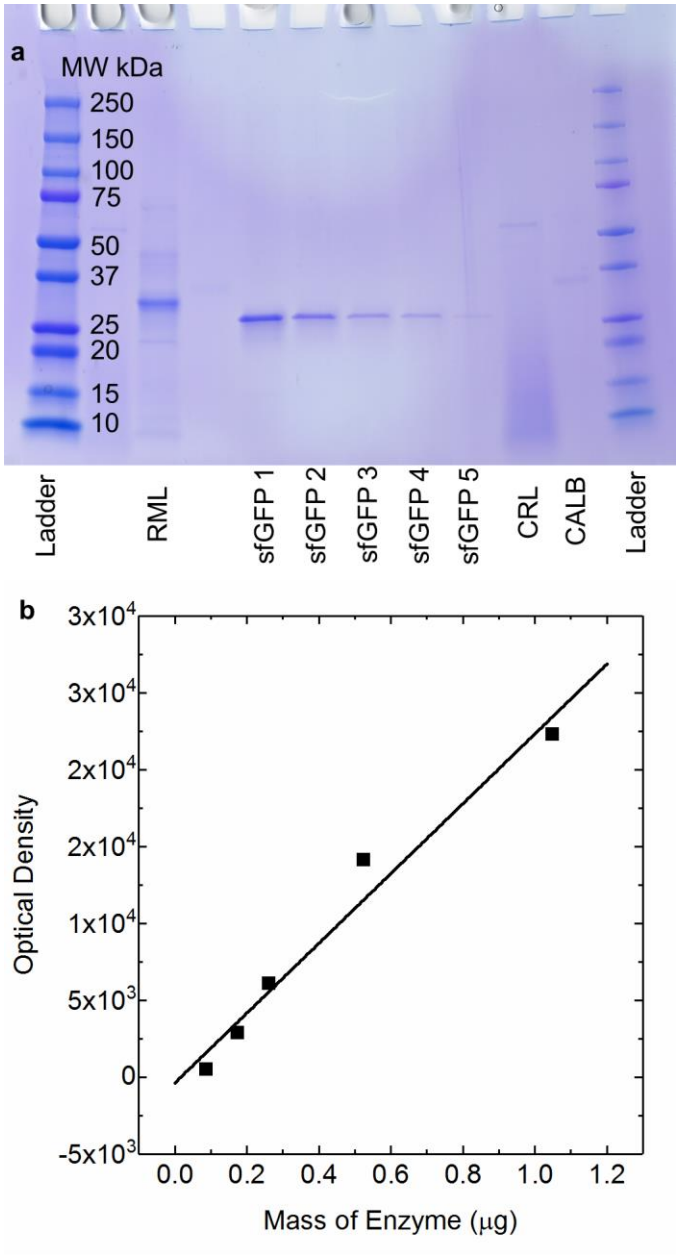

Figure D-7: Quantification of RML, CRL, and CALB by SDS-PAGE densitometry. (a) SDS-PAGE of RML, CRL, and CALB after reconstitution and extensive dialysis against 50 mM sodium phosphate, pH 7.5. Samples were run on a 4-12% acrylamide gradient gels (Biorad mini PROTEAN TGX 4-20% acrylamide gel) and stained with Coomassie. Lanes labeled with sfGFP were loaded with purified superfolder green fluorescent protein (sfGFP), which was used to generate a standard curve for optical density (from intensity of Coomassie staining) versus mass of enzyme. (b) Standard curve of the mass of sfGFP versus the optical density of the band within a given lane as quantified by the imageJ gel analyzer.

Appendix E : Supporting Information for Chapter 4

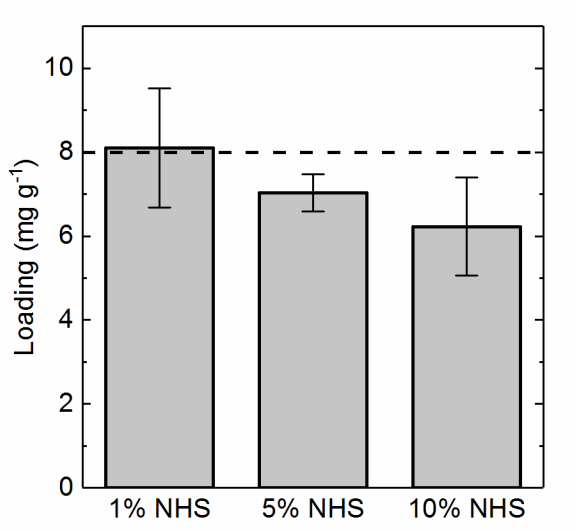

Figure E-1: Quantification of enzyme loading on 1 μm silica particles. After immobilization reactions, particles were sedimented and the concentration of unreacted enzyme remaining in the supernatant was quantified by the activity of this solution. The loading of enzyme on the particles, expressed as mg lipA per g of particles, was calculated from the mass balance between concentration of enzyme in the initial immobilization reaction and remaining enzyme in the supernatant after the 24-hour immobilization. Supernatant was aspirated and discarded, and particles were resuspended in fresh buffer containing 50 mM sodium phosphate at pH 7.5. Subsequently, particles were re-sedimented, and this rinsing procedure was repeated two additional times, with no residual activity due to enzyme leaching was observed in any rinse. The dotted line represents the maximum theoretical monolayer coverage of the enzyme assuming a 3 nm by 3 nm rectangular two-dimensional projected area of the immobilized enzyme. Error bars represent the standard deviation from three replicate activity measurements for each condition.

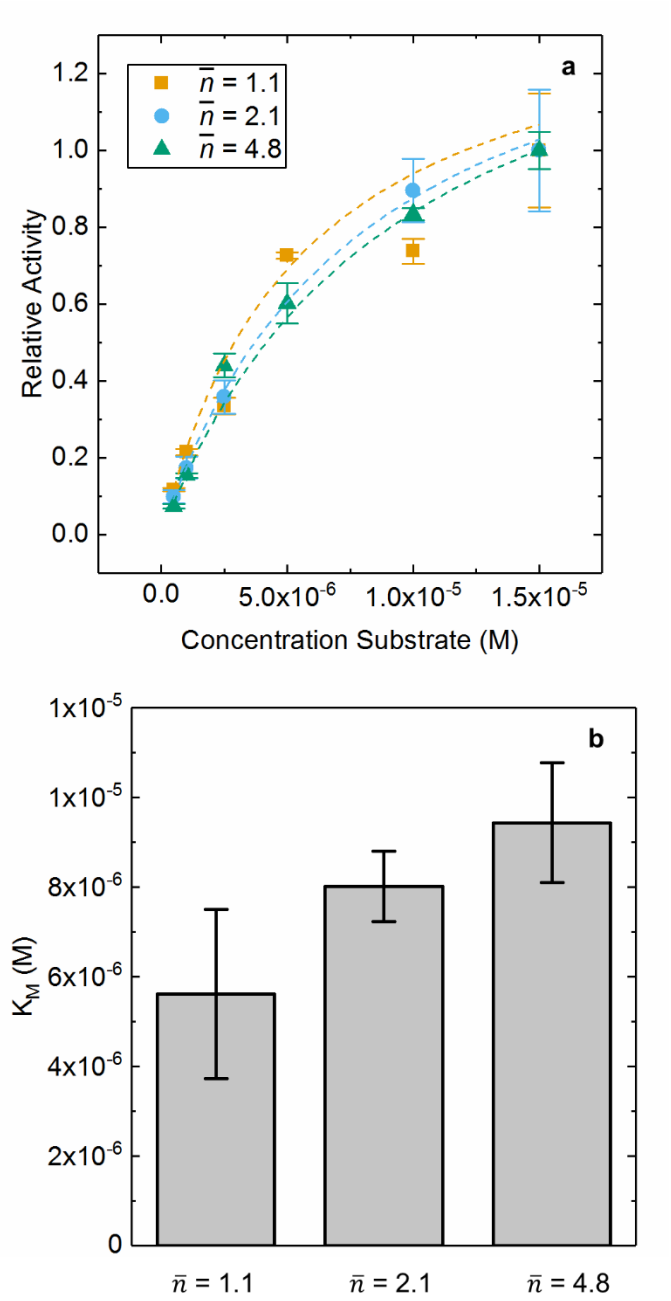

Figure E-2: Michaelis-Menten kinetics of immobilized lipA. (a) Substrate concentration dependence of relative activity of immobilized lipA with non-linear Michaelis-Menten fits. Error bars represent the standard deviation from three experimental replicates. (b) Michaelis constant (K_M) for immobilized lipA on the three supports. Error bars represent the standard error of the non-linear fit.

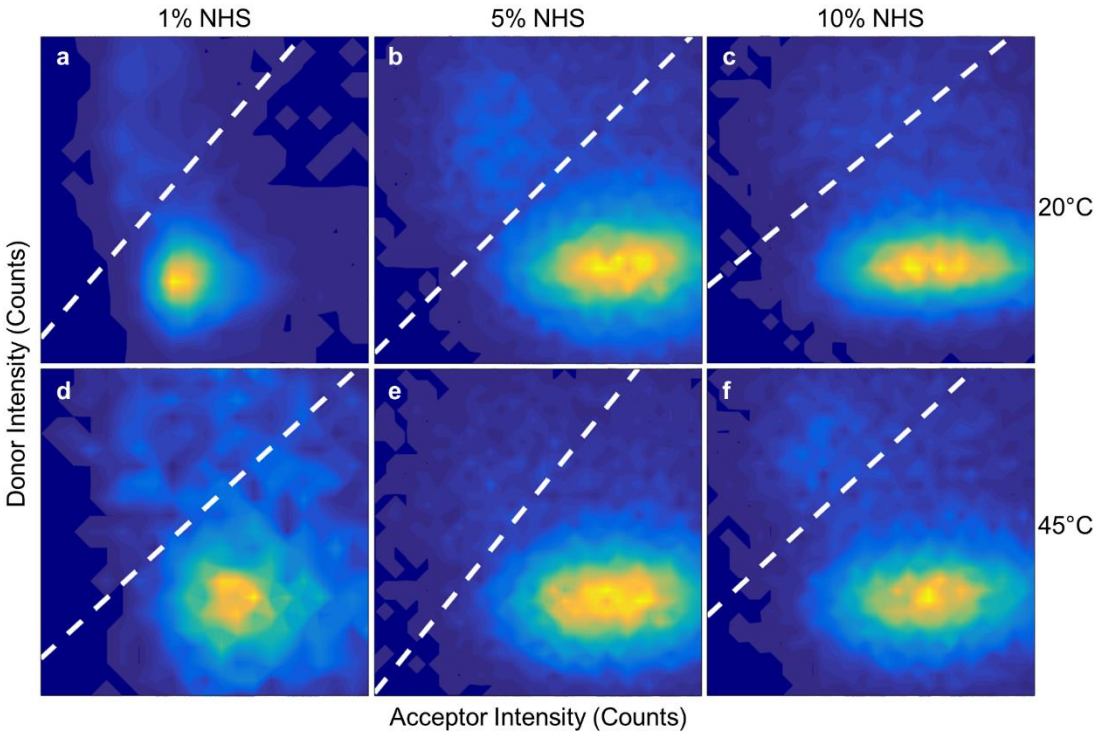

Figure E-3: Donor-acceptor intensity histograms. Two-dimensional histograms of donor-acceptor intensity pairs for each SM observation of lipA immobilized on polymer brushes synthesized with (a) 1% NHS ($\bar{n}$ = 1.1), (b) 5% NHS ($\bar{n}$ = 2.1), and (c) 10% NHS ($\bar{n}$ = 4.8) at 20°C and (d) 1% NHS ($\bar{n}$ = 1.1), (e) 5% NHS ($\bar{n}$ = 2.1), and (f) 10% NHS ($\bar{n}$ = 4.8) at 45°C. Dashed lines represent the threshold for state determination obtained from a pattern search that minimized the integrated number of observations underneath the threshold line. Observations below the threshold exhibited low donor and high acceptor emissions and were assigned as folded. Observations above the threshold exhibited high donor and low acceptor emission and were assigned as unfolded, consistent with both the site-specific labeling design and previous SM observations of this FRET-labeled construct.

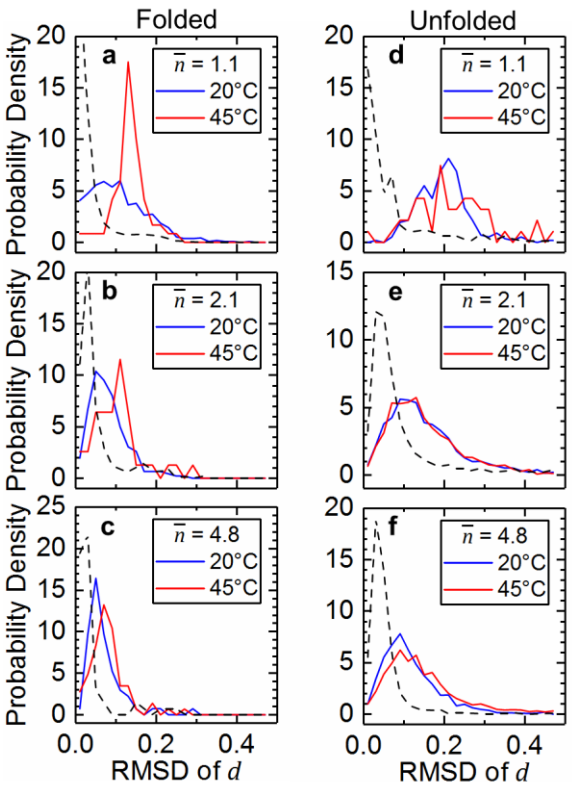

Figure E-4: Experimental and simulated RMSDs of d for immobilized lipA. Distributions of the RMSD of d at 20ºC (blue lines) and 45ºC (red lines) and simulations based on the measured uncertainties of donor and acceptor intensity (black dashed lines) for trajectories that remained folded for (a) $\bar{n}$ = 1.1, (b) $\bar{n}$ = 2.1, (c) $\bar{n}$ = 4.8 and for trajectories that remained unfolded for (d) $\bar{n}$ = 1.1, (e) $\bar{n}$ = 2.1, (f) $\bar{n}$ = 4.8. Simulations were performed for the same number of trajectories of the same duration for each condition. The time-averaged d value was varied randomly in these simulated trajectories based on the measured uncertainty in intensity measurements for each observation. The RMSD of d was calculated for each simulated trajectory in a given condition and plotted as a probability density function. Notably, these simulated RMSDs of d were significantly less than the observed distributions of RMSDs of d, indicating that the observed fluctuations in intensity were not due to camera noise.

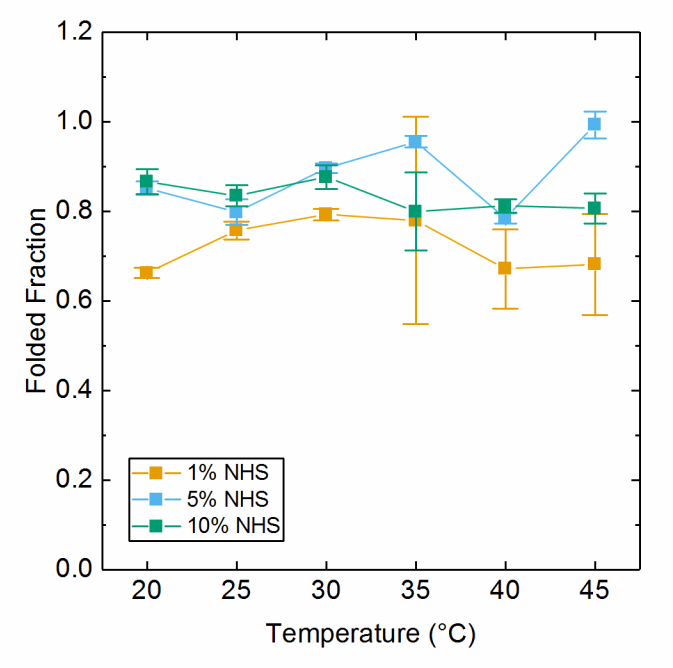

Figure E-5: LipA folded fractions from SM observations. Folded fraction versus temperature for lipA immobilized on polymer brush supports for lipA immobilized on 1% NHS supports ($\bar{n}$ = 1.1, gold squares), 5% NHS supports ($\bar{n}$ = 2.1, blue squares) and 10% NHS ($\bar{n}$ = 4.8, green squares). Folded fractions were obtained from thresholded, two-dimensional donor-acceptor histograms for all SM observations of immobilized lipA. Error bars represent estimates of the standard deviation obtained from jackknife sampling of trajectories for each condition.

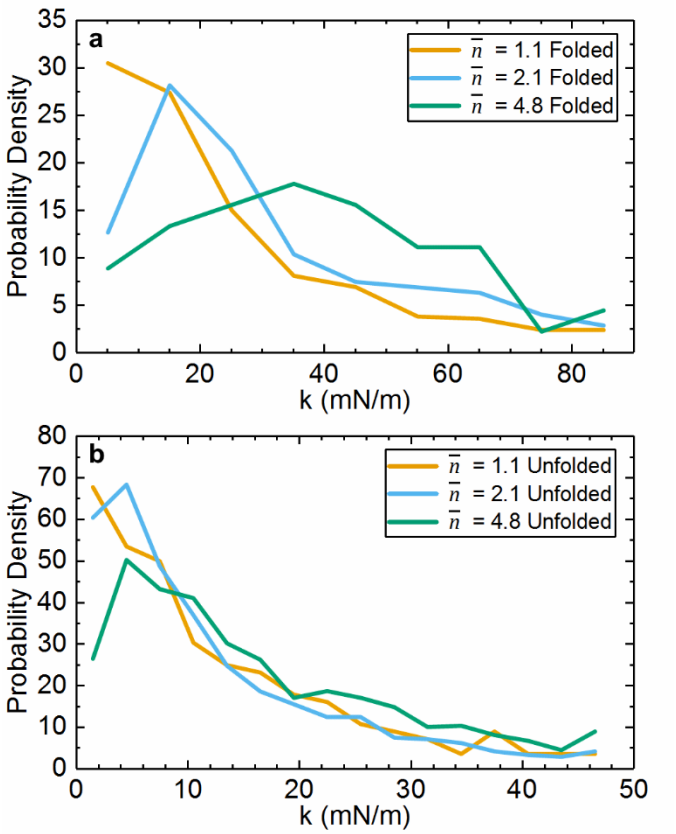

Figure E-6: Distribution of spring constants of immobilized lipA. Probability density functions of enzyme stiffnesses measured from observed SM d value fluctuations. Distributions of spring constants, expressed as Millinewtons per meter, for (a) folded lipA and (b) unfolded lipA immobilized on brushes synthesized with 1% NHS ($\bar{n}$ = 1.1, yellow lines), 5% NHS ($\bar{n}$ = 2.1, blue lines), and 10% NHS ($\bar{n}$ = 4.8, green lines).

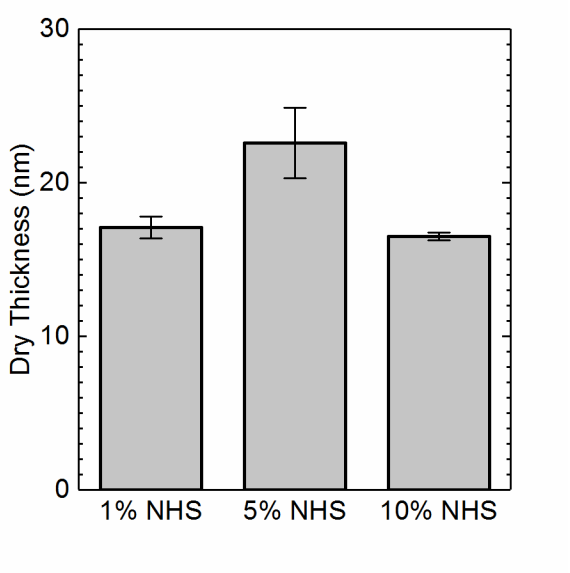

Figure E-7: Thickness of polymer brush supports. Dry thicknesses were measured on polymer brushes synthesized from 2” silicon wafers and measured with a variable-angle spectroscopic ellipsometer. The thickness of the native oxide layer, monolayer of initiator, and brush were measured independently on different samples to provide an accurate measurement of the dry brush. Error bars represent the standard deviation of three experimental replicates.

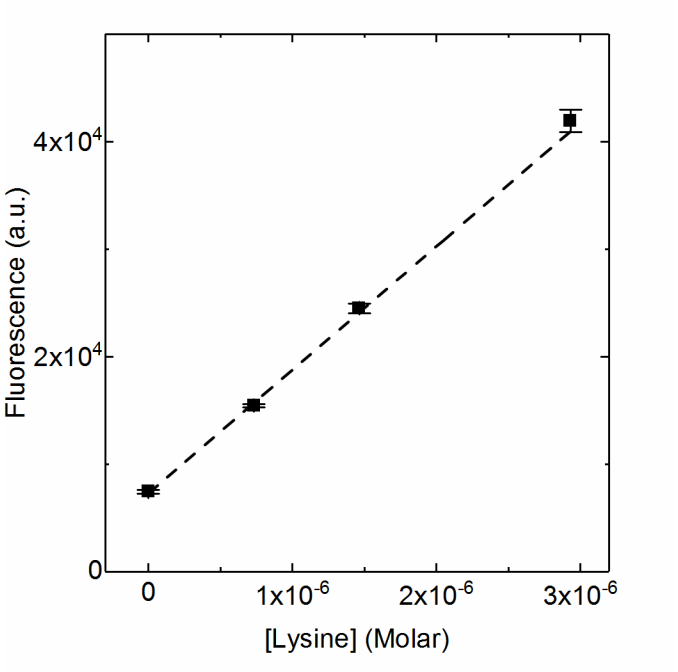

Figure E-8: Calibration curve of fluorescamine. Fluorescamine fluorescence versus molar concentration of lysine used as the standard for determining primary amine concentration in 50mM sodium phosphate, pH 7.50. Fluorescamine fluorescence was measured in an Infinite M Plex (Tecan) plate reader by measuring fluorescence emission at 470 nm with excitation at 365 nm.

$\bar{n}$	1.1	2.1	4.8
20ºC	2,930	2,254	1,725
45ºC	2,099	2,110	1,645

Table E-1**:** Number of single-molecule trajectories for each condition.

Folded

$\bar{n}$	1.1	2.1	4.8
20ºC	375	204	608
45ºC	313	706	295

Unfolded

$\bar{n}$	1.1	2.1	4.8
20ºC	291	144	142
45ºC	239	171	117

Table E-2: Number of single-molecule trajectories for RMSD of d analysis for folded and unfolded lipA.